



KTH ROYAL INSTITUTE
OF TECHNOLOGY

DEGREE PROJECT IN MECHANICAL ENGINEERING
SECOND CYCLE, 30 CREDITS

Modeling of Energy Consumption in Milling Process to Assess their Environmental Impact

**PENG LIANG
VASANTH KUMARAN ASHOK KUMAR**

Modeling of Energy Consumption in Milling Process to Assess their Environmental Impact

Peng Liang and Vasanth Kumaran Ashok Kumar

10/30/2023

Master's Thesis

Examiner
Andreas Archenti

Academic advisor
Theodoros Laspas

Industrial advisor
Coskun Islam

KTH Royal Institute of Technology
School of Industrial Engineering and Management (ITM)
Department of Production Engineering and Management
SE-100 44 Stockholm, Sweden

Abstract

This thesis presents a method for modeling energy consumption in milling process to assess their environmental impact, by a simple experimental approach. The factors influencing the environmental impact in the milling processes are analyzed with life cycle assessment principles and their climate change impact is calculated with examples of dry milling experiments.

The model to predict the energy consumption is inspired by the mechanistic model of milling operation. The tangential cutting force coefficients are approximated using experimental data to estimate the spindle power. The developed model can predict the energy consumption for given cutting parameters and conditions.

The results show that 1) the energy consumption of the milling process estimated by the proposed mechanistic-based model agrees well with the experimentally measured results, 2) the experimental approach to build the model is easy and fast, and 3) the consumption of the solid cutting tool contributes the most to the environmental impact in dry milling processes.

The analysis presented in this thesis also provides insight into how to improve energy efficiency and reduce the environmental impact of milling processes.

Keywords

Milling process, Energy consumption, Mechanistic model, Environmental impact, Life cycle assessment

Sammanfattning

Denna avhandling presenterar en metod för att modellera energiförbrukning i fräsningsprocessen för att bedöma deras miljöpåverkan genom en enkel experimentell metod. Faktorer som påverkar miljöpåverkan i fräsningsprocesser analyseras med principer för livscykelbedömning och deras klimatpåverkan beräknas med exempel på torrfräsningsförsök.

Modellen för att förutsäga energiförbrukningen är inspirerad av den mekaniska modellen för fräsningsoperation. Koefficienter för tangentIELL skärkraft approximeras med experimentella data för att uppskatta spindelkraften. Den utvecklade modellen kan förutsäga energiförbrukningen för givna skärparametrar och villkor.

Resultaten visar att 1) energiförbrukningen i fräsningsprocessen uppskattad med den föreslagna mekanikbaserade modellen överensstämmer bra med experimentellt uppmätta resultat, 2) den experimentella metoden för att bygga modellen är enkel och snabb, och 3) förbrukningen av det fasta skärverktyget bidrar mest till miljöpåverkan i torrfräsningsprocesser.

Analysen som presenteras i denna avhandling ger också insikt i hur man kan förbättra energieffektiviteten och minska miljöpåverkan i fräsningsprocesser.

Nyckelord

Fräsningsprocess, Energiförbrukning, Mekanisk modell, Miljöpåverkan, Livscykelbedömning

Acknowledgments

We would like to express our sincere gratitude to our advisors, Dr Coskun Islam and Theodoros Laspas, for their invaluable support and guidance throughout this thesis, particularly on metal cutting theory, experiments, and thesis revision. We would like to thank Dr Sayyed Shoaib Ul Hasan for generously sharing his insights about topics related to environmental impact assessment. We are also grateful to Jenny Hörlund for gathering information regarding the cutting tool carbon footprint.

We take this opportunity to thank KTH Royal Institute of Technology, and the Department of Production Engineering and Management for providing the facility to conduct experiments and helping us to learn and gain experience through this thesis work.

We thank Sandvik for providing us with the opportunity to work on this innovative thesis topic and for the support with the supply of material for the experiments.

Peng Liang would like to thank Scarlett Roa for her guidance on sustainability reporting.

Finally, we would like to thank our family and friends for their continuous love and support which kept us motivated throughout this thesis period.

Peng Liang

Vasanth Kumaran Ashok Kumar

Stockholm, June 2023

Table of Contents

Modeling of Energy Consumption in Milling Process to Assess their Environmental Impact.....	1
Abstract.....	i
Keywords	i
Sammanfattning	iii
Nyckelord.....	iii
Acknowledgments.....	v
Table of Contents	vii
List of Figures.....	ix
List of Tables	xi
List of Symbols.....	xiii
List of Acronyms and Abbreviations.....	xv
1. Introduction	1
2. Literature Review	3
2.1 Sustainable Manufacturing	3
2.2 Energy Consumption Prediction	3
2.3 Previously Suggested Frameworks	5
2.4 Milling and Cutting Mechanisms	7
3. Environmental Impact Assessment Methodology	9
3.1 System Boundary.....	9
3.2 Functional Unit	11
3.3 Environmental Impact Calculation Method	12
3.3.1 Electricity.....	12
3.3.2 Cutting Tool.....	12
4. Modeling of Energy Consumption.....	13
4.1 Cutting Force Simulation Models	14
4.1.1 Milling Force Simulation Algorithm:	15
4.1.2 Milling Tangential Force Calculation Algorithm:	17
4.2 Spindle Air-cutting Power Calculation.....	18
4.3 Cutting Power Prediction	18
4.3.1 Approach 1.....	19
4.3.2 Approach 2.....	24
4.4 Axis Power Prediction	27
4.5 Idle Power Calculation	28
4.6 Summary of the Modelling Approach	28
4.7 Experimental Procedures	29
4.7.1 Design of Tests	30
4.7.2 Experimental Setup.....	32
4.8 Data Processing Approach	34
5. Results	36
5.1 Power Prediction with Slot Cutting Experiments	36
5.1.1 Spindle Air-cutting Power	36
5.1.2 Cutting Power	38

5.1.3	Axis Motor Power	43
5.1.4	Idle Power.....	45
5.1.5	Power Prediction Validation	45
5.1.6	Practical Approach Example	53
5.2	Environmental Impact Calculation.....	55
5.2.1	Electricity	56
5.2.2	Cutting Tool	57
5.2.3	Total Environmental Impact.....	57
5.3	Uncertainty Discussion.....	59
6.	The Framework – top to bottom.....	61
7.	Conclusions and Future Work	63
References		65
Appendix A: Supplementary Figures and Tables		69

List of Figures

Figure 1 The GHG Emissions Categorized by the GHG Protocol for a Company Manufacturing Product X (adapted from [5]).....	1
Figure 2 Process Map of the Milling Processes in Question	10
Figure 3 Power Consumption in a Typical Milling Operation	13
Figure 4 Power Prediction Model Process Map	14
Figure 5 Algorithm 1 Simulation Comparison – Tool A and B	21
Figure 6 Algorithm 1 Simulation Comparison – Tool A and C	22
Figure 7 Algorithm 1 Simulation Comparison – Tool A and D	22
Figure 8 Algorithm 1 Simulation Comparison – Tool A $ap = 3$ mm and $ap = 5$ mm.....	23
Figure 9 Synthetic Experiments	24
Figure 10 Linear Regression for the Synthetic Experiments	24
Figure 11 Cutting Power Prediction for the Synthetic Experiments	24
Figure 12 Average Power vs MRR for Different Cutting Speeds (Varying Axial and Radial Depths of Cut, and Feed per Tooth Values).....	26
Figure 13 Schematic Representation of Diagonal Slot Cutting [Feed Speeds: Cut 1<Cut 2<Cut 3<Cut 4<Cut 5]	30
Figure 14 The Workpiece held on a Standard Bench Vise	33
Figure 15 Power Analyzer Wiring Diagram [54].....	33
Figure 16 Spindle Air-Cutting Power Curve for the Three End Mills.....	37
Figure 17 Average Spindle Air-Cutting Power Curve.....	37
Figure 18 Slot-cutting Experiments Results	39
Figure 19 Mechanistic Model Simulation Result for Slot-cutting Experiments	40
Figure 20 Linear Regression Result of 8 mm End Mill Slot-cutting Experiments	41
Figure 21 Linear Regression Result of 10 mm End Mill Slot-cutting Experiments	41
Figure 22 Linear Regression Result of 12 mm End Mill Slot-cutting Experiments	42
Figure 23 Comparison of Linear Regression Models.....	42
Figure 24 8 mm End Mill Pcutting Prediction Confidence Intervals	43
Figure 25 Pcutting Prediction Maximum One-side Confidence Intervals	43
Figure 26 Linear Regression for Axis Motor Power	44
Figure 27 Machine Idle Power	45
Figure 28 Total Power Comparison between Prediction and Experiments	49
Figure 29 SEC Comparison between Prediction and Experiments	49
Figure 30 Cutting Power Prediction Bias	50
Figure 31 Process Power Prediction Bias	50
Figure 32 Total Power Prediction Bias	51
Figure 33 SEC Prediction Bias.....	51
Figure 34 10 mm End Mill Linear Regression Model for Calculating Ktc and Kte	54
Figure 35 10 mm End Mill Linear Regression Models for Px and Py	55
Figure 36 The Contribution of Impact Sources for the Face Mill Experiment (Market-based)	58
Figure 37 The Contribution of Impact Sources from the Simulation with Inserted Cutters	59
Figure 38 Process Map of the Framework	61
Figure 39 Simulated and Calibrated Average Power Values vs MRR	69
Figure 40 Absolute Error in the Power Values Predicted using the Empirical Model Vs MRR	69
Figure 41 Slots Cut along X Axis	70
Figure 42 Slots Cut along Y Axis	70
Figure 43 Diagonal Slots	71

Figure 44 Face Milling Tool Path along Y Axis	71
Figure 45 Pocketing Tool Path Cutting Outward from the Center	72
Figure 46 Shoulder Milling Tool Path and Machined Surfaces	72

List of Tables

Table 1 Summary of Energy Consumption Models	4
Table 2 Summary of Previous Frameworks	6
Table 3 Functional Units in Previous Studies	11
Table 4 Tool Geometry Parameters for Simulation.....	20
Table 5 Experimental Parameters and Values for Creating the Empirical Model.....	26
Table 6 Cutting Conditions for Validating the Approach	27
Table 7 List of Cutting Tools Used in the Experiments	29
Table 8 Design of Experiments for Developing the Prediction Model.....	30
Table 9 Design of Experiments for Validating the Prediction Model	32
Table 10 List of Trace Variables Chosen to be Recorded During the Experiments	34
Table 11 Spindle Air-Cutting Power Curve Control Points.....	38
Table 12 The Spindle Speed and the Corresponding Air-cutting Power in the Slot- Cutting Experiments	38
Table 13 Linear Regression Models for Cutting Power Calculation	40
Table 14 Calculated K_{tc} and K_{te}	41
Table 15 Linear Regression Models for Axis Motors	44
Table 16 Shoulder Mill Experiments Parameters for the 12 mm End Mill	46
Table 17 Experiment and Prediction Result of the 12 mm End Mill Shoulder Mill Experiment (W, Wh/cm ³).....	47
Table 18 Bias and Relative Error of the 12 mm End Mill Shoulder Mill Prediction (W, Wh/cm ³).....	47
Table 19 Face Mill Experiments Parameters for the 10 mm End Mill	52
Table 20 Experiment and Prediction Result of the 10 mm Tool Face Mill Experiment.....	53
Table 21 Bias and Relative Error of the 10 mm Tool Face Mill Prediction	53
Table 22 10 mm End Mill Diagonal Slot Milling Tests Results.....	54
Table 23 10 mm End Mill Spindle Power Linear Regression Result	54
Table 24 10 mm End Mill Axis Power Linear Regression Result.....	55
Table 25 Practical Approach Prediction Comparison	55
Table 26 Total CO ₂ Intensity Calculation for Market-Based Method (Electricity Supply for the KTH Campus)	56
Table 27 Total CO ₂ Intensity Calculation for Location-Based Method (Sweden)	56
Table 28 Environmental Impact of the End Mills.....	57
Table 29 Total g CO ₂ -eq/FU of the Shoulder Mill Experiment (12 mm End Mill) in Section 5.1.5.1	58
Table 30 Predicted Total Power and g CO ₂ -eq/FU in 10 mm End Mill Scenario	59
Table 31 Trace Variables	73
Table 32 Experimental and Predicted Data for Calculating the Variables in Table 17	74
Table 33 Life Cycle Emission Factors for Electricity Generation Technologies (g CO ₂ - eq/kWh) [56]	74

List of Symbols

D	Diameter of cutting tool
E	Energy consumed in total
$E_{cutting}$	Energy consumed for cutting
E_{idle}	Energy consumed in machine idle state
$E_{process}$	Energy consumed for process
F_t	Tangential cutting force
K_{tc}	Tangential cutting coefficient
K_{te}	Tangential edge coefficient
N	Number of cutting edges
P_{avg}	Average spindle power consumption
$P_{cutting}$	Cutting power
P_{idle}	Idle power
$P_{process}$	Process power
$P_{sp\ air}$	Spindle air-cutting power
P_x	X-axis motor power consumption
P_y	Y-axis motor power consumption
V_c	Cutting speed
V_f	Feed rate
a_e	Radial depth of cut
a_p	Axial depth of cut
c	Feed per tooth
n	Spindle speed
α	Rake angle
β	Helix angle
ϕ	Immersion angle
η	Efficiency

List of Acronyms and Abbreviations

CAM	Computer Aided Manufacturing
CNC	Computer Numerical Control
CSRDI	Corporate Sustainability Reporting Directive
Expt.	Experiment
FU	Functional Unit
GHG	Greenhouse Gas
It.	Interpolation
LCA	Life Cycle Assessment
MRR	Material Removal Rate
P.A.	Power Analyzer
Pred.	Prediction
Rel. Err.	Relative Error
SEC	Specific Energy/Electricity Consumption
Tr.	Trace
avg	Average

1. Introduction

Milling is a type of machining operation moving a rotary cutter into a workpiece to remove material. It forms a critical part of the production in a wide range of industrial products, from small and delicate watch parts to big and heavy spacecraft components. Assessing the environmental impact of milling processes is crucial for several reasons. First, such assessment aids in sustainable decision-making in manufacturing, for example, in the selection of energy-efficient cutting parameter combinations. Second, it is necessary in product life cycle accounting and reporting for manufacturers, particularly when the milling process is a part of the product's cradle-to-grave or cradle-to-gate life cycle inventory. Finally, it is essential in corporate greenhouse gas (GHG) emission calculation and reporting, thereby fulfilling the regulatory requirements of the Non-Financial Reporting Directive (NFRD) [1] and the Corporate Sustainability Reporting Directive (CSRD) [2, 3].

For example, the GHG protocol corporate standard [4], stipulates that electricity consumption during milling processes should be reported under Scope 2, which includes indirect GHG emissions associated with electricity. The remaining GHG emissions from milling processes should be reported under Scope 3, which covers other indirect GHG emissions. In this scope, cutting tools and cutting fluid fall under Category 1 – ‘purchased goods and services’, while metal chips and waste cutting fluid are classified under Category 5 – ‘waste generated in operations.’ Therefore, it is crucial to fully understand and accurately evaluate milling processes’ environmental impact. Figure 1 illustrates the GHG emission categorization method for a product involving milling as a part of production. The blue blocks divide the GHG emission into Scope 1, 2, and 3. The red path is the product life cycle emission phases. Milling processes are part of the production phase.

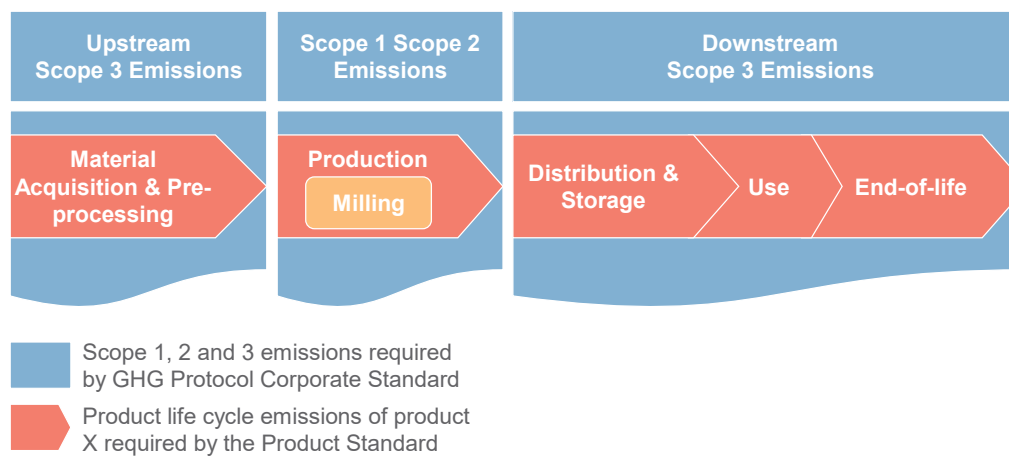


Figure 1 The GHG Emissions Categorized by the GHG Protocol for a Company Manufacturing Product X (adapted from [5])

Existing environmental impact databases typically evaluate the environmental impact footprint of manufacturing processes based on average energy consumption values, such as the energy required to remove 1 cm³ of material. Previous research has enhanced the accuracy of these predictions by linking energy consumption to the Material Removal Rate (MRR), these estimations still lack sufficient granularity when applied at the process planning level. Moreover, manufacturers and process planners lack a straightforward approach to assess the machining processes' specific environmental impact using their machines and cutting tools.

Therefore, the primary goals of this thesis are:

1. To establish a method for creating a dry milling energy consumption model that is conducive to experimentation and is grounded in the mechanistic modeling principles of metal cutting. This methodology should account for the effects of various combinations of milling parameters on energy consumption, surpassing the simplification that links milling processes only with MRR.
2. To analyze the environmental impact sources of dry milling processes and their proportions, and to propose a robust framework for assessing the indirect GHG emissions from these processes.

This thesis is structured into six chapters. Chapter 2 provides a literature review on sustainable manufacturing, machining energy consumption models, frameworks for evaluating machining energy efficiency/carbon emissions, and cutting mechanisms. In Chapter 3, the methodology guidelines of the work are detailed, the system boundaries and the functional unit are defined, and the models and approaches developed for power prediction and the environmental impact calculation are explained, along with a presentation of the experimental procedures designed for this study. Chapter 5 presents and discusses the results derived from the milling experiments, validates the prediction model, showcases practical examples of the proposed experimental approach, and computes the environmental impact of milling processes. Chapter 6 illustrates and explicates the proposed framework, and the conclusions of the thesis are drawn in Chapter 7.

2. Literature Review

2.1 Sustainable Manufacturing

Human activities are predominantly responsible for increased greenhouse gas emissions into the atmosphere. Manufacturing ranks among the most significant human activities globally [6] and, as such, contributes substantially to these emissions. A recent analysis by European Statistics indicates that manufacturing is the second largest contributor to global greenhouse gas emissions. The energy sector, which includes the energy demands of the manufacturing sector, is the most significant contributor.

The term 'carbon footprint' rose to prominence in the early 2000s. It is used in relation to different products and activities to measure the quantity of associated greenhouse gas emissions. Carbon dioxide contributes to most of the greenhouse gases. Thus, the carbon footprint of a product or activity is defined as the amount of greenhouse gases it emits, expressed as an equivalent mass of carbon dioxide [7].

Given that industrial processes are leading contributors to carbon dioxide emissions, numerous studies have sought to identify and investigate carbon-intensive steps and improve these processes to reduce their emissions [8–11]. Manufacturing processes primarily use electrical energy, significantly contributing to carbon emissions. Consequently, the carbon emissions associated with a manufacturing process can be calculated by multiplying the electrical energy consumed by a carbon emission factor associated with that energy source. This carbon emission factor depends on how the energy is generated; thus, it varies from place to place.

2.2 Energy Consumption Prediction

Since energy consumption in manufacturing processes is the principal contributor to carbon emissions, measuring this energy consumption is the initial step in evaluating the carbon footprint of a manufacturing process. Manufacturing activities can be divided into three levels: process, machine, and system [12], all three consuming electrical energy. The process level pertains solely to the manufacturing process; the machine level includes auxiliary equipment while the system level comprises all other facets of manufacturing, such as material and tool production, transportation, and disposal. Various studies have been conducted to measure energy consumption across these three levels [13, 14].

Before reading more in detail about the energy consumption models, it is necessary to know about how the machine energy consumption states are categorized. Palasciano et al. [15] outlined two primary machine states: idle and busy, further dividing the idle state into five machine energy states. In the 'Off' state, all components are switched off. The 'Stop' state occurs during operations such as setting up a new workpiece, with only the CNC active. With minimal power consumption, the 'Pre-processing' state sees the CNC controlling axis positions, ready for movement. The 'Ready' state is a standby mode post-cutting, maintaining low energy consumption. The 'Processing' state executes the cutting program, leading to medium to high power consumption by axis motors and the spindle.

There have been several attempts to predict energy consumption associated with a manufacturing process. For instance, Balogun et al. [16] developed a mathematical model to forecast the direct energy requirements in a machining operation. The energy predicted using their model includes the basic and ready state power, and the coolant pumping power requirements. The power consumed by non-cutting air movements is also included. Their study sheds light on the individual impact of machine components, auxiliary units, and other states of motion on the electrical energy demand to plan machining processes more energy-efficiently. Reducing energy consumption is the first step towards sustainable manufacturing. A study by Li et al. [17] aims to maximize the energy efficiency of

a multi-pass face milling process by selecting optimal cutting parameters. The authors conclude that the milling process can be divided into multiple periods from the power consumption point of view – the machine start-up period, standby period, acceleration and deceleration of the spindle, air-cutting and machining periods. Their study analyzes the electrical energy consumption associated with the machining process, including all the above-mentioned periods, and uses this analysis to create an optimized parameter model for reducing energy consumption.

Other researchers (Pawar et al. [18]) have developed an energy consumption prediction model for a variable material-removal rate machining process. By charting the power profile of an end-face turning process (a variable material-removal rate machining process), it is observed that power consumption fluctuates over the cutting time. The energy consumed to remove material is a function of power over the machining time; hence, energy consumption is calculated by integrating power with respect to cutting time. An empirical model was created to predict power consumption by using this approach. After conducting experiments to determine the coefficients to include in the model, it was validated to be about 95% accurate.

Similarly, Rahimifard et al. [19] and Seow et al. [20] presented a model capable of calculating the total energy consumption of a product during its manufacturing phase. The authors categorized energy consumption during manufacturing into two types—direct and indirect. Direct energy consumption is the energy consumed during the production process, such as machine consumption and auxiliary consumption during machine operation. Conversely, indirect consumption is the energy used to maintain the production environment where the manufacturing processes take place, such as lighting, heating, and ventilation. Their simulation model outputs energy consumption based on the process, product, and process energy efficiency ratios. The model is designed to assist product designers in creating more energy-efficient products and engineers in selecting process routes for energy-efficient manufacturing.

Zhou et al. [21] have developed an energy consumption model that can determine a workpiece's Energy-Consumption Allowance (ECA) in a manufacturing system. The ECA of a workpiece is defined as the reasonable quantity of energy consumed during the entire machining process of the workpiece in a manufacturing system. The machining process is broken down into smaller steps, divided into several sub-steps with basic-energy consumption to calculate the total energy consumption.

Table 1 summarizes these energy consumption models, providing an overview of the various methodologies and parameters considered in each.

Table 1 Summary of Energy Consumption Models

Authors	Energy Consumption Model	
Balogun et al.	$E_t = P_b t_b + (P_b + P_r) t_r + P_{air} t_{air} + (P_b + P_r + P_{cool} + k\dot{v}) t_c$ <p>E_t – direct total energy requirement P_b – basic power P_r – ready state power P_{cool} – coolant pumping power t_b, t_r, t_c – times for basic, ready-state and cutting k – specific cutting energy v – rate of material processing</p>	[16]
Li et al.	$E_{total} = E_{start-up} + E_{standby} + \sum_{i=1}^m (E_{air}^i + E_{machining}^i) + E_{tc}$ <p>E_{start-up} – start-up energy E_{standby} – standby energy E_{air} – air cutting energy E_{machining} – machining energy</p>	[17]

	$E_{tc} - \text{tool changing energy}$ $i=1 \text{ to } m - \text{number of milling passes}$	
Pawar et al.	$E_c = \int_0^t P_c dt$ <p>$E_c - \text{material-removal energy consumption}$ $P_c - \text{material-removal power as a function of cutting speed (v), feed rate (f) and depth of cut (d)}$</p>	[18]
Rahimifard et al. And Seow et al.	$DE = \sum_{i=1}^n (TE(i) + AE(i))$ <p>$DE - \text{total direct energy consumption}$ $TE - \text{theoretical energy for process}$ $AE - \text{auxiliary energy for supporting activities}$ $i=1 \text{ to } n - \text{number of processes}$</p>	[19, 20]
Zhou et al.	$E_M = (E_R + E_S + E_I + E_A + E_C) + E_{workshop} \cdot T^M$ <p>$E_M - \text{machining energy consumption}$ $E_R - \text{standby energy consumption}$ $E_S - \text{starting energy consumption}$ $E_I - \text{idling energy consumption}$ $E_A - \text{air cutting energy consumption}$ $E_C - \text{cutting energy consumption}$ $E_{workshop} - \text{auxiliary energy consumption}$ $T^M - \text{energy ratio of auxiliary systems}$</p>	[21]

Despite the previous works focusing on various aspects of predicting and analyzing energy consumption during machining, the existing models' specificity to specific machining scenarios is a limitation. They are not abstract enough to be scalable and adaptable across various machining situations. Given machining operations' diverse and complex nature, an abstract and versatile model is essential for accurately predicting energy consumption across various machining scenarios. Therefore, there is an evident need for an encompassing, abstract model to predict the energy consumption of the machining process in a way that is both scalable and adaptable to different manufacturing circumstances.

2.3 Previously Suggested Frameworks

Several studies have strived to devise frameworks assessing manufacturing processes' sustainability, energy efficiency, and cost effectiveness. Bhanot et al. [8] introduced a framework that evaluates a turning process's sustainability from economic and environmental perspectives. This study incorporates a comprehensive process cost analysis, employing strategies to optimize costs and improve economic efficiency. The framework aims to reduce energy consumption by determining optimal cutting parameters and provides a model for assessing carbon emissions based on this calculated energy consumption.

Similarly, Newman et al. [22] proposed a theoretical framework for energy-efficient process planning. They developed an objective function that includes various components like workpiece geometry, sequences of operations, and the cutting parameters to execute these operations. This function is designed to model and optimize process plans. Their study also compares experimental energy consumption between two distinct machining processes - finish cutting and semi-finishing an aluminum block. This comparison highlights the energy consumption variability in interchangeable machining processes, thus integrating energy consumption as a component in the objective function to optimize process planning.

Salem et al. [23] showcased an integrated approach offering machining process designers optimized cutting parameters to enhance process sustainability. This approach encompasses two significant parts: firstly, the assessment of existing machining processes based on proposed sustainable machining metrics, and secondly, a decision-making procedure to determine optimized machining parameters using a multi-objective optimization technique. This approach verified using two case studies, yields parameters outperforming experimentally determined optimal machining parameters. The sustainable machining metrics serve as important indicators for assessing machining processes. Metrics such as cost efficiency and energy and resource consumption offer insights into potential process expenses and resource wastage.

Lu et al. [24] proposed a framework for developing such metrics related to both the process and product, aiming to enhance manufacturing sustainability. This study highlights energy consumption as a key determinant in the process metrics.

Branker et al. [25] presented a new microeconomic model optimizing machining process cutting parameters by considering all energy and environmental costs. Energy costs encapsulate the expenses associated with electricity consumption during the process and consumption by ancillary or peripheral equipment. Environmental costs, on the other hand, are associated with carbon emissions throughout the entire process. The model calculates the total CO₂ emissions from various aspects of the process, such as the material, cutting tool, metal chips processing, and coolant disposal. When multiplied by the carbon cost value, these emission values determine the environmental costs. The study emphasizes that electricity consumption is the primary contributor to CO₂ emissions, suggesting the conversion of energy consumption data into emission data using the Carbon Emission Signature (CES) [26].

Dahmus et al. [27] developed a model to analyze the environmental impact of machining, not only focusing on just the cutting process but also associated processes such as material preparation and coolant preparation. The energy analysis in this study show that the energy consumption associated with the material removal process is very less compared to the total energy consumption by the machine. Also, the authors have concluded that the energy intensity of the material being machined is an important factor in total energy consumption.

Narita et al. [28] have developed an environmental burden analyzer, based on LCA concept, to evaluate a CAM program from the perspective of its environmental impact. This model simulates a cutting process from the parameter values of a program to estimate energy consumption. Following that, using emission intensities the CO₂ emissions linked to the process is calculated. This model includes the effect of peripheral devices and activities such as the coolant system and metal chips management.

Table 2 summarizes these frameworks suggesting the objective and purpose of each.

Table 2 Summary of Previous Frameworks

Authors	Framework Description	
Bhanot et al.	Determines optimal cutting parameters to reduce energy consumption and hence optimises cost and improves economic efficiency.	[8]
Newman et al.	Developing a function that models and optimizes process plans with a view of making them energy efficient	[22]
Salem et al.	To assess existing machining processes and to develop a decision-making procedure to optimize machining parameters	[23]
Lu et al.	Developing process and product metrics to enhance sustainability in manufacturing	[24]

Branker et al.	Optimising cutting parameters of a machining process considering the energy and environmental costs	[25]
Dahmus et al.	Environmental analysis of machining process including associated processes	[27]
Narita et al.	Analysing environmental burden of a machining process considering the influence of peripheral devices	[28]

Although, these frameworks are developed mostly to model and analyze energy consumption with an environmental perspective, almost none of them have used the LCA concept. Knowing the inputs and outputs of a process, defining the system boundaries and using a functional unit to assess and analyze the environmental impact of the process can be fundamental.

2.4 Milling and Cutting Mechanisms

It is important to read about the cutting mechanism of milling operation. Studies from literature and texts are helpful to gain deeper understanding on the topic. Altintas has given a very fine insight into the cutting mechanisms behind orthogonal and oblique cutting operations in his book 'Manufacturing Automation' [29]. The mechanistic model, proposed by Altintas, for orthogonal cutting and oblique cutting in milling processes have been the base for several studies to create cutting forces prediction models. Also in his book, Altintas has described a pseudocode for simulating the cutting process by entering the cutting parameters and cutting conditions as inputs. The pseudocode has been derived by several researchers to generate algorithms to simulate the milling processes to study the effect of cutting parameters on the cutting forces. Going through several studies on predicting the cutting forces linked with milling gives a clear picture about the cutting mechanisms and how to model the cutting force prediction.

Campatelli et al. [30] created a model to predict the cutting forces in milling operation using Aluminum 6082. This model was created based on a study of the influence of feed per tooth and cutting speed of the process. The authors have built the force prediction model by understanding the cutting process, simulating it, and with an aim of using the model to optimize cutting parameters. The same approach has inspired the current thesis. Wu Baohai et al. [31] designed a cutting force prediction model for circular end milling process. When traditional cutting forces prediction models focus on linear milling process, this study presents an improved prediction model for also predicting force in circular milling paths. This model is adopted from the commonly used mechanistic model proposed by Altintas. The model proves to predict the cutting forces in circular milling process with high accuracy. This study can be inspiring for the thesis to model energy consumption model for complex milling paths.

There are other studies which have presented prediction models as a part of optimizing the milling process. Dikshit et al. [32] measured and analyzed the cutting force components in high-speed ball-end milling, with an aim of creating a prediction model to optimize the cutting parameters. The model was based on a quadratic fitting for prediction of force components. Grossi et al. [33] present an instantaneous prediction method based on genetic algorithm to identify cutting force coefficients which are speed-varying. This model is also capable of estimating the tool run outs simultaneously with cutting forces prediction. Advanced prediction models are a good starting point to predict cutting forces which is the base for energy consumption modeling of milling process.

3. Environmental Impact Assessment Methodology

This research is designed to understand and evaluate the energy consumption and environmental impact of milling processes. Milling processes typically involve the following inputs [34, 35]: resources, such as metal; services, like energy supply; and ancillary materials, including cutting tools and cutting fluid. During these processes, metal chips and waste-cutting fluid are generated. Depending on the solution, recycling, reuse, and disposal methods, cutting fluid can be a source of eco-toxicity [36]. Notably, there is either no or infinitesimal direct greenhouse gas emission.

The research focuses specifically on dry milling performed on low-alloy steel (SS2541). Without the use of cutting fluid, the environmental impact categories, climate change and eco-toxicity are confined solely to climate change. Given this scope, utilizing greenhouse gas (GHG)-only inventory and a corresponding assessment methodology is practical, as there is no apparent non-GHG environmental impact.

The scope of this study is focused on dry milling processes without using a coolant. The rationale behind this decision lies in three key factors:

1. The dry milling process presents a simplified scenario that eliminates the complexities introduced by coolant use, such as considerations around coolant type, disposal, and its environmental impacts. By doing so, the research can concentrate on the fundamental aspects of energy consumption in milling operations, providing a solid foundation for subsequent, more complex studies.
2. Dry milling is an increasingly common practice in modern manufacturing due to its environmental benefits, thus enhancing the practical relevance of our research findings.
3. Given the constraints of the research timeframe and resources, focusing on dry milling without coolant has allowed researchers in this study to conduct a thorough and in-depth investigation rather than spreading our efforts too thin over a broader scope.

While the absence of coolant may limit the generalizability of the findings to all types of milling operations, it does allow for a more rigorous exploration of a critical subset of these processes.

Considering the characteristics of the object under study, the following two standards serve as guidelines for the assessment methodology:

- ISO 14044:2006 Environmental management – Life cycle assessment – Requirements and guidelines [34] (hereinafter referred to as ISO 14044), and
- Greenhouse Gas Protocol Product Life Cycle Accounting and Reporting Standard [5] (hereinafter referred to as the Product Standard).

ISO 14044 is part of the well-known 14000 series of ISO environmental management standards. ISO 14044 and ISO 14040 are two standards developed to assure life cycle assessment comparability. ISO 14044 defines specifications and principles for LCA. It includes LCA studies and life cycle inventory studies [37].

The Product Standard was created by World Resources Institute (WRI) and World Business Council for Sustainable Development (WBCSD) as guidelines for organizations to utilize in measuring the life cycle GHG emissions of their products. The fundamental goal of this standard is to provide a general framework for companies to make informed choices to reduce GHG emissions from the products (goods or services) they design, manufacture, sell, purchase, or use [38].

3.1 System Boundary

The Product Standard outlines the following steps to establish boundary setting:

- Identify the processes attributable along the life cycle directly connected to the studied product and its ability to perform its function.
- Group these attributable processes into life cycle stages.
- Identify the service, material, and energy flows required for each attributable process.
- Illustrate the product's life cycle processes via a process map.

As per ISO 14044, ‘the selection of the system boundary should be consistent with the study's goal’, ‘the criteria used in setting the system boundary should be identified and explained’, and ‘any decision to omit life cycle stages, processes, inputs, or outputs should be clearly stated, with explanations and implications for their omission.’ ISO 14044 also suggests depicting the system using a process flow diagram.

The milling processes in our study occur during the production stage of products' life cycles. The attributable and non-attributable processes, along with their justification, are as follows:

- Due to its nature as a capital good [5], the machine tool is considered non-attributable
- The cutting tool collet, with a lifespan of 500 machine hours [39] or two to three months based on an eight-hour workday [40], greatly outlasts the milling process duration in this study (minute level) and is thus non-attributable.
- The input metal blank and the output milled metal (metal with finished milled features) are considered non-attributable in this study, as it specifically focuses on the metal cutting process. The metal input may be better included in the inventory when the assessment extends to the full production stage or product life cycle. The milled metal, being the input for the next production phase, is considered outside the boundary of this milling phase.
- The electricity consumed during the machining process is attributable.
- The cutting tools, being consumables, are considered attributable.
- Peripheral activities related to machining, including auxiliary power consumption, workshop lighting, and machine maintenance, are non-attributable.
- Waste management of the metal chips and the used tools is considered attributable. This part is not included in the study because the waste management for the laboratory is different from common production workshops. It should be included in actual practice.

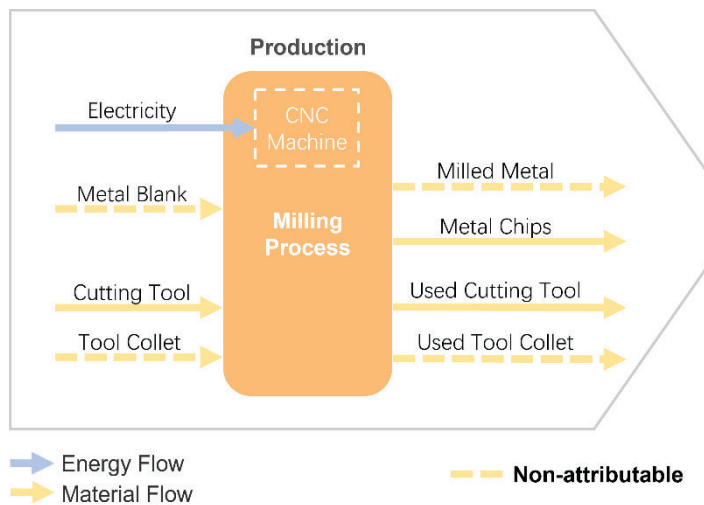


Figure 2 Process Map of the Milling Processes in Question

Therefore, this study's system boundary is demarcated by attributable and non-attributable processes and is illustrated in Figure 2.

3.2 Functional Unit

As defined by ISO 14044, the functional unit serves as a reference unit for quantifying a product system's performance. The Product Standard interprets three general parameters of a functional unit:

1. The magnitude of the function or service.
2. The duration or service life of that function or service.
3. The expected level of quality.

Functional units enable the objective comparison of products or systems that serve the same functions [41].

The performance of manufacturing approaches is a function that has been compared in previous studies. Specific energy/electricity consumption (SEC) and material removal rate (MRR) are commonly used to compare the performance and construct energy models. Gutowski et al. used specific electricity requirements as a function of the rate of material processed to reveal the energy requirement difference for various manufacturing processes [42]. Li and Kara adapted the framework introduced by Gutowski and modeled the energy consumption of turning and milling processes as $SEC = C_0 + C_1/MRR$ [43, 44], where C_0 and C_1 are the machine specific coefficients. C_0 is the coefficient of the inverse model, and C_1 is the coefficient of the predictor. They are derived from cutting experiments. Priarone et al., Campatelli et al., and Lunetto et al. applied this model further in their energy efficiency, environmental, and economic performance comparison studies between additive and subtractive manufacturing approaches [45–47].

Researchers have made diverse choices regarding functional units aligned with their study objectives (Table 3).

Table 3 Functional Units in Previous Studies

Authors, Year	Functional Unit	Purpose
Li and Kara, 2011	The specific energy consumption: the energy consumed to remove 1 cm ³ of material	To compare the machining energy consumption under different cutting conditions
Priarone et al., 2019	A single manufactured part	To compare the environmental and economic performance of additive manufacturing and machining
Campatelli et al., 2020	A single produced part	To compare the energy efficiency of additive-subtractive and pure subtractive manufacturing
Lunetto et al., 2021	A generic batch of components	To compare the environmental and economic performance of additive manufacturing and machining
He et al., 2022	The weight of the material cut from the part	To compare the environmental impact of machining process scenarios

In this study, to consider both the volume of removed material and the processing time, the MRR (i.e., the volume of material removed per unit time) is used for comparing the energy consumption and GHG emission across different cutting parameter combinations. The functional unit in this thesis is defined as the following:

“Conducting rough milling with a determined MRR to remove 1 cm³ of material.”

Different cutting parameter combinations with the same MRR are comparable using this functional unit. The electricity consumption (in Wh) and the environmental impact (in g CO₂-eq) for serving one unit function are compared between cutting parameter sets with the same MRR.

3.3 Environmental Impact Calculation Method

As discussed in the system boundary section, the GHG inventory comprises electricity and cutting tool consumption.

3.3.1 Electricity

Laboratory-based metal-cutting experiments are conducted to gather data on electricity consumption. A model predicting electricity consumption during milling is formulated by using these collected experimental data. The indirect GHG emissions from electricity use are calculated using market- and location-based methods, according to the dual reporting approach for Scope 2 emission reporting [49]. The results of both methods are required by the upcoming European Sustainability Reporting Standards (ESRS), which will be mandatory for companies under the CSRD to comply with from 2024 [50]. The location-based method reflects the average emission intensity of the power grids from which electricity is drawn. The market-based method indicates the emissions from the electricity that businesses have chosen on the market [50].

The environmental impact by electricity consumption is calculated with Equation (3.1):

$$\begin{aligned} & \text{Environmental impact of electricity consumption} \\ & = \text{Total CO}_2 \text{ intensity} \times \text{Electricity consumption} \end{aligned} \quad (3.1)$$

The total CO₂ intensity is calculated based on the energy mix.

$$\text{Total CO}_2 \text{ intensity} = \sum_i (\text{CO}_2 \text{ intensity } i \times \text{Share of source type } i) \quad (3.2)$$

3.3.2 Cutting Tool

Carbon footprint data for cutting tools are approximated using publicly available data, and tool life is evaluated using the tool catalogue from the tool manufacturer. The environmental impact of cutting tool consumption is calculated using Equation (3.3):

$$\begin{aligned} & \text{Environmental impact of cutting tool consumption} \\ & = \text{Cutting tool CO}_2 \text{ indicator} \times \text{Tool weight} \\ & \times \frac{\text{Cutting length}}{\text{Catalogue tool life length in the cutting condition}} \end{aligned} \quad (3.3)$$

The total environmental impact is the summation of electricity and cutting tool consumption impacts. An uncertainty assessment follows the result.

4. Modeling of Energy Consumption

The energy consumption of the milling processes in this thesis comes solely from the electricity usage. Therefore, by modeling the electric power, i.e., the transfer of electrical energy over time, the energy consumption can be easily deduced by integration. The problem of modeling the energy consumption is transferred to modeling the electric power in the milling process phases.

The power consumption in a typical milling process is shown in Figure 3. There are three major stable phases in a typical operation process – idle, air-cutting, and cutting. The variation in power consumption during the three phases can be clearly seen. Electricity is consumed to maintain the idle state of the control system and motors in idle states. Extra power is consumed when the spindle starts to rotate and air-cut. The required power steeply increases when the cutting tool touches the workpiece and cuts. The value of the cutting power depends on cutting parameters and conditions. A model for predicting energy consumption should take into account all these phases. Transitional phases are not in consideration in this study.

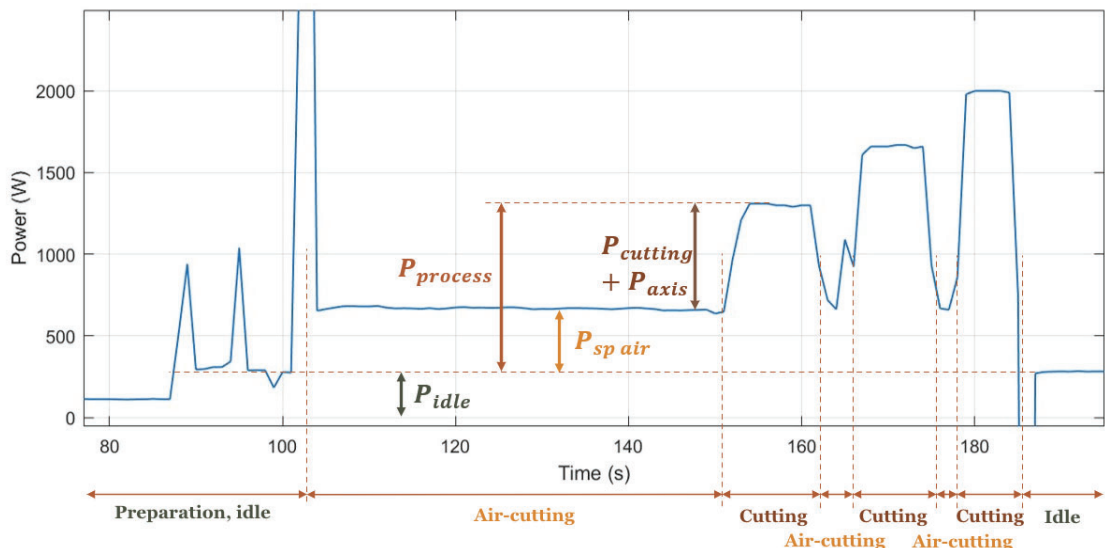


Figure 3 Power Consumption in a Typical Milling Operation

The construction of the power prediction model involves conducting three distinct types of experiments: spindle air-cutting experiments, slot-cutting experiments, and idle power experiments.

- Spindle air-cutting experiments:** These experiments are designed to quantify the power consumed by the spindle while air-cutting (not engaged with the workpiece). This power consumption, denoted as $P_{sp\ air}$, is established by plotting the spindle power consumption against spindle speed.
- Slot-cutting experiments:** This set of experiments is further divided into two sub-categories to predict the spindle and axis power separately. The power exclusively consumed by the spindle due to cutting ($P_{cutting}^{(Expt.)}$) is derived by deducting $P_{sp\ air}$ from the experimental spindle power consumption during slot-cutting experiments. This power value assists in calculating the approximate tangential cutting forces transmitted to spindle drive, subsequently allowing the cutting coefficients to be estimated. These coefficients are then used to predict the power the spindle consumes due to cutting. In parallel, the experimental power consumption values of the X and Y axes are utilized to construct the prediction model

for axis power. The sum of the predicted axis power and the predicted spindle power values results in the power consumption value for the process ($P_{process}$).

3. **Idle power experiments:** The final set of experiments is designed to estimate the machine's power consumption in its idle state. Rather than conducting separate experiments for this purpose, the machine's power consumption before and after the cutting is recorded and used to calculate the idle power (P_{idle}).

The total predicted power (P) is then calculated by adding P_{idle} to $P_{process}$.

In the second section, two different methods for the spindle power prediction are discussed and validated using a simulation model (Section 4.1) before implementing one of them. An overview of the power prediction model is illustrated as a process map in Figure 4. All the symbols used in the figure are discussed in the following sections.

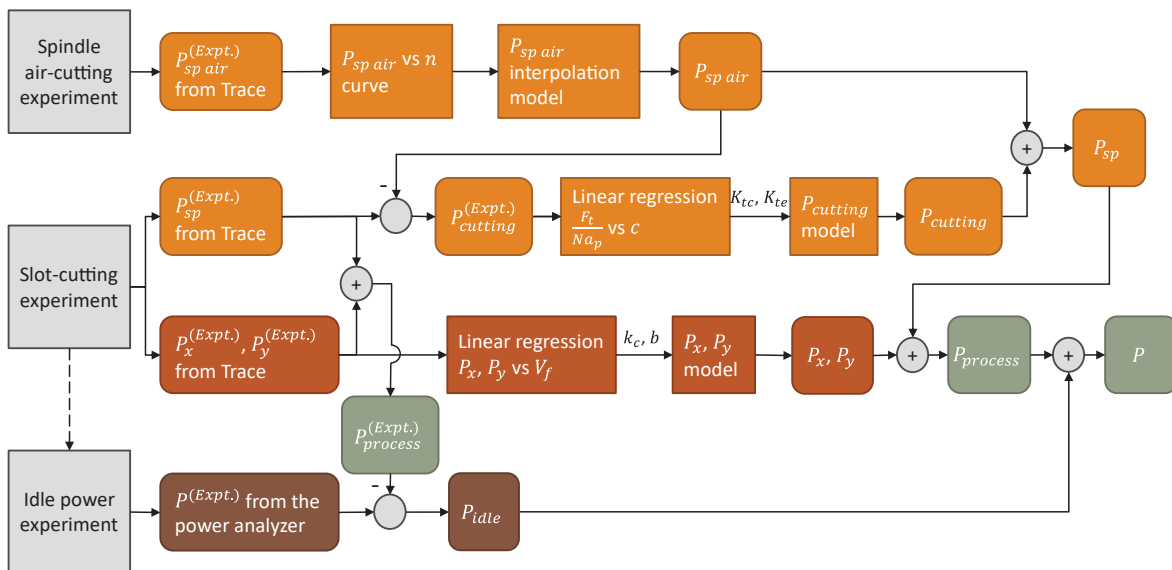


Figure 4 Power Prediction Model Process Map

4.1 Cutting Force Simulation Models

The simulation models are designed to calculate cutting forces and subsequent power consumption by the spindle. The model inputs include cutting conditions, tool geometry, and cutting coefficients. The force calculations are based on a mechanistic model of milling [29].

The cutting tool is discretized into discs along the axial direction, effectively creating oblique cutting tool segments to approximate the cutting edges (angular and axial integration numbers used in simulation can be found in Section 4.3). The tool's rotational motion is then broken down into incremental angular steps. At each rotational position in a complete revolution of the tool, engagement conditions with the workpiece are evaluated for each oblique cutting segment. The differential forces at each cutting segment can be calculated by Equations (4.1) to (4.3):

$$dF_t = [K_{tc}h(\phi) + K_{te}]dz \quad (4.1)$$

$$dF_r = [K_{rc}h(\phi) + K_{re}]dz \quad (4.2)$$

$$dF_a = [K_{ac}h(\phi) + K_{ae}]dz \quad (4.3)$$

where ϕ is the instantaneous immersion angle, and $h(\phi)$ is the instantaneous chip thickness.

$$h(\phi) = c \sin \phi \quad (4.4)$$

$$dF_x = -dF_t \cos \phi - dF_r \sin \phi \quad (4.5)$$

$$dF_y = dF_t \sin \phi - dF_r \cos \phi \quad (4.6)$$

4.1.1 Milling Force Simulation Algorithm:

This model helps to simulate laboratory experiments, which can be used to create the prediction model. To be more specific, this model is used in this thesis as a standard simulation model representing the approximate actual cutting forces. However, it does not reflect the truth without bias. The cutting coefficients input is obtained from orthogonal cutting experiments, which is one of the methods to define material behavior in the mechanistic modeling of metal cutting.

Pseudocode:

Inputs:

Cutting conditions –

End milling type - Up/Down/Slot
 a_n - axial depth of cut [mm]
 a_e - radial depth of cut [mm]
 c - Feed per tooth [mm/rev]
 V_c - Cutting speed [m/min]
 n - Spindle speed [rpm]

Tool geometry –

D - Tool Diameter [mm]
 N - Number of cutting flutes
 β - Helix angle [rad]
 α - Rake angle [rad]

Cutting coefficients –

K_{te} - Tangential edge constant [N/mm]
 τ_s - Average shear flow stress [MPa]
 ϕ_n - Shear angle [rad]
 β_a - Average friction angle [rad]

Integration numbers –

K - Number of angular integration steps
 L - Number of axial integration steps

Outputs:

T_c - Cutting torque [N · mm]
 P - Cutting power [W]
 P_{avg} - Average cutting power [W]

Assumptions:

Chip flow angle (η) = Oblique angle (i) = Helix angle (β)

Code:

[Module 1 – Inputs and initializations]

Input all the required values.

Calculate the cutter pitch angle (ϕ_p): $\phi_p = \frac{2\pi}{N}$

Calculate the normal friction angle (β_n): $\beta_n = \tan \beta_a \cos \eta$

Calculate the cutting coefficients (K_{tc} , K_{rc} , K_{ac}) using:

$$K_{tc} = \frac{\tau_s}{\sin \phi_n} \frac{\cos(\beta_n - \alpha) + \tan i \tan \eta \sin \beta_n}{\sqrt{\cos^2(\phi_n + \beta_n - \alpha) + \tan^2 \eta \sin^2 \beta_n}} \quad (4.7)$$

Calculate the integration angle ($\Delta\phi$) and integration depth (Δa): $\Delta\phi = \frac{2\pi}{K}$ $\Delta a = \frac{a_p}{L}$

Assign the entry and exit immersion angles (ϕ_{st} , ϕ_{ex}):

If End milling type equals ‘Up’

Assign zero to ϕ_{st} and $\pi - \cos^{-1}\left(\frac{2a_e}{D} - 1\right)$ to ϕ_{ex}

Else if End milling type equals ‘Down’

Assign $\cos^{-1}\left(\frac{2a_e}{D} - 1\right)$ to ϕ_{st} and π to ϕ_{ex}

Else if End milling type equals ‘Slot’

Assign zero to ϕ_{st} and π to ϕ_{ex}

End if block

[Module 2 – Integration Loops]

Initialize the tangential force register (F_t) to zeros.

Calculate the forces for every integration step:

Loop 1: Loop from j equals 1 till j equals K (Angular Integration Loop)

Start of loop 1

Initialize the tangential differential force register (dF_t) to zeros.

Calculate immersion angle of flute’s bottom edge (ϕ): $\phi = \text{mod}\left(\frac{(j-1)\Delta\phi}{2\pi}\right)$

Loop 2: Loop from k equals 1 till j equals N (Contribution of all the Flutes Loop)

Start of loop 2

Calculate immersion angle of tooth k (ϕ_l): $\phi_l = \text{mod}\left(\frac{\phi + (k-1)\phi_p}{2\pi}\right)$

Loop 3: Loop from l equals 1 till l equals L (Axial Integration Loop)

Start of Loop 3

Calculate axial position (a): $a = l\Delta a$

Calculate updates immersion angle with helix lag angle (ϕ_2):

$$\phi_2 = \phi_l - \frac{2a}{D} \tan \beta$$

Check if the edge at the immersion angle is engaged in cutting:

If $\phi_{st} \leq \phi_2 \leq \phi_{ex}$

Calculate instantaneous chip thickness at that point (h): $h = c \sin \phi_2$
 Calculate differential forces using Equation (4.1):

$$dF_t = \Delta a(K_{tc}h + K_{te})$$

End Loop 3

End Loop 2

Sum the differential forces and save in the force registers:

$$F_t(j) = F_t(j) + dF_t$$

End Loop 1

Calculate the final output values (T_c , P for each j, and P_{avg}):

$$T_c = \left(\frac{D}{2} \right) F_t$$

$$P = \frac{\pi n T_c}{30000}$$

$$P_{avg} = mean(P)$$

4.1.2 Milling Tangential Force Calculation Algorithm:

A simplified version of the above discussed simulation model is developed as a part of the prediction model. In this version, only the slot milling experiment determined K_{tc} and K_{te} are the cutting coefficients inputs. Orthogonal cutting experiments are not required.

Pseudocode:

Inputs:

Cutting conditions –

End milling type - Up/Down/Slot
 a_n - axial cut depth [mm]
 a_e - radial cut depth [mm]
 c - Feed per tooth [mm/rev]
 V_c - Cutting speed [m/min]
 n - Spindle speed [rpm]

Tool geometry –

D - Tool Diameter [mm]
 N - Number of cutting flutes
 β - Helix angle [rad]

Cutting coefficients –

K_{te} - Tangential edge constant [N/mm]
 K_{tc} - Tangential cutting coefficient [N/mm²]

Cutting positions –

K - Number of angular integration steps
 L - Number of axial integration steps

Outputs:

T_c - Cutting torque [N·mm]
 P - Cutting power [kW]
 P_{avg} - Average cutting power [kW]

Assumptions:

$$\text{Chip flow angle } (\eta) = \text{Oblique angle } (i) = \text{Helix angle } (\beta)$$

Code:

[Module 1 – Inputs and initializations]

Input all the required values.

$$\text{Calculate the cutter pitch angle } (\phi_p): \phi_p = \frac{2\pi}{N}$$

$$\text{Calculate the normal friction angle } (\beta_n): \beta_n = \tan \beta_a \cos \eta$$

$$\text{Calculate the integration angle } (\Delta\phi) \text{ and integration depth } (\Delta a): \Delta\phi = \frac{2\pi}{K} \quad \Delta a = \frac{a_p}{L}$$

Assign the entry and exit immersion angles (ϕ_{st}, ϕ_{ex}):

If End milling type equals ‘Up’

$$\text{Assign zero to } \phi_{st} \text{ and } \pi - \cos^{-1}\left(\frac{2a_e}{D} - 1\right) \text{ to } \phi_{ex}$$

Else if End milling type equals ‘Down’

$$\text{Assign } \cos^{-1}\left(\frac{2a_e}{D} - 1\right) \text{ to } \phi_{st} \text{ and } \pi \text{ to } \phi_{ex}$$

Else if End milling type equals ‘Slot’

$$\text{Assign zero to } \phi_{st} \text{ and } \pi \text{ to } \phi_{ex}$$

End if block

[Module 2 – Integration Loops]

This module is the same as Module 2 in the previous algorithm.

4.2 Spindle Air-cutting Power Calculation

The spindle consumes significant power while spinning in the air without cutting the workpiece. Identifying and including this consumption in the power prediction model is essential. The approach to do this is by recording the power consumption by the spindle while air-cutting at different spindle speeds. The recorded power values are plotted against the varying spindle speeds. A relation between the two values can be obtained by doing linear interpolation. The spindle power consumption for any spindle speed can be estimated by using this method.

4.3 Cutting Power Prediction

Spindle power is the key contributor to total power consumption during machining. This study explores two methods for predicting the energy the spindle utilizes, each founded on the mechanistic modeling of cutting forces during milling operations. The milling force simulation algorithm in Section 4.1.1 (hereinafter referred to as Algorithm 1) is employed to validate and compare these methodologies before choosing the most appropriate framework proposed in this thesis. The angular and axial integration numbers are 360 and 50 for all the following simulations.

The first approach uses mechanistic modeling to predict power and torque under various tool-workpiece engagement conditions. This model requires spindle-specific tangential cutting coefficients that are determined by slot-milling tests. These identified coefficients are derived from sampled spindle drive data signals. Nevertheless, due to system dynamics and the sampling capabilities of the servo drive, transmission losses are present, which impact the accurate

transmission of dynamic torque changes at the cutting region to the spindle drive. Therefore, this approximation is solely used to represent spindle power consumption, and the actual cutting torque values at the cutting region may vary.

In the second approach, a direct correlation between power and the Material Removal Rate (MRR) is sought by collecting data under a range of cutting conditions.

4.3.1 Approach 1

The primary concept of this approach is to use the convenience of full-immersion milling experiments for identifying cutting coefficients [29]. These coefficients are utilized to model the average tangential force on the cutting tool, from which the cutting power is then calculated.

From Equation (4.1), it is known that for each oblique cutting segment

$$dF_{t0} = [K_{tc}h(\phi) + K_{te}]dz \quad (4.8)$$

Multiply $d\phi$ to both sides of Equation (4.8), and substitute $h(\phi) = c \cdot \sin\phi$ to the equation. We have

$$dF_{t0}d\phi = (K_{tc}c \sin\phi + K_{te})dzd\phi \quad (4.9)$$

For slot milling with an axial depth of cut a_p ,

$$\int_0^\pi \int_0^{a_p} F_{t0} d\phi dz = \int_0^\pi \int_0^{a_p} (K_{tc}c \sin\phi + K_{te}) dz d\phi \quad (4.10)$$

Here we have for an engaged cutting edge, the average tangential cutting force per tooth period F_{t0}

$$\pi F_{t0} = a_p (-K_{tc}c \cos\phi + K_{te}\phi) \Big|_0^\pi \quad (4.11)$$

$$F_{t0} = \frac{2a_p K_{tc}}{\pi} c + a_p K_{te} \quad (4.12)$$

The average number of engaged cutting edges is

$$m = \frac{\phi_{ex} - \phi_{st}}{\phi_p} \quad (4.13)$$

For full-immersion milling

$$m = \frac{\pi}{2\pi/N} = \frac{N}{2} \quad (4.14)$$

Therefore, we have the average tangential force:

$$\bar{F}_t = m F_{t0} \quad (4.15)$$

Substitute F_{t0} and m to the equation, the relation between the average tangential force \bar{F}_t and the cutting coefficients are simplified as follows:

$$\bar{F}_t = \frac{Na_p}{\pi} K_{tc} c + \frac{Na_p}{2} K_{te} \quad (4.16)$$

In a simplified case, the average tangential cutting force \bar{F}_t can be evaluated from the measured spindle power with Equation (4.17).

$$\bar{F}_t^{(sp)} = \frac{P_{cutting}}{V_c} = \frac{P_{sp} - P_{sp\ air}}{V_c} \quad (4.17)$$

where P_{sp} is the active power of the spindle while cutting, and $P_{sp\ air}$ is the active power while air-cutting with the same spindle rotational speed. Therefore, $K_{tc}^{(sp)}$ and $K_{te}^{(sp)}$ can be estimated by linear regression of the data with Equation (4.16). In order to make the linear regression independent to a_p and N for a simpler experimental approach, Equation (4.18) is derived from Equation (4.16).

$$\frac{\bar{F}_t^{(sp)}}{Na_p} = \frac{K_{tc}^{(sp)}}{\pi} c + \frac{K_{te}^{(sp)}}{2} \quad (4.18)$$

The problem is simplified to experimentally finding the coefficients in the linear function:

$$F = F_c c + F_e \quad (4.19)$$

where,

$$F = \frac{\bar{F}_t^{(sp)}}{Na_p}, F_c = \frac{K_{tc}^{(sp)}}{\pi}, F_e = \frac{K_{te}^{(sp)}}{2} \quad (4.20)$$

$$K_{tc}^{(sp)} = \pi F_c, K_{te}^{(sp)} = 2F_e \quad (4.21)$$

Once $K_{tc}^{(sp)}$ and $K_{te}^{(sp)}$ are identified, they are used in the simulation model in Section 4.1.2 (hereinafter referred to as Algorithm 2) for predicting tangential cutting force and cutting power in other cutting conditions.

Note that the superscript '(sp)' is used in this section to distinguish that the force components are deducted from the spindle signals. It does not represent the exact tangential cutting force due to system behavior limitations (structural dynamics, control system sampling limitations, etc.)

To simplify the notation, the superscript '(sp)' is omitted from $\bar{F}_t^{(sp)}$, $K_{tc}^{(sp)}$, and $K_{te}^{(sp)}$ in the following paragraphs.

To further explain the system and the approach, slot milling simulations are first conducted with Algorithm 1 for the following four end mills with $a_p = 3$ mm. Note that only one geometry parameter varies from Tool A to Tool B, C, and D. An extra simulation is performed for Tool A with $a_p = 5$ mm.

Table 4 Tool Geometry Parameters for Simulation

Tool Code	D (mm)	N	β	α
A	10	3	30°	9°
B	10	4	30°	9°
C	10	3	45°	9°
D	10	3	30°	12°

The cutting coefficient inputs are approximated using orthogonal to oblique transformation (coefficients derived from orthogonal cutting tests). The coefficients K_{te} , τ_s , ϕ_n , and β_a are V_c , α , and chip load \bar{h} dependent. \bar{h} can be calculated with Equation (4.22) [29]. It is also noteworthy that the simulations are not using the slot milling test-based method, suggesting that the goal here is to explain the suggested approach via simulation data rather than directly demonstrating its application. This approach offers an opportunity to understand the basic principles and impacts of different parameters on cutting forces and energy consumption before applying the proposed method in real-world scenarios.

$$\bar{h} = \frac{c(\cos \phi_{st} - \cos \phi_{ex})}{\phi_{ex} - \phi_{st}} \quad (4.22)$$

Figure 5 to Figure 8 present the simulation results of F_t , $P_{cutting}$, and $F_t/(N \cdot a_p)$ from Algorithm 1. It can be seen that F_t increases linearly with V_c for the same c value. The offsets between the lines for different V_c are independent to c . $P_{cutting}$ is the product of F_t and V_c (Equation (4.17)), therefore, varies with these two variables. However, it is important to remember that these trends and relationships may not be universally applicable. They are specific to the low alloy steel SS2541 material that was modeled in this case.

Now consider the four tool geometry parameters D , N , β , and α . From Equation (4.16), we know that F_t changes proportionally with N (Figure 5) and a_p (Figure 8). F_t increases when β gains (Figure 6). When α increases, F_t decreases (Figure 7). F_t , and therefore $P_{cutting}$ and $F_t/(N \cdot a_p)$, are all independent of D (not presented with a figure). When $F_t/(N \cdot a_p)$ is taken as the variable for obtaining the cutting coefficient inputs of Algorithm 2, $F_t/(N \cdot a_p)$ is only dependent on β and α . The end mills with the same β and α share the same model line regardless of the chosen a_p in slot milling experiments.

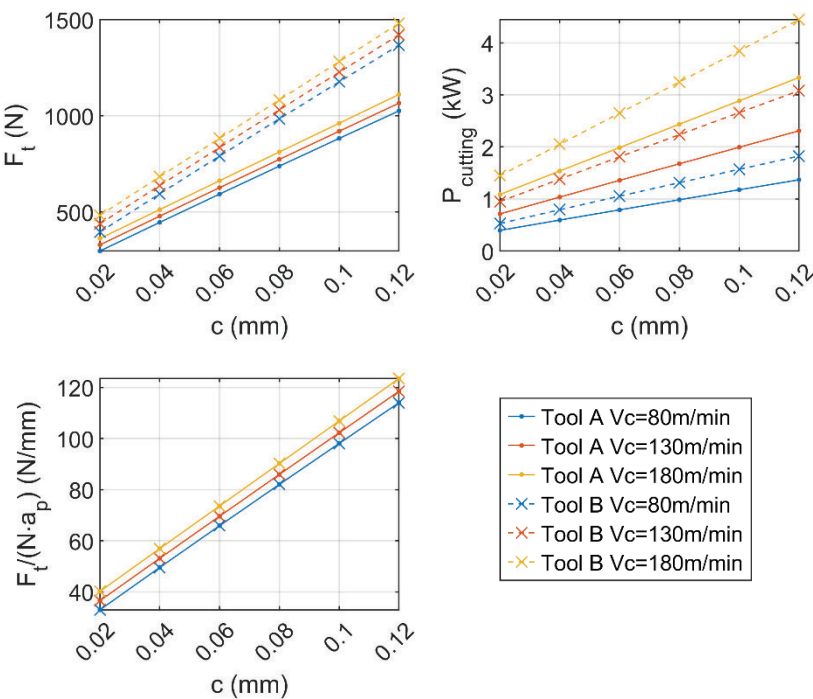


Figure 5 Algorithm 1 Simulation Comparison – Tool A and B

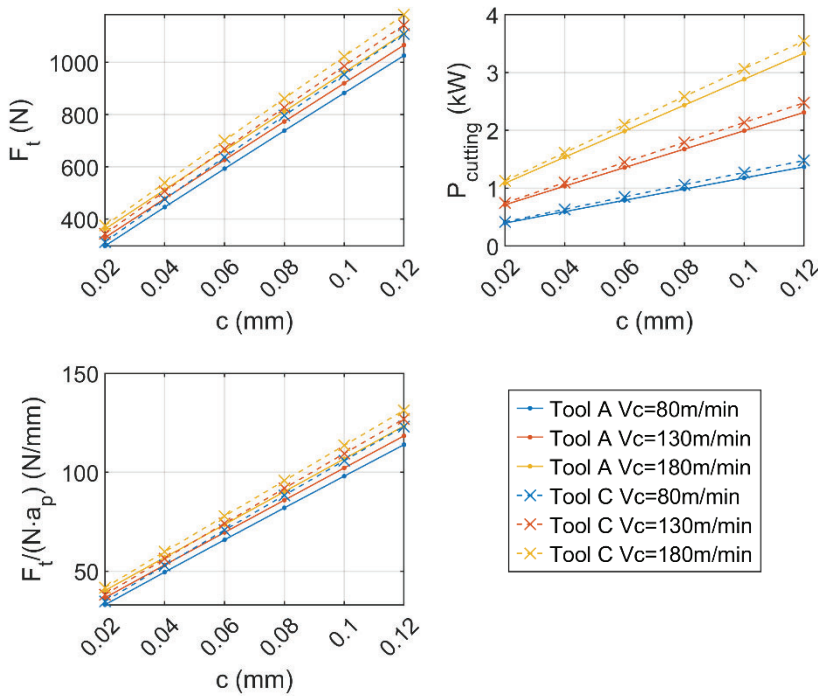


Figure 6 Algorithm 1 Simulation Comparison – Tool A and C

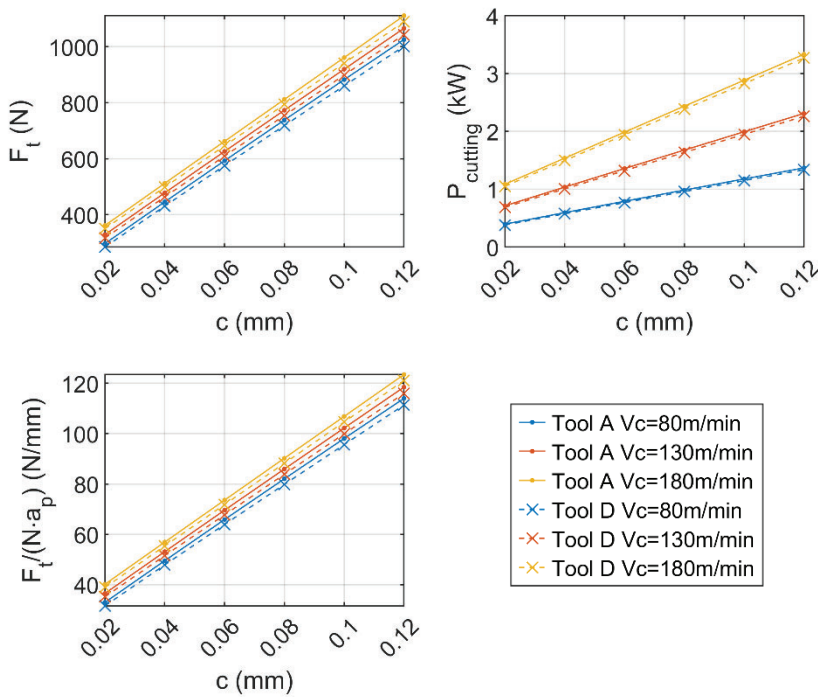


Figure 7 Algorithm 1 Simulation Comparison – Tool A and D

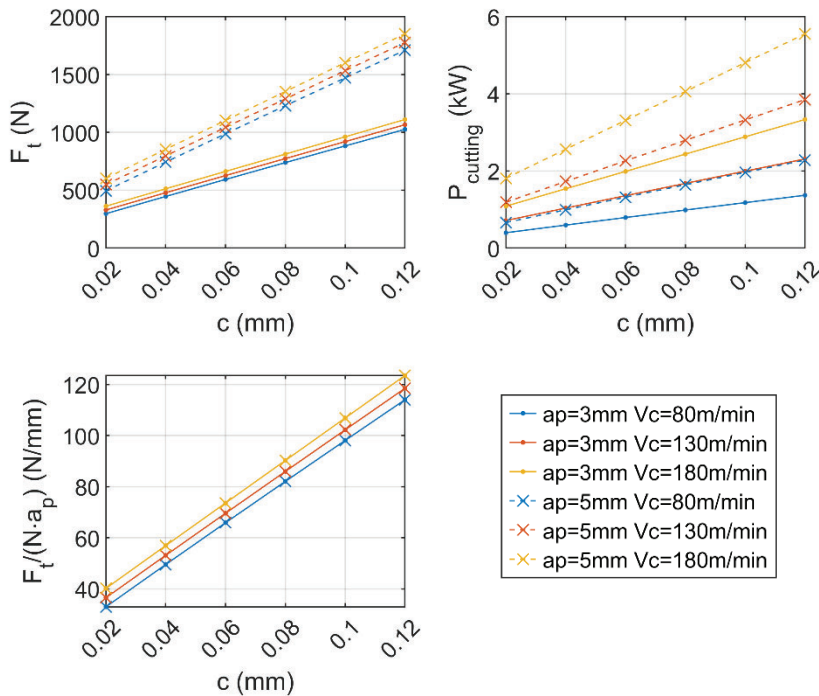


Figure 8 Algorithm 1 Simulation Comparison – Tool A $a_p = 3 \text{ mm}$ and $a_p = 5 \text{ mm}$

Theoretically, the constant offsets in $F_t/(N \cdot a_p)$ lines caused by the variation of V_c can be modeled with a correction factor. However, these offsets are small. They might be covered by the error and noise in the experimental measurement. In order to understand the effect of error and noise on Algorithm 2, a synthetic experiment is performed by adding artificial noise to the simulation result of Algorithm 1.

The random-generated noise follows a Gaussian distribution with zero mean and a standard deviation of 2.5 % of the mean value of all the $P_{cutting}$ in the synthetic experiments generated by Algorithm 1. This means that, statistically, 95 % of the random-generated points fall in a band centered at $P_{cutting}$ and with a width of 10 % of the average value of all the generated $P_{cutting}$ values. The bias between the data points with and without noise are illustrated in Figure 9. The P values with noise simulate the power values obtained in real slot milling experiments.

The corresponding $F_t/(N \cdot a_p)$ values are calculated from $P_{cutting}$ with noise, and linear regression models are built between $F_t/(N \cdot a_p)$ and c (Figure 10). With the noise present, the linear regression models intersect each other and do not reflect the constant offsets caused by V_c as in Figure 5. Using the K_{tc} and K_{te} calculated for every V_c does not provide a significantly more accurate $P_{cutting}$ prediction (maximum relative error 6.5 %, average relative error 0.4 %) than using the K_{tc} and K_{te} for $V_c = 130 \text{ m/min}$ for all V_c values (maximum relative error 6.1 %, average relative error 0.6 %, Figure 11).

Based on this result, it was decided to perform the real slot milling experiments with several different V_c for analysis but taking all $P_{cutting}^{(Expt.)}$ data points for different V_c together for linear regression. The linear regression models, therefore, omit the difference in V_c .

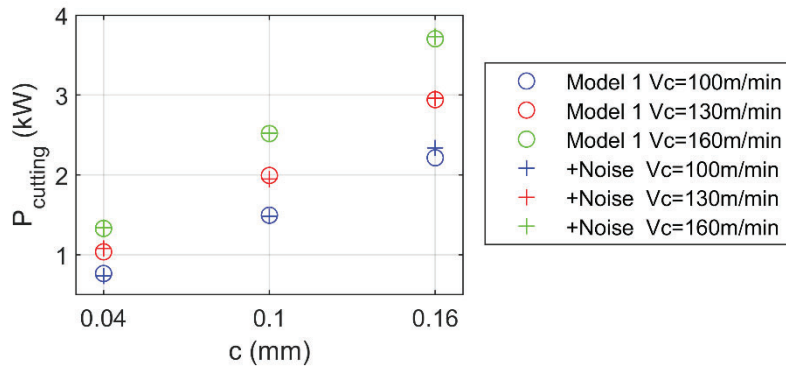


Figure 9 Synthetic Experiments

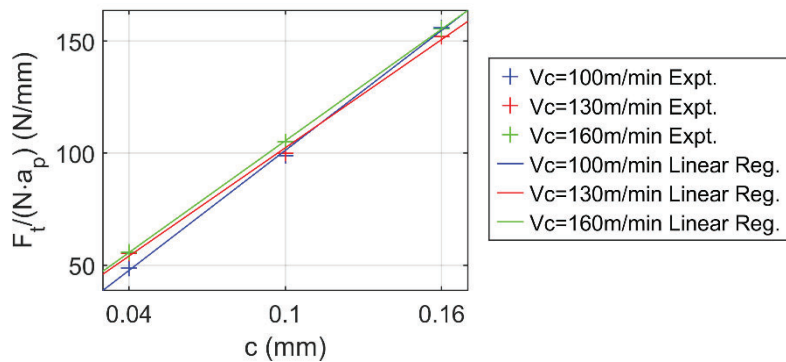


Figure 10 Linear Regression for the Synthetic Experiments

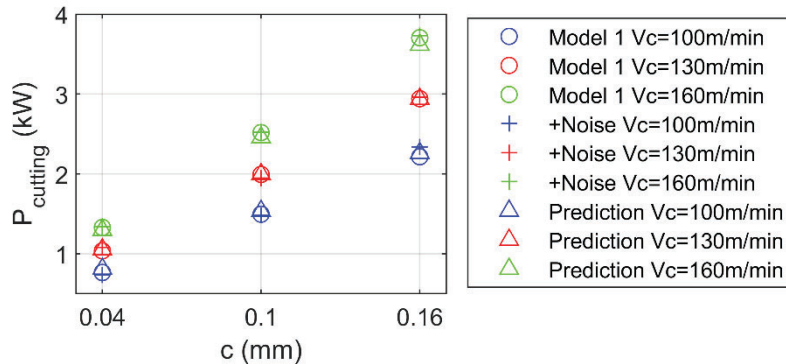


Figure 11 Cutting Power Prediction for the Synthetic Experiments

It is to be noted that the estimation is specific to the machine used to perform the experiments. However, to predict the power consumption for milling operations to be performed in the same machine, this approach is adequate.

4.3.2 Approach 2

The core concept of this approach is to determine a relationship between power consumption and cutting parameters through a function. Material Removal Rate (MRR) is selected for this purpose as it can be expressed as a function of the cutting parameters.

$$MRR = \frac{a_e a_p c V_c N}{\pi D} \quad (4.23)$$

where a_e is the Radial Depth of Cut, a_p is the Axial Depth of Cut, c is the Feed per Tooth, V_c is the Cutting Speed, N is the Number of Cutting Tooth, and D is the Diameter of the Cutting Tool.

Material Removal Rate (MRR) is the material volume removed per unit time by machining. It can be expressed in several ways, and the simplest will be the product of cutting speed and the area of the chip section.

$$MRR = A_{chip} V_c \quad (4.24)$$

where A_{chip} is the Area of the Chip section.

The area of the chip section can be calculated as the product of chip thickness (h) and the axial depth of cut (a_p).

$$A_{chip} = h \quad (4.25)$$

The cutting forces are related to the chip thickness [51], and because of that, the MRR relates to the power consumed in the cutting process. MRR can be a function of different cutting parameters. Hence, forming an association between MRR and the power consumed can give the power consumption an indirect relation to the cutting parameters. This is the planned approach to predict power consumption by knowing the cutting parameters. The MRR used, in this case, must be expressed as a function of as many cutting parameters as possible to relate the power consumption strongly to the parameters.

Experiment:

In this method: The experiment can be planned by cutting with different MRRs. The MRR is changed by keeping the cutting speed (V_c^1) constant and modifying the other parameters (i.e., a_p , c , a_e). The experiments can thus be repeated for five more cutting speeds (V_c^2 , V_c^3 , ..., V_c^6). The machine's trace function can monitor the spindle's power consumption during cutting. A trace variable specific to the spindle drive motors can be selected. The power consumed can be plotted against the changing MRR for the six different V_c values by analyzing the collected data. It can be observed that there is a linear relationship between power and MRR, and the three plots have varying slopes. The first observation indicates a linear relationship between power consumed and MRR, while the second observation suggests that the variable slope (K), can be expressed as a function of V_c . Hence the resulting linear expression will be as the following:

$$P_{avg} = K \cdot MRR + b \quad (4.26)$$

where P_{avg} is the average power consumption by the spindle, and b is the Y-intercept of the plot.

The intercept is minimal and can be disregarded. Thus, power will be equivalent to the product of the slope and MRR. Further, plotting the slopes against cutting speeds makes a linear relationship between them evident. Presuming linearity, the slope can be expressed as a function of cutting speed.

$$K = AV_c + B \quad (4.27)$$

where A and B are the plot's slope and Y-intercept, respectively.

By solving the above equation, the values of A and B can be found, and hence get an expression for K as a function of V_c . This expression can be substituted in the power and MRR relation in Equation (4.26). The expression will now be an empirical model where power consumed is expressed in terms of cutting parameters like cutting speed, axial and radial cutting depths, and feed per tooth.

This empirical model can predict the power consumed by just having the values of the cutting parameters. The empirical model is expressed as:

$$P_{avg} = (AV_c + B)MRR \quad (4.28)$$

where A and B are the slope and Y-intercept of the plot (K vs V_c).

This approach enables the linking of power consumption to the cutting parameters and may be suitable for this case, as cutting parameters are available during the process planning stage. The approach is validated using the simulation model before application. Once the model is created using data from the planned experiments, the power consumed is calculated using the suggested model.

Table 5 Experimental Parameters and Values for Creating the Empirical Model

Parameters	Values
Cutting Speed (V_c)	150 to 200 (step of 10) m/min
Feed per tooth (c)	0.05 to 0.2 (step of 0.01) mm
Axial depth of Cut (ap)	0.5 to 4 (step of 0.2) mm
Radial depth of Cut (ae)	0.5 to 4 (step of 0.2) mm

The power consumed under these conditions can be calculated by varying other parameters for the different cutting speeds (Table 5).

The resulting average power values are plotted against the varying MRR. Figure 12 illustrates that the slope consistently increases with ascending cutting speeds, with almost zero y-intercepts observed in all cases.

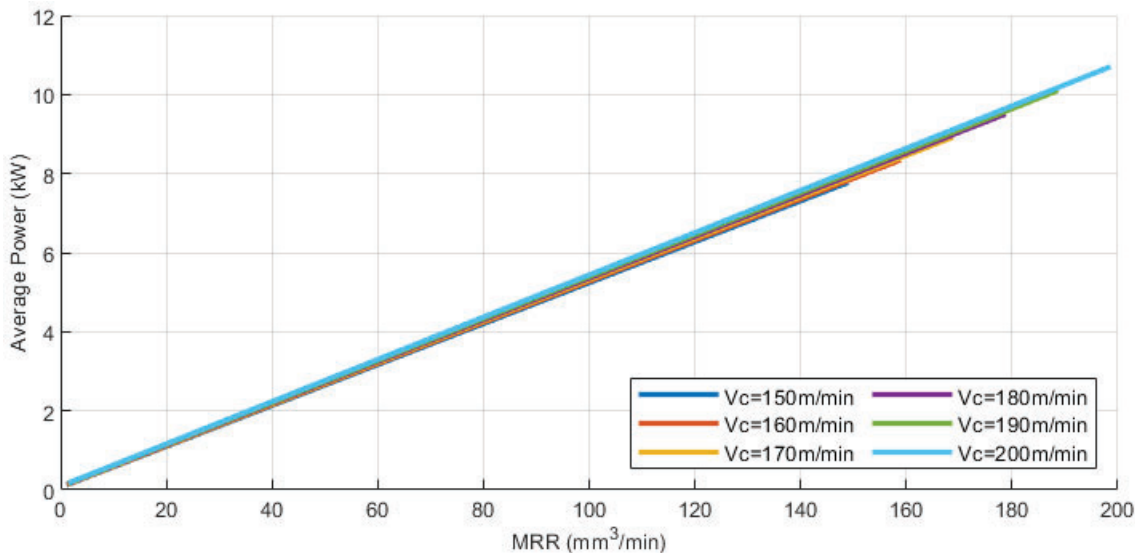


Figure 12 Average Power vs MRR for Different Cutting Speeds (Varying Axial and Radial Depths of Cut, and Feed per Tooth Values)

The slopes are identified and are plotted against the changing cutting speeds. It is assumed that there is a linear relationship between them. The empirical model is thus created using these simulated values in Equation (4.29).

$$P_{avg} = (3.403 \times 10^{-5} V_c + 0.048)MRR \quad (4.29)$$

The empirical model thus formulated is used to predict power consumption for a set of cutting conditions (Table 6). The simulation model generates power consumption values for the same set of cutting conditions. The power values from both models are compared to validate the empirical model (Figure 39 in Appendix A). It can be observed that the absolute error is relatively high. When

compared to the first approach, the error in this approach is higher, showing that the second approach is less reliable.

Table 6 Cutting Conditions for Validating the Approach

Parameters	Values
Cutting Speed (Vc)	150 m/min
Feed per tooth (c)	0.1 to 0.2 (step of 0.01) mm/rev
Axial depth of Cut (ap)	2 to 4 (step of 0.5) mm
Radial depth of Cut (ae)	0.5 to 4 (step of 0.2) mm

This unreliability can be linked to a couple of factors. Firstly, the error in the power prediction is very inconsistent (Figure 4o in Appendix A). It changes significantly with the changing parameter values. Finding the correct combinations of parameters to create the empirical model is complex. Secondly, more data points are required to make the model more accurate, which requires more experiments to be performed to build the model. Hence, the first approach is chosen over the second.

4.4 Axis Power Prediction

The spindle is the primary contributor to power consumption and is not the only factor to consider during milling operations. The power consumption of axis motors also must be accounted for. This consumption arises from the torque exerted on the motors by the forces of inertia, friction, and cutting loads. The total torque on the motor τ_m can be expressed as [52]:

$$\tau_m = K_t i_{act} = J_e \frac{d\omega}{dt} + B_e \omega + \tau_f + \tau_c \quad (4.30)$$

where K_t is the motor constant, and i_{act} is the actual current value; τ_f and τ_c are the coulomb friction and cutting torque respectively; ω is the angular velocity of the rotating shaft (in rad/s); J_e is the equivalent inertia and B_e is the equivalent viscous friction coefficient delivered on the motor. The cutting force acts as a disturbance torque to x and y servo drive system, therefore τ_c term corresponds to the disturbance torque in servo feed drive systems [53].

Equation (4.30) helps to develop an expression for the axis power P_{axis} which includes two components - power due to friction $P_{friction}$ and power due to cutting disturbance P_d (Equation (4.31)). The inertia term $J_e d\omega/dt$ is zero while the rotational speed reaches a stable plateau, i.e., the axis motor is running in a stable phase but not in a transitional phase. P_d is considered to be a minor fraction with respect to $P_{friction}$, hence not modeled.

$$P_{axis} = P_{friction} + P_d \quad (4.31)$$

$P_{friction}$ includes the power consumed as an effect of motor torque's viscous and friction components in Equation (4.30). The viscous and the friction components are together termed as the friction torque $\tau_{friction}$ (Equation (4.32)).

$$\tau_{friction} = B_e \omega + f_c L \quad (4.32)$$

where L is the load causing the coulomb friction and f_c is the coulomb friction coefficient.

Multiplying the friction torque with the angular velocity of the rotating shaft ω gives $P_{friction}$ (Equation (4.33)).

$$P_{friction} = \omega \tau_{friction} \quad (4.33)$$

Substituting Equation (4.32) in Equation (4.33) gives:

$$P_{friction} = B_e \omega^2 + f_c L \omega \quad (4.34)$$

The conversion between the rotational speed ω and the feed rate V_f is:

$$\omega = \left(\frac{2\pi}{lead} \right) V_f \quad (4.35)$$

where *lead* is the linear distance traveled for each complete rotation of the ball screw.

Substituting Equation (4.35) in Equation (4.34) gives an expression for $P_{friction}$:

$$P_{friction} = k_v V_f^2 + k_c V_f \quad (4.36)$$

where $k_v = \left(\frac{4\pi^2}{lead^2} \right) B_e$ and $k_c = \left(\frac{2\pi}{lead} \right) f_c L$.

The k_v and k_c terms represent the viscous and Coulomb friction components, and k_v and k_c can be estimated by quadratic regression between experimental recorded $P_{friction}$ and V_f .

A set of air-cutting experiments are planned to record the power consumption for different feed rates. Air-cutting is done so that there is no cutting load and the friction component due to cutting is eliminated. In the experiments, the feed drive motors are used to move the worktable diagonally. A diagonal path is chosen to work both the x and y axis motors simultaneously. The table is moved along the path in 3 different feed rates ($V_f = 300, 1000$, and 3000 mm/min). The recorded power values are plotted against the changing feed rates. The coefficients in Equation (4.36) are determined by quadratic regression. The quadratic term $k_v V_f^2$ is found minimal and negligible. Therefore, a linear relationship is assumed between V_f and $P_{friction}$, as in Equation (4.37).

$$P_{friction} = k_c V_f + b \quad (4.37)$$

where b is the constant term in the linear regression.

Equation (4.37) is used to predict the axis power consumption once the coefficient k_c and the constant term b are determined by experimental data.

4.5 Idle Power Calculation

The idle state of a machine refers to the period when no productive tasks (such as cutting the workpiece) are occurring [15]. During this time, the machine still consumes electricity to operate peripheral equipment. For instance, the coolant system might consume power to keep the coolant's temperature within a specified range. The drives are active and ready, hence consuming low power. The power consumed by the machine in this state is referred to as idle power, and it is crucial to calculate and include this in the prediction model.

During the experiments, the recording of power values commenced before the start of the cutting process. These power values represent the machine's consumption in its idle state. Average idle power consumption can be determined by taking the average of these values.

4.6 Summary of the Modelling Approach

A custom-built, manufacturing process-focused approach is utilized to determine the environmental impact of milling processes. This approach begins by defining a system boundary, where we distinguish between processes that contribute and those that do not contribute to the milling part of a product's production process.

Two contributors identified within the system boundary are electricity consumption and the consumption of cutting tools during milling. Their indirect GHG emissions contribute notably to environmental impact.

Following this identification, a functional unit is established to evaluate and compare electricity consumption and environmental impact. For this study, the functional unit is defined as rough milling at a determined Material Removal Rate (MRR) to remove a unit volume of material. This functional unit allows the comparison of milling processes with different combinations of cutting parameters.

The next step involves creating a model to predict the electricity consumption of the milling process based solely on the cutting parameters and conditions. It is aimed to develop a detailed power prediction model inspired by the mechanistic model of milling operations. Experimental data obtained from cutting experiments are required to establish this model, as outlined in Section 4.7. These experiments aid in estimating the cutting coefficients for the prediction model.

Given the cutting parameters and conditions, the developed model can predict the electricity consumption for milling processes. The output is the power consumption of the process (in Watts), which is converted to electrical energy consumption (in Watt-hours) using the process time.

Identifying the source of electrical energy used for the process is crucial, as it significantly influences the evaluation of environmental impact. Once the energy source is identified, carbon emission intensities for those sources are collected.

The final step of the developed approach is calculating the impact using these intensity data and the energy consumption values derived from the prediction model. This step also includes calculating the impact of cutting tool consumption during the process. This calculation is done by gathering information on the emissions associated with tool production, estimating the weight of cutting tools consumed, and knowing the estimated tool life for the process.

Thus, using the developed approach, the environmental impact of milling processes can comprehensively be assessed, focusing on electricity, and cutting tool consumption.

4.7 Experimental Procedures

Planning for the cutting operations involves measuring the power consumption during the process and deriving coefficients from this consumption. These coefficients are similar to the cutting coefficients and can substitute in the simulation model, thereby predicting power usage.

As discussed in Section 4.3.1, a full immersion cutting mechanistic model is employed to derive these coefficients. Using the chosen cutting tools, the slot-cutting operation will be performed on the selected material, SS2541. The tools include end mills with 8mm, 10mm, and 12mm diameters, as outlined in Table 7.

Table 7 List of Cutting Tools Used in the Experiments

#	Tool Diameter	Tool Type	Number of Cutting Edges	Helix Angle	Radial Rake Angle
1	8 mm	End Mill for Medium Roughing	4	45°	10.5°
2	10 mm	End Mill for Heavy Roughing	3	30°	9°
3	12 mm	End Mill for Heavy Roughing	3	30°	9°

4.7.1 Design of Tests

The development of the model depends on the planning and execution of the slot-cutting experiments. These experiments use three distinct cutting tools, each operated at three different cutting speeds. The experiments are further diversified by altering the cut direction for each cutting speed (Table 8), yielding three distinct experiments for every speed.

The cutting operations are carried out along the X and Y axis, with each experiment resulting in five evenly spaced slots, each cut at a different feed per tooth value (Figure 41 and Figure 42 in Appendix A). For operations conducted diagonally the feed per tooth values are adjusted to ensure that higher feed speeds correspond to longer cutting paths (demonstrated in Figure 43 in Appendix A). This strategy ensures sufficient data gathering during the cutting time.

Figure 13 provides a schematic representation of how the diagonal cuts are planned to guarantee longer cuts for higher feed speeds. However, the diagonal cutting experiment was divided and performed on two different surfaces when the cutting time was exceptionally short for high feed speeds (as was the case when using the 12 mm mill). This allowed for longer cutting paths for all feed speeds, thereby ensuring a consistent data collection process for the development of the model.

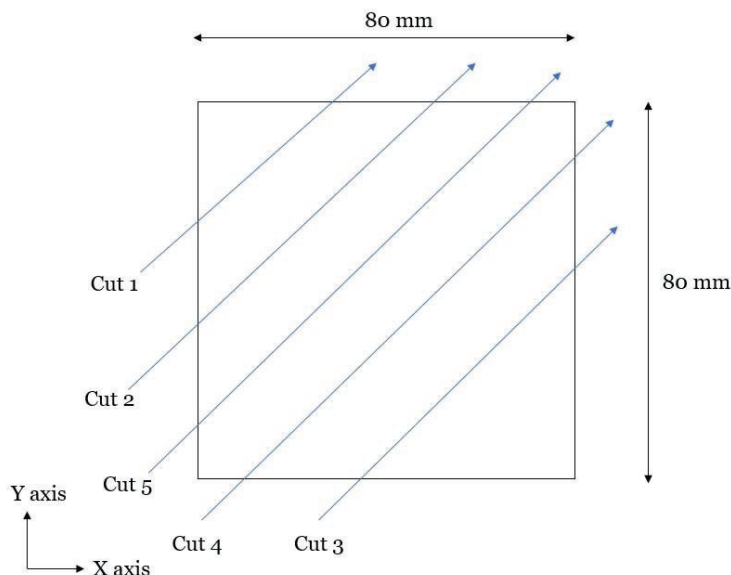


Figure 13 Schematic Representation of Diagonal Slot Cutting [Feed Speeds: Cut 1<Cut 2<Cut 3<Cut 4<Cut 5]

Table 8 Design of Experiments for Developing the Prediction Model

Tool	Cutting operation	Cutting Parameters		Direction of Cut
		Cutting Speed (V_c) [m/min]	Feed per Tooth (c) [mm/rev]	
8 mm	Slotting	130	0.03,0.04,0.05,0.06,0.07	Along Y Along X Diagonal
		150	0.03,0.04,0.05,0.06,0.07	Along Y Along X Diagonal
		170	0.03,0.04,0.05,0.06,0.07	Along Y Along X Diagonal
10 mm	Slotting	130	0.03,0.05,0.07,0.09,0.11	Along Y Along X Diagonal
		150	0.03,0.05,0.07,0.09,0.11	Along Y Along X Diagonal
		170	0.03,0.05,0.07,0.09,0.11	Along Y Along X Diagonal
12 mm	Slotting	130	0.03,0.05,0.07,0.09,0.11	Along Y Along X Diagonal
		150	0.03,0.05,0.07,0.09,0.11	Along Y Along X Diagonal
		170	0.03,0.05,0.07,0.09,0.11	Along Y Along X Diagonal
Other parameters: $a_p = 3$ mm				

To validate the model, three distinct cutting operations are executed using the three specified cutting tools, as outlined in Table 9. These operations include face milling, pocketing, and shoulder milling.

During the face milling operation, milling is carried out in a back-and-forth motion along the Y axis, as depicted in Figure 44 (Appendix A).

In the case of pocketing, a unique tool path is implemented, initiating from the center of the workpiece, and progressing outwards, as illustrated in Figure 45 (Appendix A). To facilitate the mill's penetration into the workpiece, a drill hole is created at the outset of the process.

Shoulder milling is performed along the X-axis in both directions, which results in both Up and Down milling. This operation is illustrated in Figure 46 (Appendix A). Shoulder milling involves varying the depth of cut, specifically implementing two different axial depths (a_p) and three different radial depths (a_e) for each axial depth.

Furthermore, within the scope of the same experiment, a slot is milled following the cutting parameters recommended in the tool catalog. This comprehensive set of operations ensures a broad and diverse dataset for validating the predictive model.

Table 9 Design of Experiments for Validating the Prediction Model

Tool	Cutting operation	Cutting Parameters			Direction of Cut
		Cutting Speed (V_c) [m/min]	Feed per Tooth (c) [mm/rev]	Depths of cut – axial (a_p) and radial (a_e) [mm]	
8 mm	Face mill	160	0.06	$a_p = 3$ mm	Along Y – Back and Forth
	Pocket (70mm×70 mm)	140	0.06	$a_p = 3$ mm	-
	Shoulder	155,135,120	0.056, 0.042, 0.0373	$a_p = 3, 1.5$ mm $a_e=2, 4, 6$ mm	Along X
	Slot	98.5	0.0208	$a_p = 3$ mm	Along X
10 mm	Face mill	160	0.06	$a_p = 3$ mm	Along Y – Back and Forth
	Pocket (70mm×70 mm)	140	0.06	$a_p = 3$ mm	-
	Shoulder	150,135,118	0.0726, 0.059, 0.052	$a_p = 5, 3$ mm $a_e=3, 5, 8$ mm	Along X
	Slot	103	0.059	$a_p = 3$ mm	Along X
12 mm	Face mill	160	0.06	$a_p = 3$ mm	Along Y – Back and Forth
	Pocket (70mm×70 mm)	140	0.06	$a_p = 3$ mm	-
	Shoulder	175,135,115	0.111, 0.0693, 0.0609	$a_p = 5, 3$ mm $a_e=2, 6, 10$ mm	Along X

4.7.2 Experimental Setup

Milling operations are conducted on AFM Defum R1000 Three Axis Vertical Milling Center, with a Siemens Sinumerik 828D CNC Controller. This milling center has the capability of moving 1000 mm along X axis, 510 mm along Y axis and 560 mm along Z axis. It has a maximum spindle speed of 8000 rpm, a spindle rated power of 9.7 kW and a maximum spindle torque of 75 Nm.

Steel blocks, of dimensions $80 \times 80 \times 40$ mm³, are used as blanks. A standard bench vise is employed to hold the blocks and parallels are utilized at the bottom to secure the blocks, providing a machinable depth of 28 mm from the top surface of the vise (Figure 14). The end mill tools are mounted on tool holders and loaded into the machine's magazine. All cutting experiments are conducted under dry-machining conditions without any coolant.

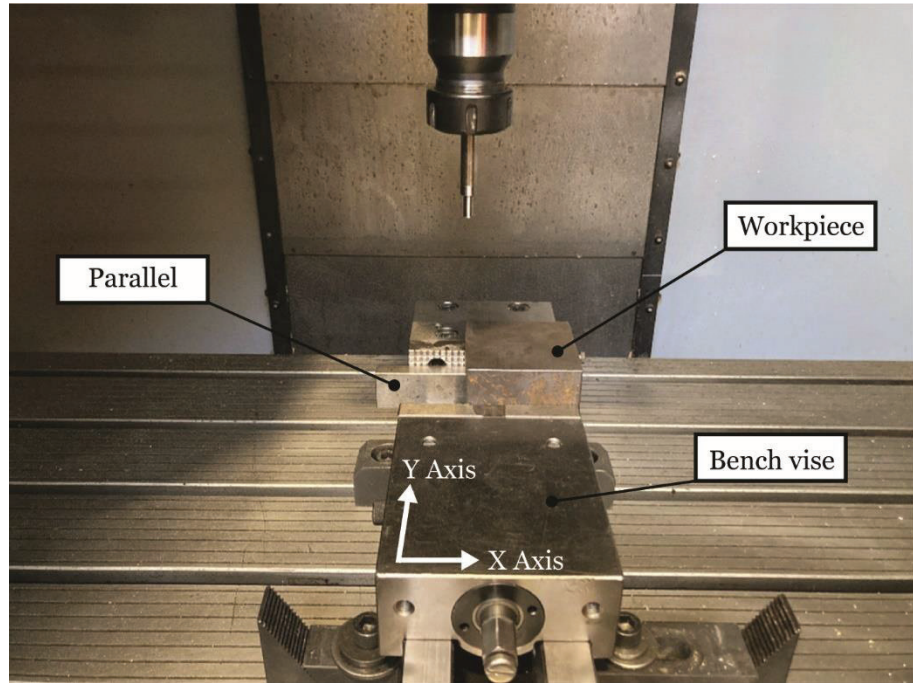


Figure 14 The Workpiece held on a Standard Bench Vise

To measure the power consumption of the entire machine during the experiments, a Yokogawa WT500 power analyzer is utilized. This device measures the active power of the three-phase three-wire system employing the two-wattmeter method with a sampling frequency of 1 Hz. The wiring diagram is shown in Figure 15. Measuring the total power consumption is vital to account for both idle and auxiliary power consumption. Idle consumption refers to the power used when the machine is ON but not processing, with only the drives active. Auxiliary consumption pertains to the machine's state between processes, during which other systems within the machine consume power [15].

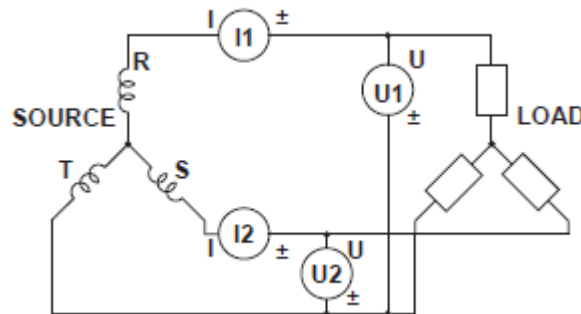


Figure 15 Power Analyzer Wiring Diagram [54]

The power analyzer is connected to the main three-phase lines supplying power to the machine. The power analyzer records the power consumption data and automatically exports the data to a '.csv' file format for further analysis. The accuracy of the measured power at 50 Hz is 0.1 % of reading + 0.1 % of measurement range [54]. The measurement ranges use in the experiments are 600 V and 40 A.

Along with capturing the overall power consumption of the entire machine, the power explicitly utilized by the machining process is also independently recorded. This is accomplished using the Trace function on the Siemens Sinumerik 828D CNC controller. The Trace function enables the real-

time capture of data directly from the drives during the machine operation, facilitating the simultaneous recording of the performance of the drive motors during the cutting experiments. The Trace function can also collect data from the Programmable Logic Controller (PLC) and other operational channels.

The performance of the drives, along with many other variables such as the position of the axes, spindle speed, feed rate of the axis, and the line number of the Numerical Control (NC) Code, can all be documented using the Trace function. A selection of variables relevant to the intended experiments are chosen for tracing (Table 10). These chosen variables will contribute to developing the prediction model. Detailed information of the Trace variables can be found in Appendix A Table 31.

The traced variables and their corresponding recorded data are stored in an '.xml' format in the controller. The active power data is sampled at a rate of 0.003 seconds. The detailed configuration can be found in Appendix A. This recorded data provides a deeper understanding of the machine's operational behavior, which contributes to creating a more accurate prediction model for power consumption.

Table 10 List of Trace Variables Chosen to be Recorded During the Experiments

#	Trace Variable Description	Units
1	Actual value of position, X axis	mm
2	Actual value of position, Y axis	mm
3	Actual value of position, Z axis	mm
4	Actual value of axis-specific feed rate, X axis	mm/min
5	Actual value of axis-specific feed rate, Y axis	mm/min
6	Actual value of axis-specific feed rate, Z axis	mm/min
7	Active power, X axis	Watt
8	Active power, Y axis	Watt
9	Active power, Z axis	Watt
10	Active power, Spindle	Watt
11	Torque-prod. Current act. Val., X axis	Ampere
12	Torque-prod. Current act. Val., Y axis	Ampere
13	Torque-prod. Current act. Val., Z axis	Ampere
14	Torque-prod. Current act. Val., Spindle	Ampere
15	Actual value of rotary speed, X axis	percent
16	Actual value of rotary speed, Y axis	percent
17	Actual value of rotary speed, Z axis	percent
18	Actual value of the interpolation feed rate	mm/min
19	Line number of current NC instruction	-
20	Spindle speed, actual value	rpm

4.8 Data Processing Approach

The data gathered from the experiments are processed using MATLAB. The power values obtained from the Trace function undergo previous neighbor interpolation to ensure continuity. A Butterworth filter of order 6 with a cut-off frequency of 10 Hz is applied to reduce noise and smooth out the signal. Following signal filtering, the distinct cutting sections from each experiment are identified and subjected to further processing. This step-by-step treatment of data aids in extracting more precise and useful information from the experimental data, enhancing the reliability of the subsequent analysis and model creation.

5. Results

46 cutting experiments, 11 spindle air-cutting experiments, and 14 table movement experiments were conducted and documented. The results were analyzed and are summarized in this chapter.

The first section of this chapter presents and discusses the prediction of active power and electricity consumption, which serves as one of the contributors to the indirect CO₂ emission in milling processes. This section is organized sequentially, the same as the four horizontal paths in Figure 4, covering spindle air-cutting power, cutting power, axis motor power, and idle power, followed by the validation results. Towards the end, an example of an application of the practical approach is provided.

The second section outlines the calculation of the environmental impact of milling processes, including the contributions from electricity, and cutting tools and the total impact.

Unless specified separately, the units of variables in this chapter are as follows:

- Length – millimeters (mm)
- Angle – radians (rad)
- Cutting speed – meters per minute (m/min)
- Feed rate – millimeters per minute (mm/min)
- Spindle speed – revolutions per minute (rpm)
- Power – Watts (W)
- Energy – Watt-hours (Wh)
- Material Removal Rate (MRR) – cubic centimeters per minute (cm³/min)
- Specific Energy Consumption (SEC) – Watt-hours per cubic centimeter (Wh/cm³)

Please note that all the power referred to in this chapter pertains to active power.

5.1 Power Prediction with Slot Cutting Experiments

The result is presented in the same order as the four horizontal paths in Figure 4. For the convenience of the readers, the components of the total power are again briefly described here.

$$\begin{aligned}
 P &= P_{process} + P_{idle} \\
 &= P_{sp} + P_x + P_y + P_{idle} \\
 &= P_{sp\ air} + P_{cutting} + P_x + P_y + P_{idle}
 \end{aligned} \tag{5.1}$$

5.1.1 Spindle Air-cutting Power

The machine tool employed in these experiments has an upper limit for spindle speed at 8000 rpm. The machine employs gears for varying speed levels. Spindle air-cutting experiments are conducted at 500 rpm intervals from 500 to 8000 rpm, calculating the average active power at steady spindle rotation for the three different end mills. The spindle active power signals are obtained from the Trace function.

Figure 16 illustrates the active power curves for the three cutting tools. The curves only show slight differences in the speed range below 4000 rpm. Between 4500 rpm and 7500 rpm, the active power slightly increases with the tool diameter. The maximum difference between the three cutting tools is found at 5000 rpm, with a 22.6 W (4.2 %) disparity between the 8 mm and 12 mm tools. The differences between the three curves diminish at 8000 rpm.

This study's experiments have spindle speeds from 3500 rpm to 7000 rpm. Given that the differences in spindle air-cutting power among different end mills are minimal, these power curves for the three tools can be simplified into a single curve by taking the average value. In the power prediction model, we obtain spindle air-cutting active power values through linear interpolation between the control points of the simplified curve depicted in Figure 17. The control points of this curve are listed in Table 11.

In practical applications of the proposed power prediction approach, creating a separate power curve for each tool would not be overly burdensome. However, for timesaving and operation simplification purposes, it is acceptable to use a single cutting tool for the test and its curve to represent other tools with little difference in rotational inertia.

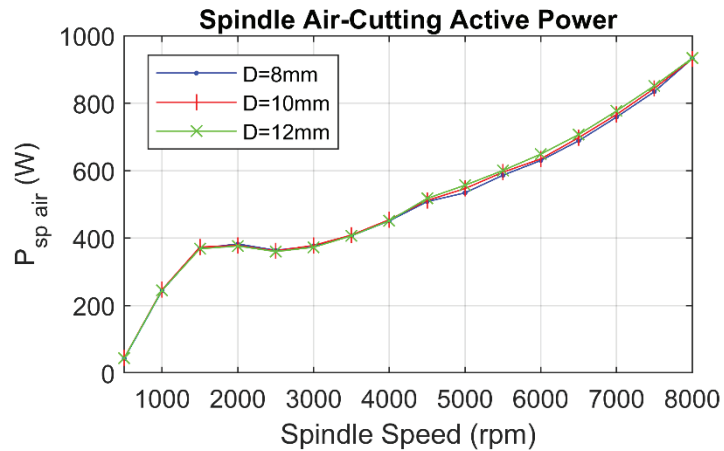


Figure 16 Spindle Air-Cutting Power Curve for the Three End Mills

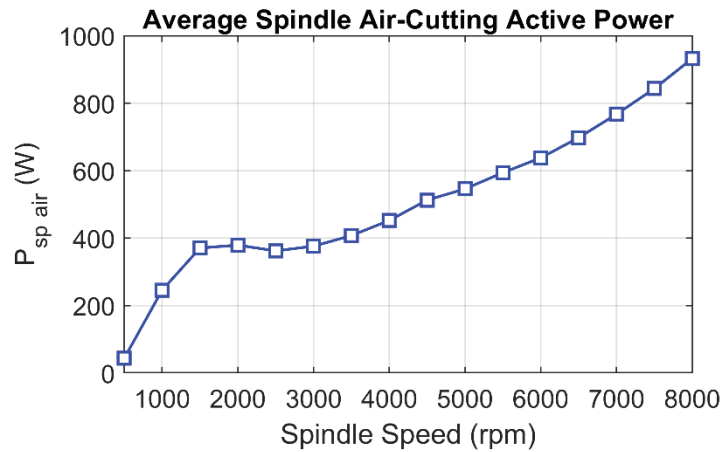


Figure 17 Average Spindle Air-Cutting Power Curve

Table 11 Spindle Air-Cutting Power Curve Control Points

n (rpm)	$P_{sp\ air}$ (W)	n (rpm)	$P_{sp\ air}$ (W)
500	43.86	4500	512.73
1000	245.78	5000	546.08
1500	370.77	5500	594.18
2000	379.34	6000	638.05
2500	362.21	6500	697.83
3000	376.30	7000	767.38
3500	407.71	7500	843.34
4000	452.58	8000	932.37

Since only three $P_{sp\ air}$ curves are obtained in the limited experiment time, it is not easy to give an uncertainty evaluation with high confidence. It is suggested taking the maximum difference between the three curves 22.6 W, as one standard deviation of the estimation. This means that the 95 % confidence interval band of $P_{sp\ air}$ prediction has a width of 90.4 W.

5.1.2 Cutting Power

Stable cutting segments are isolated from the spindle power signals derived from the Trace function. Utilizing the average spindle power, denoted as $P_{sp}^{(Tr)}$, from each stable cutting segment and interpolated spindle air-cutting power, denoted as $P_{sp\ air}^{(It)}$, the experimental power of material removal $P_{cutting}$ is calculated using the given Equation (5.2). Subsequently, the value of $P_{cutting}$ is inserted into Equation (5.3) to solve for $F_t/(N \cdot a_p)$.

Table 12 shows the cutting speed (V_c), spindle speed (n), and interpolated spindle air-cutting power ($P_{sp\ air}^{(It)}$) for the three end mills. The $F_t/(N \cdot a_p)$ values are represented against feed per tooth (c) in Figure 18 for all 135 slot-cutting experiments. Different end mills are distinguished by color, and the cutting speeds are differentiated by marker.

$$P_{cutting} = P_{sp}^{(Tr)} - P_{sp\ air}^{(It)} \quad (5.2)$$

$$\frac{F_t}{N \cdot a_p} = \frac{60P_{cutting}}{V_c N \cdot a_p} \quad (5.3)$$

Table 12 The Spindle Speed and the Corresponding Air-cutting Power in the Slot-Cutting Experiments

D (mm)	V_c (m/min)	n (rpm)	$P_{sp\ air}^{(It)}$ (W)
8	130	5170	562.44
	150	5970	635.42
	170	6760	734.00
10	130	4140	469.42
	150	4770	530.74
	170	5410	585.52
12	130	3450	404.57
	150	3980	450.78
	170	4510	513.40

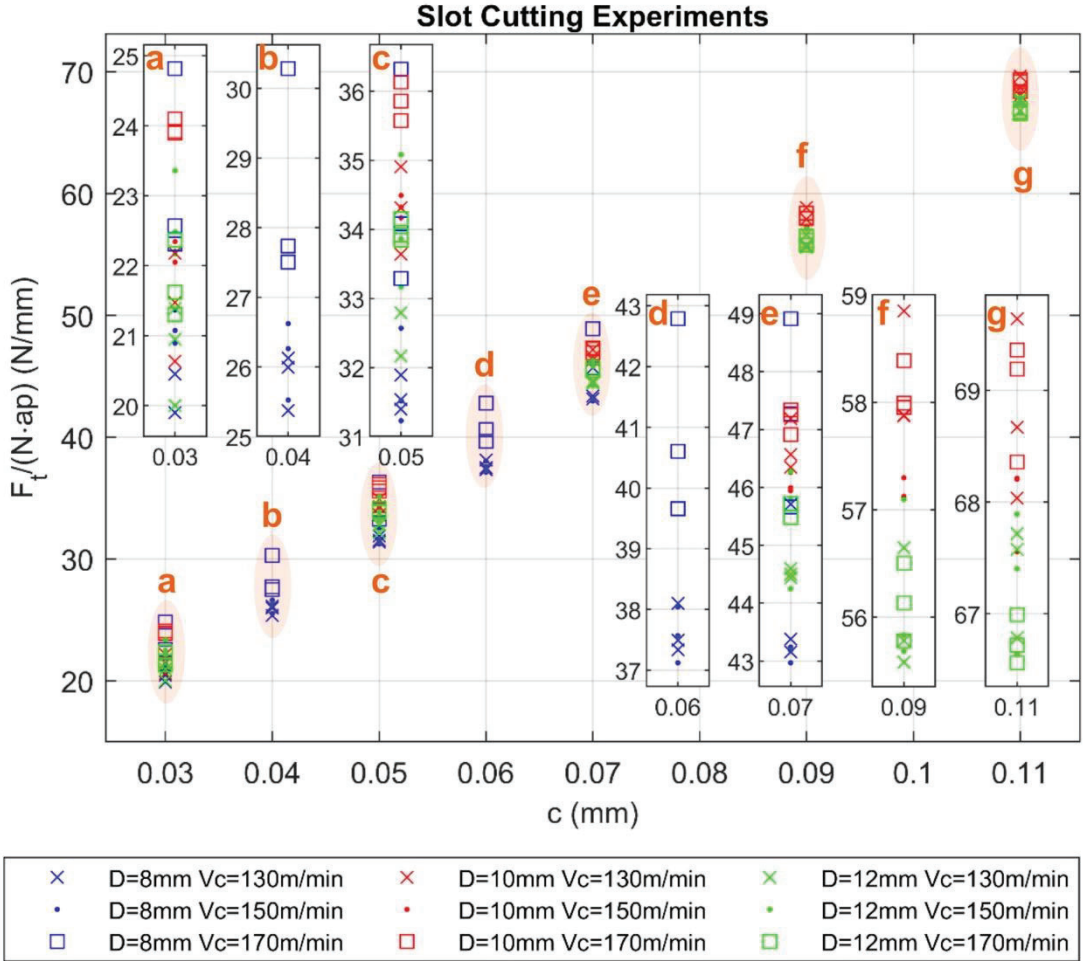


Figure 18 Slot-cutting Experiments Results

The analysis of experimental data shows variations across different end mills. The 8 mm end mill results displayed a more significant dispersion than the other two. Also, the increase in cutting power with the rising cutting speed is more pronounced for this end mill.

For the 8 mm and 10 mm end mills, the outcome difference for varying cutting speeds is more evident at lower c values. In the case of the 10 mm end mill, there is no noticeable difference between the results for cutting speeds of 130 m/min and 150 m/min. However, at a cutting speed of 170 m/min, the values are notably higher when c is small. This difference disappears as c exceeds 0.07 mm.

For the 12 mm end mill, no significant differences are seen across varying cutting speeds. Interestingly, the cutting power of the 10 mm end mill surpasses that of the 12 mm end mill for all values. This observation deviates from the results predicted by Algorithm 1. As per the theoretical predictions discussed in the methodology Section 4.3.1, 10 mm and 12 mm end mills with the same number of cutting edges N , helix angle β , and radial rake angle α should exhibit identical values of $F_t/(N \cdot a_p)$ (as shown in Figure 19.). This discrepancy emphasizes the importance of experimental validation in power prediction models.

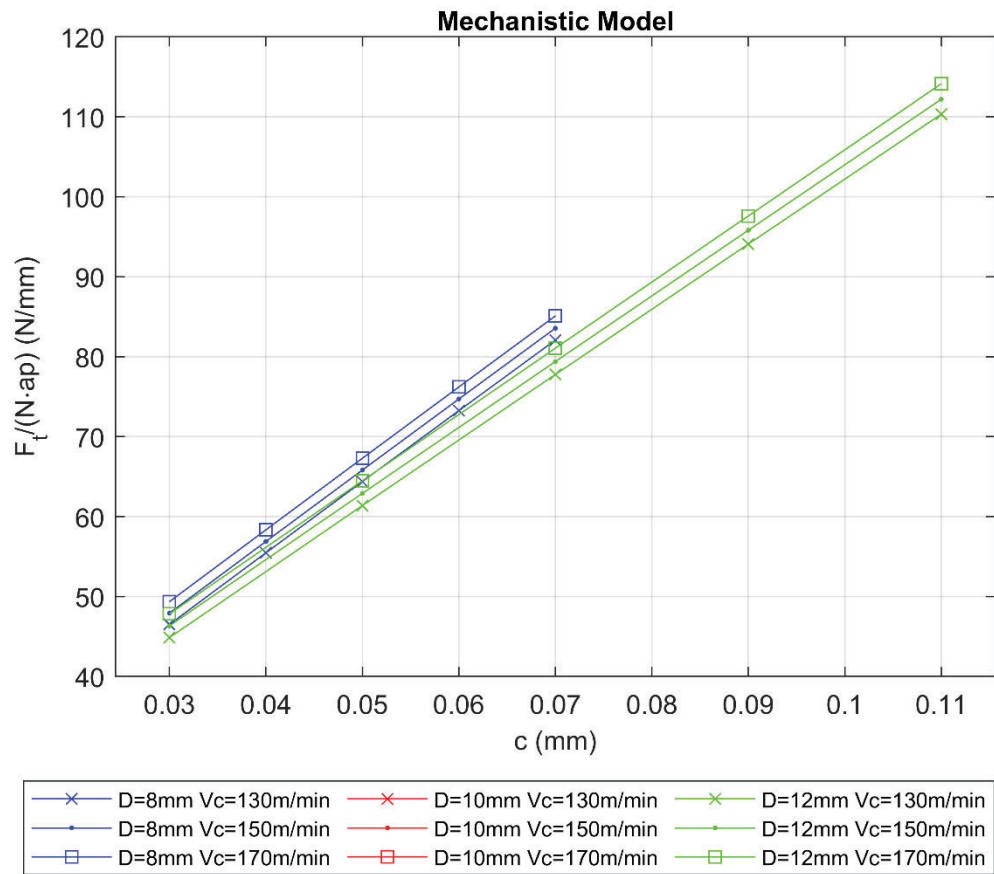


Figure 19 Mechanistic Model Simulation Result for Slot-cutting Experiments

* The results for the 10 mm end mill are identical to the simulation results for the 12 mm end mill and are therefore covered by the green lines and markers.

Figure 20 to Figure 22 display the linear regression models for the three end mills and their respective 95 % confidence intervals. Figure 23 provides a comparative view of the three models, and Table 10 summarizes the model equations and their R-squared (R^2) values. The dispersion in the 8 mm end mill data points results in a lower R^2 value than the other two end mills.

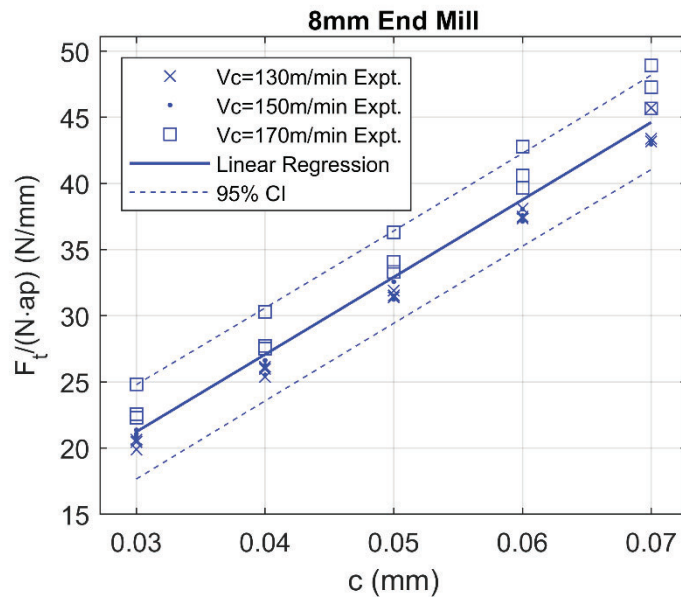
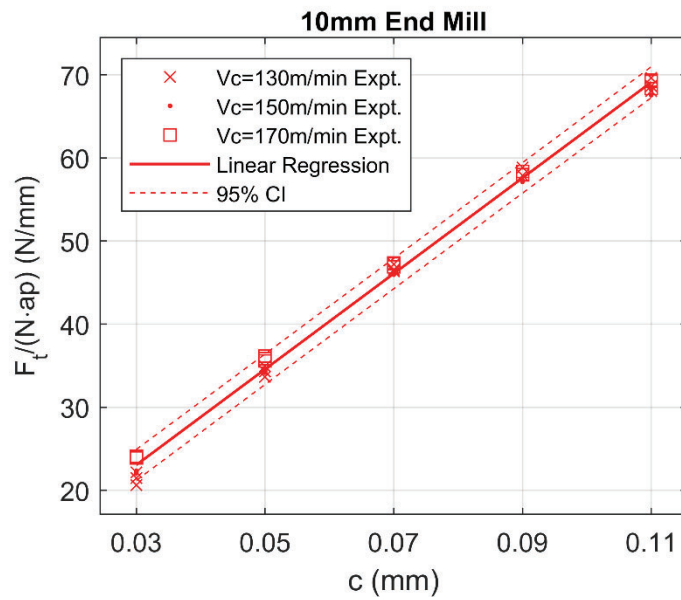
Using Equation (4.21), K_{tc} and K_{te} (the cutting coefficients) are calculated and presented in Table 14. It is crucial to note that these coefficients provide valuable insights into the behavior of the different end mills under various cutting conditions. They play a significant role in the power prediction model, as a base for calculating the cutting forces and, subsequently, the power consumed during the cutting process.

Table 13 Linear Regression Models for Cutting Power Calculation

D (mm)	Linear Regression Model	R^2
8	$y = 584.71x + 3.69$	0.9600
10	$y = 575.51x + 5.80$	0.9971
12	$y = 566.97x + 5.05$	0.9978

Table 14 Calculated K_{tc} and K_{te}

D (mm)	K_{tc} (N/mm ²)	K_{te} (N/mm)
8	1836.92	7.37
10	1808.01	11.59
12	1781.20	10.10

**Figure 20 Linear Regression Result of 8 mm End Mill Slot-cutting Experiments****Figure 21 Linear Regression Result of 10 mm End Mill Slot-cutting Experiments**

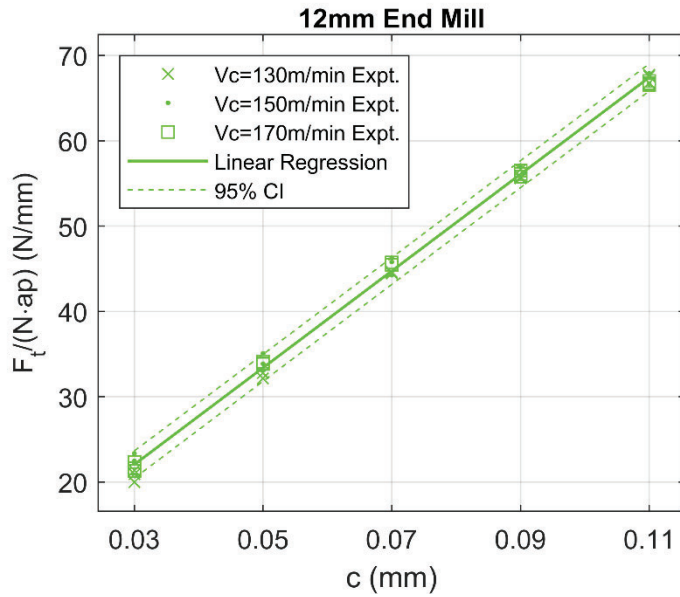


Figure 22 Linear Regression Result of 12 mm End Mill Slot-cutting Experiments

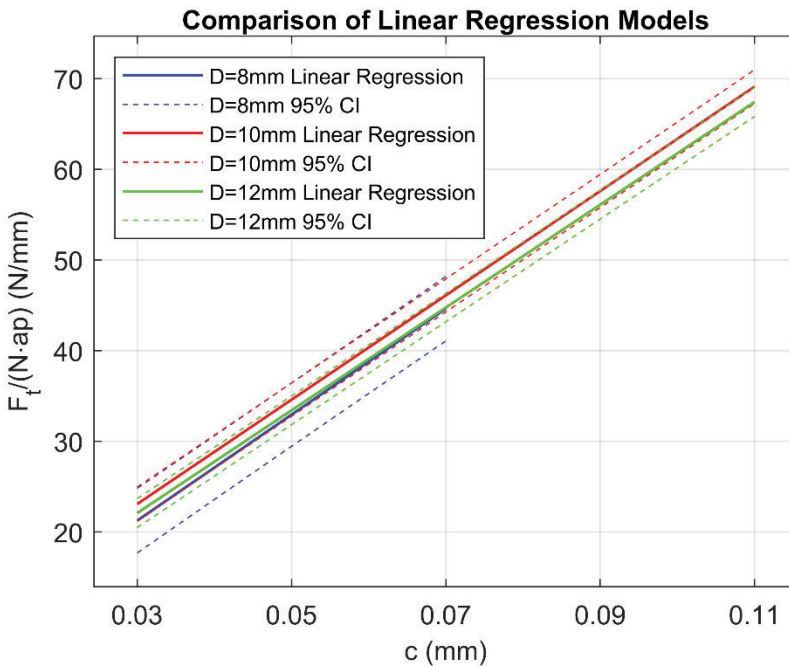


Figure 23 Comparison of Linear Regression Models

When the uncertainty in the linear regression models is propagated to $P_{cutting}$, the width of the confidence interval escalates with increases in V_c and c . Figure 24 depicts the propagated confidence interval on the prediction of $P_{cutting}$. The parameters of the 8 mm end mill are employed in the simulation. The confidence interval of full-immersion $P_{cutting}$ prediction can be estimated using Equation (5.4), where CI_F represents the confidence interval for the linear regression model of $F_t/(N \cdot a_p)$, as illustrated by the dashed line in Figure 23.

Confidence intervals for non-full-immersion milling can be estimated using empirical Equations (5.5) and (5.6), where k_{pc} is the correction factor, and IR represents the radial immersion ratio. It should be noted that Equation (5.6) does not account for variations in chip load, leading to potential overestimation, particularly for small radial immersions.

Figure 25 depicts the models' maximum one-side 95 % confidence interval for $a_p = 3$ mm slot milling. The values in Figure 25 are evaluated within the range of tested c values. For the 8 mm end mill, the range extends from $c = 0.03$ to 0.07 mm. The range for the 10 mm and 12 mm end mills is $c = 0.03$ to 0.11 mm.

$$CI_{slot} = CI_F a_p V_c N / 60 \quad (5.4)$$

$$CI_{shou} = k_{pc} CI_{slot} \quad (5.5)$$

$$k_{pc} = \frac{1}{\pi} \arccos(1 - 2IR) \quad (5.6)$$

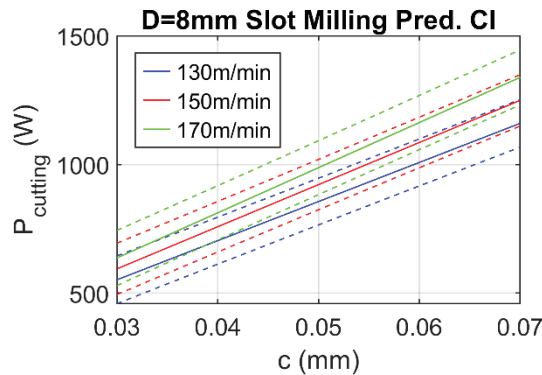


Figure 24 8 mm End Mill $P_{cutting}$ Prediction Confidence Intervals

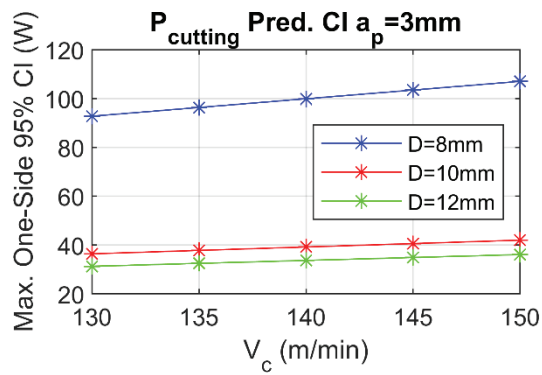


Figure 25 $P_{cutting}$ Prediction Maximum One-side Confidence Intervals

5.1.3 Axis Motor Power

The power consumption of X and Y axis are tested with various feed rates with repetitions. As discussed in Section 4.4, the viscous friction component in the axis power was found negligible from

the experimental data, and axis motor power P_{axis} is modeled with a linear relation with feed rate V_f for X and Y axis separately.

Table 15 and Figure 26 present the linear regression models and the 95 % confidence intervals of the average power consumed by the axis motors, calculated from the Trace function signals across different feed rates. The linear regression plot for the Y-axis in Figure 26 reveals a hysteresis in the power consumption of the Y-axis of the machine used for the experiments. In this context, hysteresis refers to the power difference between forward and reverse feed; the power consumed during forward feed is lower than during reverse feed.

The experimental data show a high level of reproducibility. There are three data points for each V_{fy} in each moving directions and the differences between the points in the same condition are so minuscule that they are hard to distinguish in the figure.

The hysteresis observed may be due to wear and tear on the ball screw, but a definitive cause requires further inspection and analysis. This hysteresis is likely the reason for the lower R^2 value for the Y-axis model.

Both linear regression models possess negative Y-intercepts, which is physically impossible. This discrepancy may be attributed to oversimplifying a quadratic model as a linear one. The viscous term $B_e \omega^2$ in Equation (4.34) and $k_v V_f^2$ in Equation (4.36) are omitted in modeling axis power. The linear regression models, therefore, become invalid when the outputs are equal to or less than zero. This is essential to consider in practical applications and further model development.

Recalling the derivation in Section 4.4 that the inertia term $J_e d\omega/dt$ is zero while rotational speed is stable and the transitional phases are not considered in this thesis, the linear regression models should only be used for predicting axis power in stationary phases.

Table 15 Linear Regression Models for Axis Motors

Axis	Linear Regression Model	R^2
X	$P_x = 0.013841V_{fx} - 2.1726$	0.9829
Y	$P_y = 0.025227V_{fy} - 0.63462$	0.6475

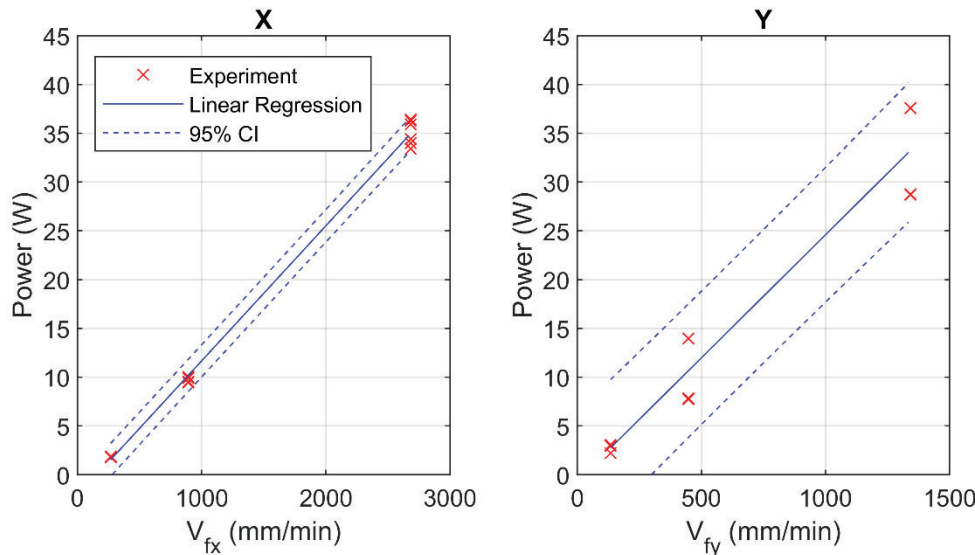


Figure 26 Linear Regression for Axis Motor Power

The linear regressions provide a maximum standard deviation of 0.86 W for P_x and 3.57 W for P_y in the tested feed rate range.

This axis motor power model contains only the Coulomb friction component, not the viscous friction and inertial torque parts. Hence, it is limited to only modeling the power at stable constant feed rate. The motor acceleration and deceleration phases, in which the inertial torque is not negligible, are short in time (< 1 s) in simple straight line milling tasks. The neglection of these phases makes minuscule change to the energy consumption result since energy is the product of power and time.

In complex milling operations with curved cutting paths, the axis motors may accelerate and decelerate continuously. Neglecting the inertial torque in these cases will underestimate the axis motor power to a visible extent. The axis motor power accounts for less than 5 % of the total power in the experiments in this thesis. If the proportion of the axis motor power in complex milling is on a similar level, the discrepancy caused by neglecting continuous acceleration and deceleration is acceptable on total power. The potential cases with high proportions of axis motor power in total power should be discussed case wise.

5.1.4 Idle Power

The active power segments during the machine's idle state, recorded by the power analyzer, are extracted from 47 experiments conducted over seven days. The average idle power is calculated for each segment, yielding a mean of 275.76 W and a standard deviation of 5.99 W. The histogram of these idle power values is depicted in Figure 27, with the mean value represented by a vertical dashed line. This analysis provides valuable insight into the average power consumption of the machine during its idle state, which is crucial for energy efficiency considerations.

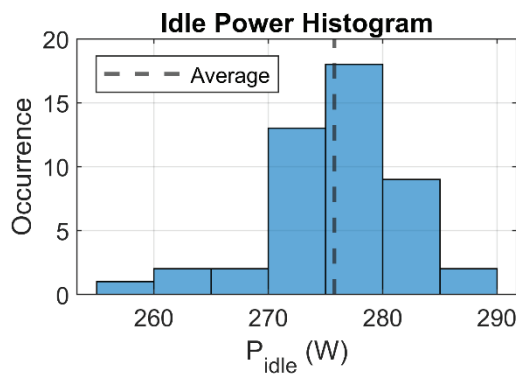


Figure 27 Machine Idle Power

5.1.5 Power Prediction Validation

So far, all four parts of the total power model – spindle air-cutting power, cutting power, axis motor power, and idle power – have been established. To verify the accuracy of this model, it is tested using several sets of non-full-immersion cutting experiments. These experiments will provide a range of scenarios to assess the model's capacity to predict power consumption accurately, thereby testing its robustness and utility. The following subsections will present the verification process and results of the power prediction model.

5.1.5.1 Shoulder Mill

Twelve shoulder mill operations are performed using the 12 mm end mill for model verification. The experiments vary in two axial depths of cut (a_p) and three radial depths of cut (a_e). The cutting parameters – namely, spindle speed (n), feed rate (V_f), cutting speed (V_c), and feed per tooth (c) - are based on the first suggestion from the end mill manufacturer's cutting parameter calculator, with slight modifications for experimental convenience. Up-milling and down-milling are utilized for each parameter combination, and all cuts are made along the X-axis. The chip load is 0.044 mm for all cuts. The comprehensive parameters for these experiments are provided in Table 16.

Table 16 Shoulder Mill Experiments Parameters for the 12 mm End Mill

#	a_p (mm)	a_e (mm)	Type	n (rpm)	V_f (mm/min)	V_c (m/min)	c (mm)	MRR (cm ³ /min)
1	5	2	Down	4640	1550	175	0.111	15.5
2	5	2	Up	4640	1550	175	0.111	15.5
3	5	6	Down	3580	744	135	0.0693	22.3
4	5	6	Up	3580	744	135	0.0693	22.3
5	5	10	Down	3050	557	115	0.0609	27.9
6	5	10	Up	3050	557	115	0.0609	27.9
7	3	2	Down	4640	1550	175	0.111	9.3
8	3	2	Up	4640	1550	175	0.111	9.3
9	3	6	Down	3580	744	135	0.0693	13.4
10	3	6	Up	3580	744	135	0.0693	13.4
11	3	10	Down	3050	557	115	0.0609	16.7
12	3	10	Up	3050	557	115	0.0609	16.7

The experiment and model prediction results are given in Table 17. On the experiment side of Table 17, $P_{cutting}$ and $P_{process}$ are calculated with Equation (5.7) and (5.8) with the data from Trace function, and P is from the power analyzer records.

$$P_{cutting} = P_{sp}^{(Tr)} - P_{sp\ air}^{(Tr)} \quad (5.7)$$

$$P_{process} = P_{sp}^{(Tr)} - P_x^{(Tr)} \quad (5.8)$$

Specific energy consumption (SEC) is calculated with Equation (5.9).

$$SEC = \frac{P}{60MRR} \quad (5.9)$$

On the prediction side, $P_{cutting}$ is predicted by the cutting power model built by slot-cutting experiments. $P_{process}$ and P are calculated with Equation (5.10) and (5.11), where P_{idle} is the average machine idle power in Section 5.1.4. SEC is also calculated with Equation (5.9).

$$P_{process} = P_{cutting}^{(Pred)} + P_x^{(Pred)} + P_{sp\ air}^{(It)} \quad (5.10)$$

$$P = P_{cutting}^{(Pred)} + P_x^{(Pred)} + P_{sp\ air}^{(It)} + P_{idle} \quad (5.11)$$

Detailed data for calculating the result of $P_{cutting}$, $P_{process}$, P , and SEC can be found in Table 32 in Appendix A.

Table 17 Experiment and Prediction Result of the 12 mm End Mill Shoulder Mill Experiment (W, Wh/cm³)

#	Experiment				Prediction			
	Tr. Calc.	Tr. Calc.	P.A.	P.A. Calc.	Pred.	Pred.	Pred.	Pred.
$P_{cutting}$	$P_{process}$	P	SEC	$P_{cutting}$	$P_{process}$	P	SEC	
1	519.2	1013.1	1244.4	1.338	519.1	1060.4	1336.2	1.437
2	529.0	1029.6	1247.9	1.342	519.1	1060.5	1336.2	1.437
3	761.5	1155.2	1392.2	1.040	747.8	1170.8	1446.6	1.080
4	780.3	1177.5	1421.3	1.061	747.8	1170.8	1446.6	1.080
5	972.6	1336.1	1600.3	0.958	933.2	1318.1	1593.9	0.954
6	1004.2	1368.6	1628.9	0.975	933.2	1318.1	1593.9	0.954
7	305.4	808.9	1015.9	1.821	310.4	851.8	1127.5	2.021
8	325.1	828.1	1036.3	1.857	312.0	853.4	1129.1	2.024
9	470.4	867.2	1082.6	1.347	449.3	872.4	1148.1	1.429
10	480.9	879.3	1099.0	1.368	448.0	871.0	1146.8	1.427
11	601.3	961.2	1190.2	1.187	559.7	944.6	1220.4	1.217
12	605.1	965.0	1194.1	1.191	560.3	945.3	1221.0	1.218

Table 18 Bias and Relative Error of the 12 mm End Mill Shoulder Mill Prediction (W, Wh/cm³)

#	$P_{cutting}$		$P_{process}$		P_{sp}		P		SEC	
	Bias	Rel. Err.	Bias	Rel. Err.	Bias	Rel. Err.	Bias	Rel. Err.	Bias	Rel. Err.
1	-0.2	-0.03%	47.4	4.7%	43.4	4.3%	91.8	7.4%	0.099	7.4%
2	-9.9	-1.9%	30.8	3.0%	33.7	3.3%	88.3	7.1%	0.095	7.1%
3	-13.7	-1.8%	15.6	1.4%	15.4	1.3%	54.4	3.9%	0.041	3.9%
4	-32.5	-4.2%	-6.6	-0.6%	-3.4	-0.3%	25.3	1.8%	0.019	1.8%
5	-39.5	-4.1%	-17.9	-1.3%	-16.2	-1.2%	-6.4	-0.4%	-0.004	-0.4%
6	-71.0	-7.1%	-50.5	-3.7%	-47.8	-3.5%	-35.0	-2.1%	-0.021	-2.1%
7	5.1	1.7%	42.9	5.3%	43.7	5.5%	111.7	11.0%	0.200	11.0%
8	-13.1	-4.0%	25.3	3.1%	25.6	3.2%	92.8	9.0%	0.166	9.0%
9	-21.1	-4.5%	5.1	0.6%	4.9	0.6%	65.5	6.1%	0.082	6.1%
10	-32.9	-6.8%	-8.2	-0.9%	-6.8	-0.8%	47.8	4.3%	0.059	4.3%
11	-41.6	-6.9%	-16.6	-1.7%	-15.3	-1.6%	30.2	2.5%	0.030	2.5%
12	-44.8	-7.4%	-19.7	-2.0%	-18.5	-1.9%	26.9	2.3%	0.027	2.3%

Table 18 lists the bias and relative errors in the prediction results of shoulder milling. The model's precision fluctuates depending on several parameters, such as a_p , a_e , the milling method (up-milling versus down-milling), and MRR.

Almost universally, the model underestimates the cutting power $P_{cutting}$ except for cut #7 ($a_p = 3$ mm, $a_e = 2$ mm, down-milling). The model omits the efficiency (η) in the relationship of the tool-tip energy consumption and the cutting power consumed by the spindle which is one of the reasons for the underestimation. The energy consumed by the spindle is not fully converted to metal removal but also to other forms of energy. This underestimation could also be attributed to the missing tool wear during the slot-cuts done with new tools. Furthermore, discrepancies may arise from variations in tool edge preparation, which can differ significantly even when using the same tool type across

different experiments. Other errors could originate from other components involved in total power approximation and possible inconsistency in workpiece material properties.

When holding a_p and a_e constant, the model's error for down-milling is less than for up-milling, likely due to improved chip formation in down-milling.

The most pronounced relative error in $P_{cutting}$ is displayed in cut #12 ($a_p = 3$ mm, $a_e = 10$ mm, down-milling), where the model underestimates by -7.4 %. This suggests that the model's precision is sensitive to MRR, but this relationship becomes inapplicable when considering different axial depths of cut.

When a_e and the milling type remain constant, the model's error is larger for a smaller a_p (3 mm) than for a larger a_p (5 mm). This observation can be correlated with a relative increase in the shearing effect as the engagement between the tool and workpiece strengthens. The power prediction model is built on the mechanistic model, which offers better accuracy for shear-dominated cutting. When plowing effects prevail, the model's precision decreases, as seen with increased tool wear (an increased effective cutting-edge radius). This nuanced interaction between the tool and workpiece and its impact on the accuracy of the power prediction model highlights an important area for further model enhancement.

The most significant relative error in the process power, $P_{process}$, is observed in cut #7. Upon comparing the biases of $P_{process}$ and P_{sp} , it's clear that the main increase in bias from $P_{cutting}$ to $P_{process}$ is driven by a persistent positive bias from $P_{sp\ air}$. Similarly, a consistent positive bias also appears in P_{idle} if comparing the biases of P and $P_{process}$. For this reason, cut #7 again emerges as the most inaccurately predicted instance when considering P and SEC.

The reason for the consistent and stable positive bias exhibited by $P_{sp\ air}$ and P_{idle} is currently unclear. If possible, it should be analyzed by further comparing data from other cutting experiments to the air-cutting experiments which determines the $P_{sp\ air}$ curve and conducting more accurate measurement of each power-consuming component of the machine.

Generally speaking, when the tool's radial immersion increases, the model's ability to accurately predict $P_{cutting}$ correspondingly decreases. The accuracy of $P_{process}$ and P prediction mainly attributes to the bias in $P_{sp\ air}$ and P_{idle} .

The comparisons of P , SEC, and the prediction bias are illustrated in the figures that follows:

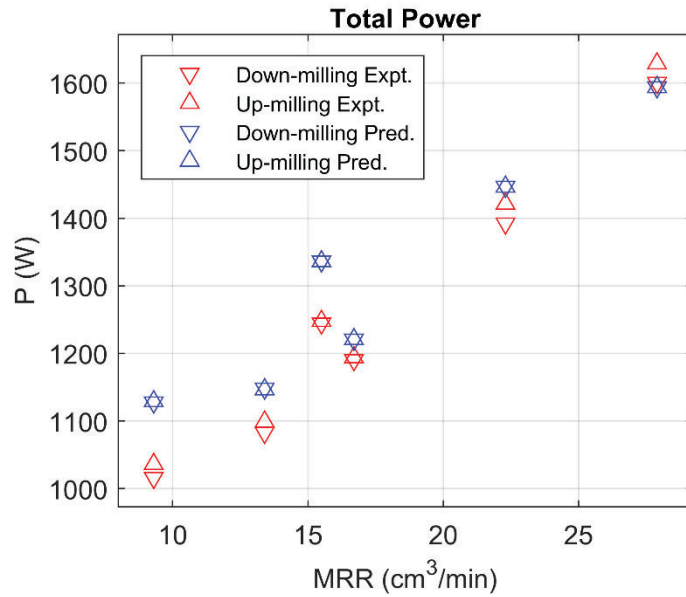


Figure 28 Total Power Comparison between Prediction and Experiments

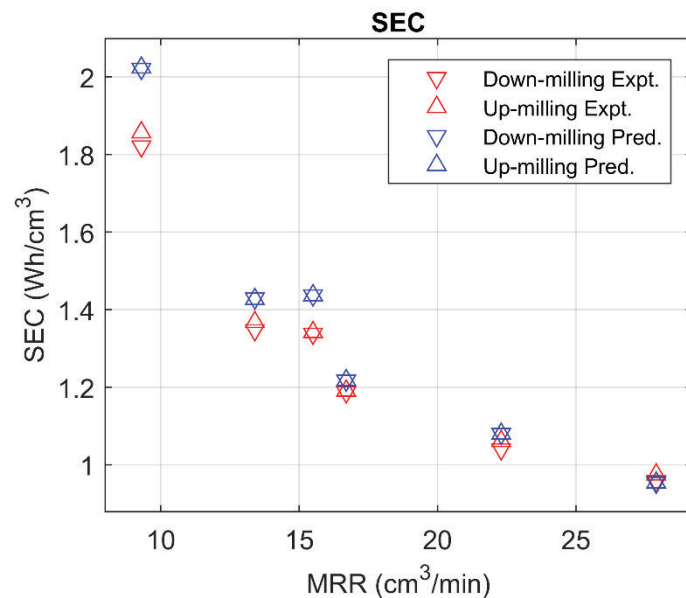


Figure 29 SEC Comparison between Prediction and Experiments

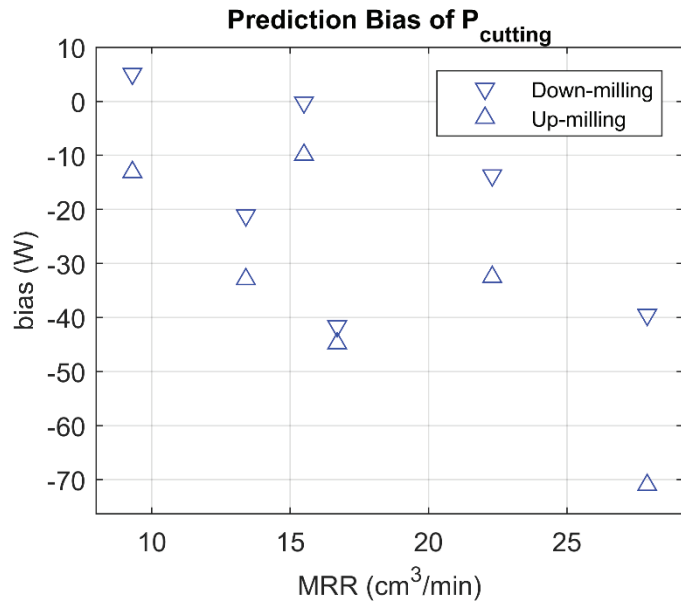


Figure 30 Cutting Power Prediction Bias

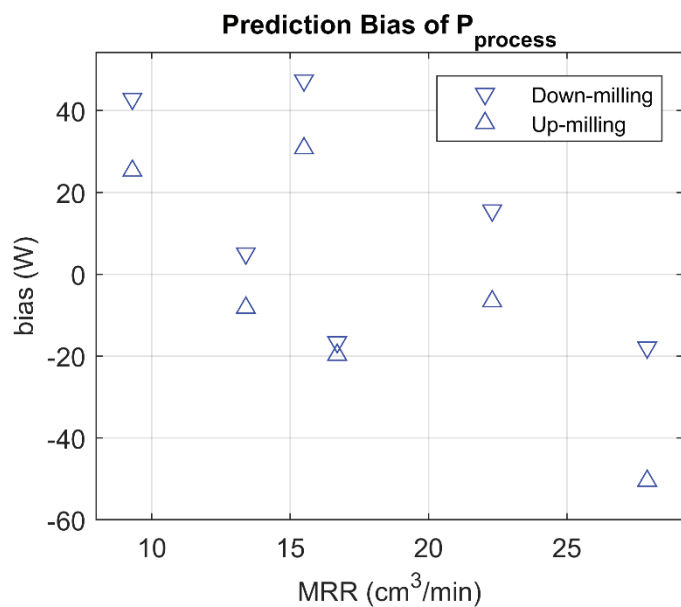


Figure 31 Process Power Prediction Bias

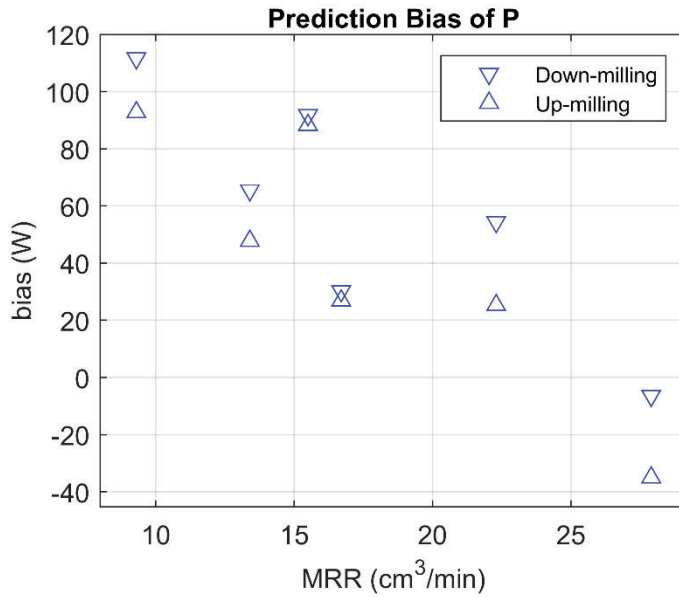


Figure 32 Total Power Prediction Bias

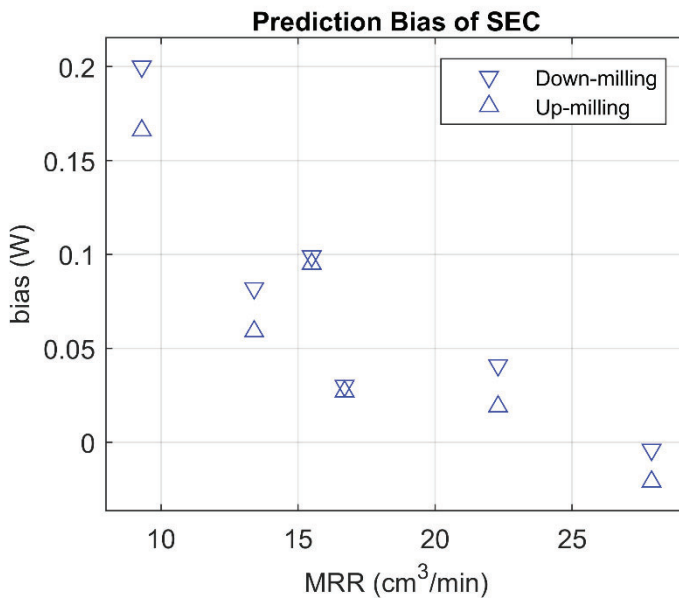


Figure 33 SEC Prediction Bias

5.1.5.2 Face Mill

Face milling with the 10 mm end mill is conducted as a validation. This process is performed in a tool path that moves back and forth along the Y-axis, cutting continuously and not exiting the workpiece. The cutting parameters (except a_e in the last pass) remain constant throughout the operation. Table 19 presents the comprehensive parameter selection for this experiment.

Table 19 Face Mill Experiments Parameters for the 10 mm End Mill

Experiment Step	a_p (mm)	a_e (mm)	n (rpm)	V_f (mm/min)	V_c (m/min)	c (mm)	MRR (cm ³ /min)	MRR _{avg} (cm ³ /min)
Face Milling (except the last pass)	3	7.5	5090	917	160	0.06	20.6	17.2
Last pass	3	5	5090	917	160	0.06	13.8	

The energy consumption from the experiment and the energy prediction using the model is listed in Table 20.

Rather than calculating the power consumption in every step of the process, the energy consumption for the entire process is calculated. The energy consumption in Wh is calculated from the recorded power values by multiplying them with the process time. The process time is found to be 74 seconds. The energy calculations for E_{idle} , $E_{sp\ air}$, and E_{axis} are as in:

$$E_{idle} = P_{idle} \left(\frac{74}{3600} \right) \quad (5.12)$$

$$E_{sp\ air} = P_{sp\ air} \left(\frac{74}{3600} \right) \quad (5.13)$$

$$E_{axis} = (P_x^{(Tr)} + P_y^{(Tr)}) \left(\frac{74}{3600} \right) \quad (5.14)$$

On the experiment side of Table 20, E is the energy value recorded using the power analyzer. The power analyzer has an in-built integration method which calculates the total energy consumption for the recorded power values. $E_{cutting}$ is the energy consumption associated with the spindle when cutting and is found by Equation (5.15). $E_{process}$ is the energy consumed for the process, including the axis motor consumption, and is found by using Equation (5.16).

$$E_{cutting} = E - (E_{idle} + E_{sp\ air} + E_{axis}) \quad (5.15)$$

$$E_{process} = E - E_{idle} \quad (5.16)$$

The average power consumption ($P_{avg}^{(face)}$) is to be known to calculate the SEC. Dividing the total energy (E) by the process time gives $P_{avg}^{(face)}$ (Equation (5.17)).

$$P_{avg}^{(face)} = E \left(\frac{3600}{74} \right) \quad (5.17)$$

SEC is calculated with Equation (5.18)

$$SEC = \frac{P_{avg}^{(face)}}{60MRR_{avg}} \quad (5.18)$$

On the prediction side, the energy consumption is again calculated from the predicted power values similar to Equations (5.12) to (5.14). $P_{cutting}$ is predicted using the cutting power model. $P_{process}$ and P are calculated as discussed in Section 5.1.5.1 (Equations (5.10) and (5.11)). $E_{process}$ and E are calculated using Equations (5.19) and (5.20).

$$E_{process} = E_{cutting}^{(Pred)} + E_{axis}^{(Pred)} + E_{sp\ air} \quad (5.19)$$

$$E = E_{process} + E_{idle} \quad (5.20)$$

SEC is found same as in Equation (5.18).

Table 20 Experiment and Prediction Result of the 10 mm Tool Face Mill Experiment

Experiment				Prediction			
Tr. Calc.	Tr. Calc.	P.A.	P.A. Calc.	Pred.	Pred.	Pred.	Pred.
$E_{cutting}$	$E_{process}$	E	SEC	$E_{cutting}$	$E_{process}$	E	SEC
13.2	25.1	27.1	1.333	12.1	22.1	23.8	1.169

Table 21 shows the bias and relative errors pertaining to the results from the face milling experiment.

Table 21 Bias and Relative Error of the 10 mm Tool Face Mill Prediction

$E_{cutting}$		$E_{process}$		E		SEC	
Bias	Rel. Err.	Bias	Rel. Err.	Bias	Rel. Err.	Bias	Rel. Err.
-1.1	-9 %	-3	-12 %	-3.3	-12 %	-0.164	-12 %

5.1.6 Practical Approach Example

This detailed example lays out a practical approach for manufacturers to apply in their operations.

1. The cutting tool and the material in question should be installed on the machine correctly.
2. Perform a series of spindle air-cutting tests in the spindle speed range of interest. This can be repeated several times as time allows.
3. Perform four or more diagonal slot-cutting tests in the feed per tooth range of interest. Only one cutting speed is required for all feed per tooth. A reasonable axial depth of cut can be chosen with practical experience. Record the active power of the spindle and the axes with Trace function.
4. If time allows, a table-movement test can be performed. It is not necessary since the axis motor power contributes little to the process power. In our experiments, the axis motor power is usually less than 5 % of the spindle power. The axis motor power model can be built with the data obtained in the slot-cutting tests.
5. If total power and energy consumption are of interest, use a power analyzer or a similar sensor to record the machine's total power for idle power estimation. This step is not necessary if only process power and energy are of concern.

A calculation example is given below with the slot-cutting experiments discussed in this chapter.

Assuming that a manufacturer would like to build a model for predicting the process electricity consumption of the machine during milling operations with the 10 mm end mill on steel SS2541.

After setting the cutting tool and the test material block in place, the manufacturer performs step 2. A series of spindle air-cutting tests is done, and the green line with x markers in Figure 16 is generated. The control points of $P_{sp\ air}$ interpolation model are obtained.

Then four diagonal slot milling tests are conducted with the cutting parameters $V_c = 130$ m/min, $c = 0.03, 0.05, 0.09, 0.11$ mm, $a_p = 3$ mm. Spindle speed is calculated from the parameters as $n =$

4140 rpm. Feed speed is calculated as $V_f = 372, 621, 1120, 1370$ mm/min. The average spindle power and axis motor power are extracted from Trace function signals (Table 22).

Table 22 10 mm End Mill Diagonal Slot Milling Tests Results

Expt. No.	1	2	3	4
c (mm)	0.03	0.05	0.09	0.11
V_f (mm/min)	372	621	1120	1370
V_{fx}, V_{fy} (mm/min)	263	439	792	969
P_{sp} (W)	871.77	1125.40	1597.95	1796.11
P_x (W)	2.44	5.35	14.16	18.62
P_y (W)	3.76	6.45	11.66	14.20

Corresponding $F_t/(N \cdot a_p)$ for each test is calculated from P_{sp} , $P_{sp\ air}$, and V_c with Equation (4.17). The linear regression model between $F_t/(N \cdot a_p)$ and c is shown in Figure 34 and Table 23. K_{tc} and K_{te} are evaluated from the parameters of the linear regression model with Equation (4.21). Therefore, $P_{cutting}$ can be predicted with Algorithm 2. The linear models for P_x and P_y are built with V_{fx} , V_{fy} , P_x , and P_y values in Table 22 and shown in Figure 35 and Table 23.

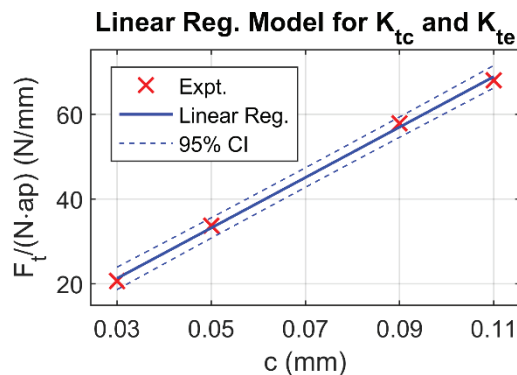


Figure 34 10 mm End Mill Linear Regression Model for Calculating K_{tc} and K_{te}

Table 23 10 mm End Mill Spindle Power Linear Regression Result

Linear Regression Model	$y = 595.18x + 3.38$
R^2	0.9985
K_{tc} (N/mm ²)	1869.83
K_{te} (N/mm)	6.77

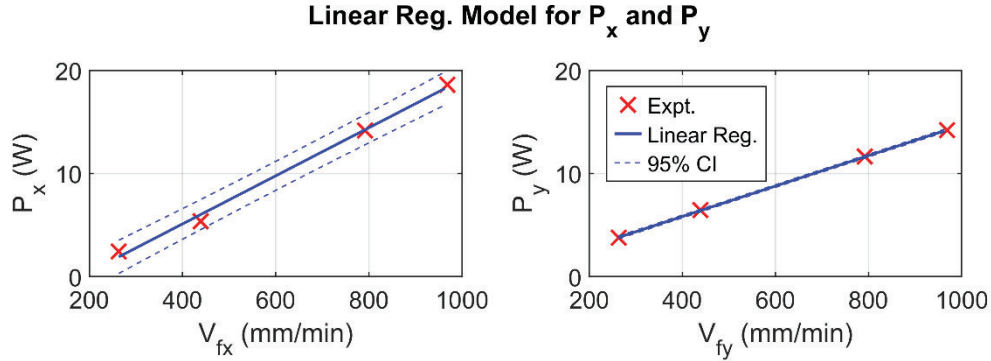


Figure 35 10 mm End Mill Linear Regression Models for P_x and P_y

Table 24 10 mm End Mill Axis Power Linear Regression Result

	X	Y
Linear Regression Model	$P_x = 0.023339V_{fx} - 4.2289$	$P_y = 0.014780V_{fy} - 0.083164$
R^2	0.9954	0.9999

Up to this point, all the models are ready for $P_{process}$ prediction. The model is used to predict $P_{cutting}$ and $P_{process}$ for four other parameter sets in Table 25. The predicted result is compared to the experiments.

Table 25 Practical Approach Prediction Comparison

V_c	c	a_p	$P_{cutting}$			$P_{process}$		
			Expt.	Pred.	Rel. err.	Expt.	Pred.	Rel. err.
130	0.07	3	948.74	878.39	-7.4%	1395.98	1366.92	-2.1%
150	0.07	3	1091.72	1013.52	-7.2%	1593.31	1566.91	-1.7%
150	0.11	3	1570.90	1549.19	-1.4%	2088.64	2118.21	1.4%
170	0.05	3	956.99	845.12	-11.7%	1523.25	1448.21	-4.9%

If time and equipment are available, step 4 and 5 can be performed. P_{idle} can be measured and total SEC can be evaluated.

5.2 Environmental Impact Calculation

The electricity CO₂ intensity and the cutting tool CO₂ emission are calculated in this section. The total environmental impact of a face mill experiment is evaluated. Energy consumption and the environmental impact are compared based on the functional unit with the experiment results of shoulder mills.

5.2.1 Electricity

The energy mix of the KTH campus is 40 % hydropower, 40 % bioenergy, and 20 % wind power. The electricity generation mix of Sweden is calculated with the data published by Statistics Sweden (SCB). The total CO₂ intensity of market-based and location-based methods are evaluated with Equation (3.2) in the two tables below.

Table 26 Total CO₂ Intensity Calculation for Market-Based Method (Electricity Supply for the KTH Campus)

	CO ₂ Intensity (g CO ₂ -eq/kWh)	Share ^(a)
Hydropower	21 ^(b)	40 %
Biopower	52 ^(c)	40 %
Wind Power	13 ^(d)	20 %
Total	32	100 %

(a) information from Akademiska Hus

(b) reservoir and run-of-river

(c) co-firing, direct combustion, gasification, gasification engine

(d) land-based and offshore

Table 27 Total CO₂ Intensity Calculation for Location-Based Method (Sweden)

	CO ₂ Intensity (g CO ₂ -eq/kWh)	Share ^(e)
Hydropower	21	43.55 %
Nuclear	13 ^(g)	30.24 %
Wind Power	13	16.08 %
Conventional Thermal Power ^(f)	486 ^(h)	9.24 %
Solar Power	43 ⁽ⁱ⁾	0.89 %
Total	60	100.00 %

(e) calculated with the latest published electricity production data by SCB for the year 2021 [55]

(f) including Combined Heat and Power (CHP) in industry, CHP in public steam and hot water works, condensing steam power, gas turbines, and others

(g) light-water reactor (including pressurized water and boiling water) only

(i) natural gas

(h) thin film and crystalline silicon photovoltaic

Note that the CO₂ intensity values are the median of total life cycle emissions factors for electricity generation technologies published by NREL in 2021 [56]. The minimum, maximum and quartiles of the statistics are given in Appendix A. The accuracy of the values is limited by the studied areas, the target technologies, and the study time of the collected references. These values may not reflect the true situation in Sweden with complete accuracy. The regional total life cycle data should be used if they are available. Particularly, the intensity factor for conventional thermal power in Table 27 is not for the technologies listed in note (f), but for natural gas-fired power generation. The conventional thermal power category published by SCB covers a wide range of different power generation technologies. The use of different fuels has a significant impact on the intensity factor of these technologies. We are unable to obtain specific data for this category, so we use the data for natural gas instead.

In Greenhouse Gas Protocol's scope division methodology, only the GHG emitted in the electricity generation phase belongs to the Scope 2 emission of the reporting body who consumes the electricity

as an end user. The GHG emitted in construction, fuel extraction, operation, transmission and distribution, and decommission is not included. Therefore, renewable energy, e.g., solar and wind power, has zero emission for end users. The emission factors used in market-based and location-based methods follow the defined emission factor hierarchies and depends on the contractual instruments of electricity-related emission. Intuitively, the emission factors considering only the generation phase are lower than full life cycle emission factor calculated by NREL's data. However, they can be higher as well, e.g., residual mix is used in market-based method. Detailed methodology can be found in GHG Protocol Scope 2 Guidance and RE-DIIS project's publications. The calculation in this section does not follow the emission factor decision trees in Greenhouse Gas Protocol but demonstrates the calculation in a straightforward manner. In reporting calculations, the decision maps of the required standard must be followed strictly.

5.2.2 Cutting Tool

The GHG emissions associated with the end mills are estimated by leveraging the CO₂ emission factor of the tool material (cemented carbide) and the tool's weight. This approach represents a compromise as the calculation only accounts for a portion of the material input during production and omits other phases of the end mills' lifecycle. Emissions generated during manufacturing, transportation, and waste management are not factored in. The precision of this calculation could be significantly improved when more comprehensive data becomes available.

According to the research by Furberg et al. [57, 58] and Ma et al. [59], the CO₂ footprint of 1 kg of typical non-Chinese tungsten carbide production is estimated at 14 kg CO₂-eq (ranging from 5 – 28 kg CO₂-eq for cases with low and high environmental impacts under various scenarios) and 69 kg CO₂-eq for production in China. The lower value has been adopted in the calculations for this study. Table 28 outlines the weight and calculated the environmental impact of the three end mills utilized in the experiments.

Table 28 Environmental Impact of the End Mills

D (mm)	Weight (kg)	Environmental Impact (g CO ₂ -eq/piece)
8	0.05	700
10	0.085	1190
12	0.13	1820

It is worth noting that the environmental impact of the tools could be further mitigated through reconditioning, which extends the lifespan of the tools and reduces the need for manufacturing new ones. Moreover, the use of inserted cutters, which only require the replacement of the cutting edges rather than the entire tool, can also contribute to reducing emissions.

5.2.3 Total Environmental Impact

The face mill experiment discussed in Section 5.1.5.2 is given as an example for the calculation of the total environmental impact. The total electricity consumption for the face mill operation is 27.1 Wh. The CO₂ emission of the electricity therefore is calculated as 0.9 and 1.6 g CO₂-eq according to market-based and location-based method, respectively. The tool used for this operation is the 10 mm end mill and the tool life consumed in this operation is 6.2 %, given by the catalogue. Hence the CO₂ emission of the cutting tool is calculated as 73.8 g CO₂-eq according to Equation (3.3). The total environmental impact of this operation therefore is 74.7 and 75.4 g CO₂-eq for market-based and location-based methods.

The material removed in this operation is 19.2 cm^3 . The MRR is $17.2 \text{ cm}^3/\text{min}$. The electricity consumption for one functional unit is 1.4 Wh . The total environmental impact per functional unit is $3.9 \text{ g CO}_2\text{-eq}$. The cutting tool consumption contributes 98 % to 99 % of the total environmental impact in this milling process. Since the emission factor of the cutting tool is underestimated, the real proportion of the cutting tool caused impact can be higher. Even assuming a better scenario where the cutting tool is used for three times the recommended cutting length and the electricity is generated only by natural gas, the percentage is still over 65 %.

The mix of the electricity consumption and environmental impact sources are illustrated in Figure 36. The electricity indirect GHG emission is calculated with the market-based method in this figure. Considering only the electricity-linked impact, the milling process accounts for 92.6 % and machine idling accounts for 7.4 %.

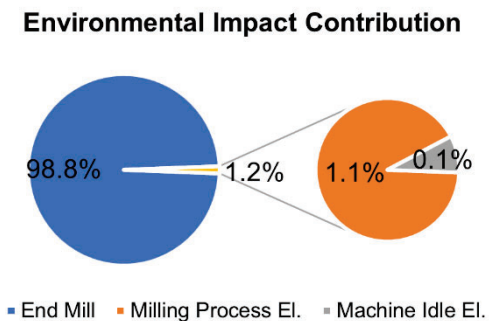


Figure 36 The Contribution of Impact Sources for the Face Mill Experiment (Market-based)

To further understand the effect of cutting parameters on the environmental impact per functional unit, the impact of the shoulder mill experiment with 12 mm end mill in Section 5.1.5.1 is calculated (Table 29). Since the impact of the cutting tool is absolutely dominant in the total impact, the results calculated for the experiment measured power and the predicted power show almost no difference. The power requirement difference in up-milling and down-milling do not appear in the total environmental impact result, therefore only down-milling cuts are shown in Table 29. The total impact per functional unit decreases considerably with increasing a_p . For the same a_p , the value decreases with increasing MRR.

A scenario of the same MRR but cutting with the 10 mm end mill is created for comparing against the 12 mm end mill result. The total power and $\text{g CO}_2\text{-eq/FU}$ are calculated with the cutting parameters in Table 30 for cut #7, 9, and 11. The c values are the first suggestion given by the catalogue. a_p and a_e of the shoulder millings are same with the 12 mm end mill experiment. By using the 10 mm end mill, a smaller $\text{g CO}_2\text{-eq/FU}$ is achieved for the same MRR.

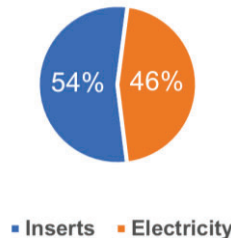
Table 29 Total $\text{g CO}_2\text{-eq/FU}$ of the Shoulder Mill Experiment (12 mm End Mill) in Section 5.1.5.1

#	MRR (cm^3/min)	Expt.	Pred.	Cutting Tool Contribution
1	15.5	3.5	3.5	98.6 %
3	22.3	3.0	3.0	98.7 %
5	27.9	2.6	2.6	98.9 %
7	9.3	5.7	5.8	98.8 %
9	13.4	4.8	4.8	99.0 %
11	16.7	4.3	4.3	99.1 %

Table 30 Predicted Total Power and g CO₂-eq/FU in 10 mm End Mill Scenario

#	V_c (m/min)	c (mm)	P (W)	Total g CO ₂ -eq/FU
7	187	0.0871	1258.0	5.0
9	140	0.0555	1262.9	4.1
11	98.8	0.0590	1255.5	3.2

With the interest of knowing how the impact contributions will change by using inserted cutters instead of solid cutting tools, a brief simulation is performed with a 40 mm diameter tool with 6 inserted cutters. Each inserted cutter has 4 cutting edges and weighs 2 grams. The 40 mm tool weighs 168 grams. The tool and the inserted cutters are all made of tungsten carbide. Using this tool and inserted cutters combination to conduct the same face milling process generated Figure 36 gives an impact contribution result in Figure 37.

**Figure 37 The Contribution of Impact Sources from the Simulation with Inserted Cutters**

The catalogue simulated electricity consumption of this process is 9.7 Wh, leading to 0.31 g (market-based) and 0.58 g (location-based) CO₂-eq. The inserted cutters lose 0.22 % of tool life. The impact from the inserted cutters is 0.36 g CO₂-eq. The total environmental impact is 0.67 g (market-based) and 0.94 g (location-based) CO₂-eq. The shares of the electricity and the cutters are in Figure 37. The impact is much lower than the experimental result from the solid cutting tool. This is a very good study aspect for future research to consider the emission reduction by using inserts and tool reconditioning methods.

5.3 Uncertainty Discussion

In the previous sections of this chapter, the uncertainty of the prediction or estimation is all presented; however, the form varies in several cases. Since it is stated in Section 5.2.3 that the consumption of the solid cutting tool is the absolute dominator in the total environmental impact, the uncertainty mostly attributes to tool life estimation and life cycle CO₂ emissions evaluation. Both are outside the research scope of this thesis.

As emission factors of the tool material, Furberg et al. [57] offer lower and upper bounds of 5 and 28 kg CO₂-eq per kg tungsten carbide. Therefore, a lower bound of 36 % and an upper bound of 200 % of the environmental impact estimation can be given for the estimation in Section 5.2.

It should be noted that the result computed with the tungsten carbide emission factor only accounts for the material production phase of the cutting tool life cycle. If a conservative estimation is made that material production accounts for 90 % of the cutting tool's full life cycle GHG emissions. The result should be multiplied by a factor of 1.1.

Due to the limited research scope of this thesis, a thorough search and collecting of existing measurements and estimations of the emission factors is not undertaken. More extensive work in the domain of life cycle assessment is expected.

While the current research result has provided valuable insights, certain aspects need further investigation. Particularly, the impact of tool wear on the overall environmental footprint could be a pivotal factor in understanding the environmental implications of milling processes more comprehensively. The longevity and performance of cutting tools significantly affect the total environmental impact, as shorter tool lifespans can lead to higher raw material consumption, energy use, and waste generation.

In addition, this study primarily dealt with small machine tools. Nevertheless, the energy consumption patterns of larger machine tools may differ significantly, especially in terms of idle and overall energy consumption. Larger machine tools generally have higher idle energy usage due to the bigger number of auxiliary systems, and their total energy consumption is typically higher as well. As such, further research into the energy consumption behaviors of larger machine tools could provide a broader and more accurate understanding of the environmental impacts associated with different scales of manufacturing operations.

Both these areas – tool wear and the effect of larger machine tools – present ample opportunities for future research to further enhance our understanding of the energy consumption patterns and environmental impacts in milling processes.

6. The Framework – top to bottom

The primary objective of this thesis is to model energy consumption for milling operation to assess its environmental impact. To accomplish this, a framework is proposed as depicted in Figure 38. This framework initiates with the process plan of machining a product and concludes with the predicted CO₂ emissions associated with this process plan. Consequently, different process plans can be compared based on their CO₂ emissions, facilitating the creation of more sustainable machining plans.

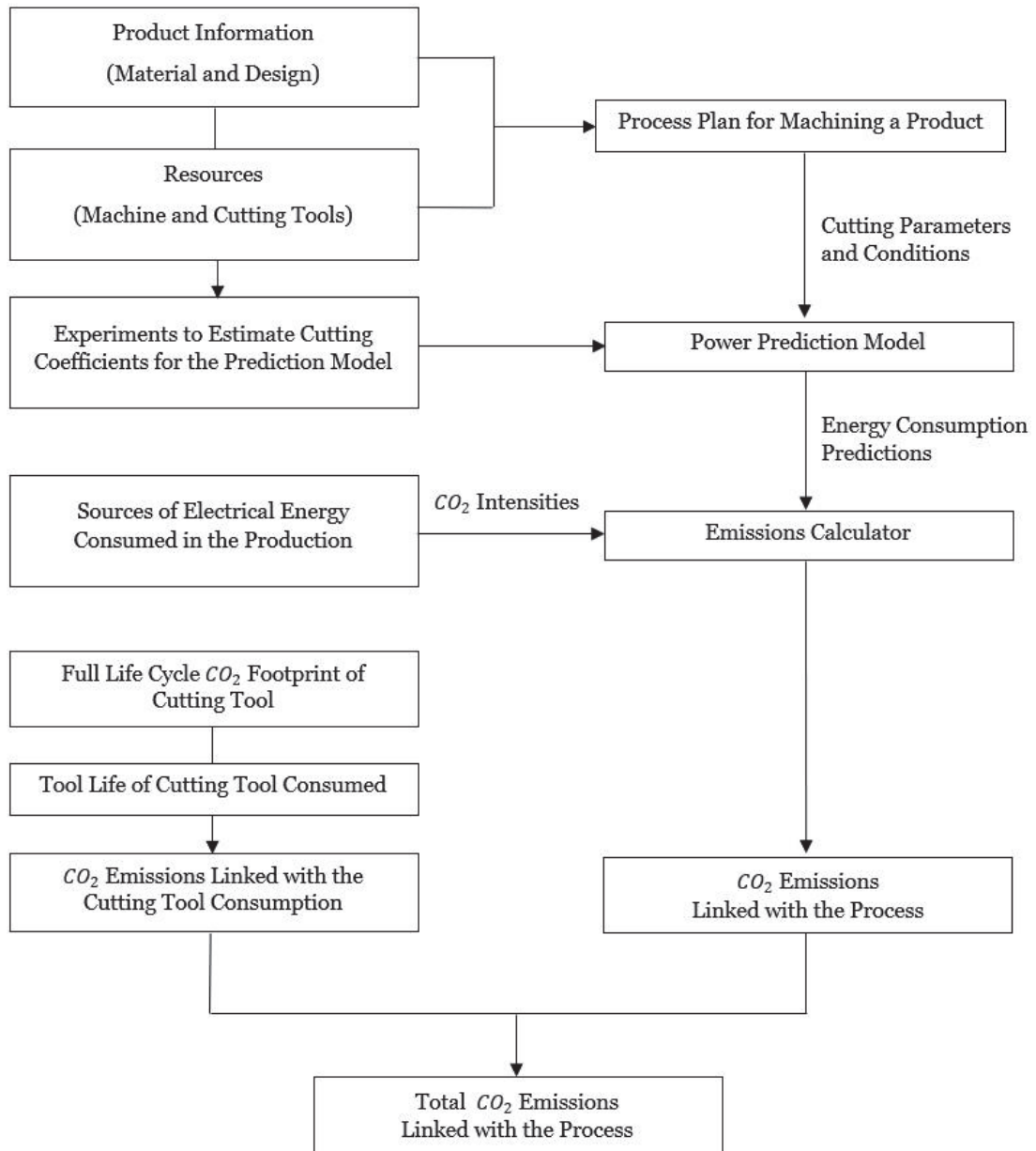


Figure 38 Process Map of the Framework

Product information (material and design of the product) and resources available for machining (machine and cutting tools) are the inputs to create process plans. The process plans are made using CAM software generating tool paths to machine the workpiece. They contain information on the cutting parameters – cutting speed, feed rate, depth of cut, and tool engagement. Also, the cutting conditions – with or without coolant, direction of cut, are defined in the process plans. These parameters are input in the prediction model to predict the power consumption by the process plan.

To obtain additional data required for constructing the prediction model, a series of simple air-cutting and material removal experiments are conducted by the practical approach outlined in Section 5.1.6. Data recorded from these experiments assist in estimating cutting coefficients which can be input to the prediction model. This prediction model is then tailored for a specific combination of material type, machine, and cutting tool. Provided the combination remains unchanged, the coefficients estimated by performing the experiments once are sufficient for the power prediction of various process plans.

The prediction model delivers power prediction values, which are subsequently used to calculate CO₂ emissions. At this point, it is important to know the sources of the electrical energy that is consumed or planned to be consumed for production. Knowing the energy sources, CO₂ intensities tied to the energy from the sources can be gathered from databases. With these intensities and the energy consumption predictions from the model, the CO₂ emissions linked to the process can be estimated.

The cutting tool is considered consumable in this process. Therefore, the CO₂ emissions linked to the cutting tool are also included in the framework. To calculate this, some information about the tool is to be input into the framework – the full life cycle CO₂ footprint of the tool and the estimated tool life for the machining operations in question. The tool life consumed during the process can be estimated, and along with the tool information, it helps to estimate the CO₂ emissions linked with the cutting tool.

Summing up the CO₂ emissions for the process and that of the cutting tool gives the total CO₂ emission values linked to the process plan. This value can be produced for different process plans, and based on this, the level of sustainability of different process plans can be compared.

7. Conclusions and Future Work

This thesis discusses two possible approaches for fast modeling the cutting power of milling processes with simple experiments, to provide a feasible framework for machine tool owners to build energy models and evaluate the environmental impact in milling processes.

Principles and guidelines of life cycle assessment are used in defining the system boundary and functional unit of the study. A method for calculating indirect GHG emissions in dry milling, per the dual reporting regulatory requirement, is given and explained by calculating the data from milling experiments.

The proposed model and the workflow for evaluating the electricity consumption in milling processes demonstrated good accuracy with a simple, practical procedure, especially for the process power and its electricity consumption.

Findings indicate that the consumption of solid cemented carbide end mills dominates the environmental impact in the milling processes examined in this thesis. Electricity consumption, particularly electricity with a high penetration of renewables, presents a minor effect on the total environmental impact. Thus, extending tool life and reducing the life cycle carbon footprint of the cutting tools emerge as viable strategies for mitigating the impact in milling processes.

Notably, implementing practices such as reconditioning tools can decrease the emission impact associated with using these tools. Furthermore, the use of inserted cutters, which involve replacing only the cutting edge rather than the entire tool, may serve as another effective strategy for further reducing declared emissions.

Future work can be done on utilizing the proposed model and framework in a cradle-to-gate life cycle assessment for a machined product, cutting parameter optimization with energy-efficient objectives at the stage of process planning, and improving the model and the uncertainty evaluation for real practice.

Machine tool is a complex system. It is not easy to comprehensively answer the question about its energy efficiency. A good amount of research work can be done on this topic. In the experiments of this study, detailed AC power time series data are recorded by the power analyzer, besides the active power used in modeling and analysis. These data include the reactive power, apparent power, power factor, voltage, current, and phase shift for two lines. For a big rotary machine, managing the reactive power could be a beneficial practice for the owner and the grid from the energy perspective. The experimental data can be useful for future studies on this topic. Additionally, the study of energy consumption of CNC machinery could be expanded further to include a more detailed analysis of mechanical inertial effects in start and stop operations. This would involve an in-depth examination of the energy spent due to the machine's start-stop operations, acceleration-deceleration cycles, and other factors linked to inertia, contributing to a more comprehensive understanding of the machine's overall energy consumption.

References

- [1] The European Parliament and the Council of the European Union, *Directive 2014/95/EU of the European Parliament and of the Council of 22 October 2014 amending Directive 2013/34/EU as regards disclosure of non-financial and diversity information by certain large undertakings and groups*. 2014 [Online]. Available: <http://data.europa.eu/eli/dir/2014/95/oj/eng>. [Accessed: 17-May-2023]
- [2] Directorate-General for Financial Stability and Financial Services and Capital Markets Union, 'Corporate sustainability reporting'. [Online]. Available: https://finance.ec.europa.eu/capital-markets-union-and-financial-markets/company-reporting-and-auditing/company-reporting/corporate-sustainability-reporting_en. [Accessed: 17-May-2023]
- [3] The European Parliament and the Council of the European Union, *Directive (EU) 2022/2464 of the European Parliament and of the Council of 14 December 2022 amending Regulation (EU) No 537/2014, Directive 2004/109/EC, Directive 2006/43/EC and Directive 2013/34/EU, as regards corporate sustainability reporting*. 2022 [Online]. Available: <http://data.europa.eu/eli/dir/2022/2464/oj/eng>. [Accessed: 17-May-2023]
- [4] GHG Protocol Initiative Team, 'The Greenhouse Gas Protocol'. World Resources Institute and World Business Council for Sustainable Development, Mar-2004 [Online]. Available: <https://ghgprotocol.org/sites/default/files/standards/ghg-protocol-revised.pdf>
- [5] GHG Protocol Team, 'Product Life Cycle Accounting and Reporting Standard'. World Resources Institute and World Business Council for Sustainable Development, Sep-2011.
- [6] *Manufacturing Systems: Theory and Practice*. New York: Springer-Verlag, 2006, Mechanical Engineering Series, ISBN: 978-0-387-25683-2 [Online]. DOI: 10.1007/0-387-28431-1
- [7] Divya Pandey, Madhoolika Agrawal, and Jai Shanker Pandey, 'Carbon footprint: current methods of estimation', *Environ. Monit. Assess.*, vol. 178, no. 1, pp. 135–160, Jul. 2011. DOI: 10.1007/s10661-010-1678-y
- [8] Neeraj Bhanot, P. Venkateswara Rao, and S. G. Deshmukh, 'An integrated sustainability assessment framework: a case of turning process', *Clean Technol. Environ. Policy*, vol. 18, no. 5, pp. 1475–1513, Jun. 2016. DOI: 10.1007/s10098-016-1130-2
- [9] Fysikopoulos Apostolos, Stavropoulos Panagiotis, Salonitis Konstantinos, and Chryssolouris George, 'Energy Efficiency Assessment of Laser Drilling Process', *Phys. Procedia*, vol. 39, pp. 776–783, Jan. 2012. DOI: 10.1016/j.phpro.2012.10.100
- [10] Qi Lu, Guang-Hui Zhou, Zhong-Dong Xiao, Feng-Tian Chang, and Chang-Le Tian, 'A selection methodology of key parts based on the characteristic of carbon emissions for low-carbon design', *Int. J. Adv. Manuf. Technol.*, vol. 94, no. 9, pp. 3359–3373, Feb. 2018. DOI: 10.1007/s00170-017-0522-8
- [11] Paolo Calefati, John Pandremenos, Apostolos Fysikopoulos, and George Chryssolouris, 'Energy Efficient Process Planning System – The ENEPLAN Project', in *Advances in Production Management Systems. Competitive Manufacturing for Innovative Products and Services*, vol. 397, C. Emmanouilidis, M. Taisch, and D. Kiritsis, Eds. Berlin, Heidelberg: Springer Berlin Heidelberg, 2013, pp. 119–126 [Online]. DOI: 10.1007/978-3-642-40352-1_16
- [12] Vasiliki Christina Panagiotopoulou, Panagiotis Stavropoulos, and George Chryssolouris, 'A critical review on the environmental impact of manufacturing: a holistic perspective', *Int. J. Adv. Manuf. Technol.*, vol. 118, no. 1–2, pp. 603–625, Jan. 2022. DOI: 10.1007/s00170-021-07980-w
- [13] A. E. Bonilla Hernández, Tomas Beno, and Claes Fredriksson, 'Energy and Cost Estimation of a Feature-based Machining Operation on HRSA', *Procedia CIRP*, vol. 61, pp. 511–516, Jan. 2017. DOI: 10.1016/j.procir.2016.11.141
- [14] Oliver Ioan Avram and Paul Xirouchakis, 'Evaluating the use phase energy requirements of a machine tool system', *J. Clean. Prod.*, vol. 19, no. 6, pp. 699–711, Apr. 2011. DOI: 10.1016/j.jclepro.2010.10.010
- [15] Claudio Palasciano, Andres Bustillo, Paola Fantini, and Marco Taisch, 'A new approach for machine's management: from machine's signal acquisition to energy indexes', *J. Clean. Prod.*, vol. 137, pp. 1503–1515, Nov. 2016. DOI: 10.1016/j.jclepro.2016.07.030
- [16] Vincent Aizebeoje Balogun and Paul Tarisai Mativenga, 'Modelling of direct energy requirements in mechanical machining processes', *J. Clean. Prod.*, vol. 41, pp. 179–186, Feb. 2013. DOI: 10.1016/j.jclepro.2012.10.015
- [17] Congbo Li, Xingzheng Chen, Ying Tang, and Li Li, 'Selection of optimum parameters in multi-pass face milling for maximum energy efficiency and minimum production cost', *J. Clean. Prod.*, vol. 140, pp. 1805–1818, Jan. 2017. DOI: 10.1016/j.jclepro.2016.07.086
- [18] Shailendra Pawanr, Girish Kant Garg, and Srikanta Routroy, 'Modelling of Variable Energy Consumption for CNC Machine Tools', *Procedia CIRP*, vol. 98, pp. 247–251, Jan. 2021. DOI: 10.1016/j.procir.2021.01.038
- [19] Shahin Rahimifard, Yingying Seow, and T. Childs, 'Minimising Embodied Product Energy to support energy efficient manufacturing', *CIRP Ann. - Manuf. Technol.*, vol. 59, pp. 25–28, Dec. 2010. DOI: 10.1016/j.cirp.2010.03.048
- [20] Yingying Seow, Shahin Rahimifard, and Elliot Woolley, 'Simulation of energy consumption in the manufacture of a product', *Int. J. Comput. Integr. Manuf.*, vol. 26, pp. 663–680, Jul. 2013. DOI: 10.1080/0951192X.2012.749533

- [21] Xiaona Zhou, Fei Liu, and Wei Cai, 'An energy-consumption model for establishing energy-consumption allowance of a workpiece in a machining system', *J. Clean. Prod.*, vol. 135, pp. 1580–1590, Nov. 2016. DOI: 10.1016/j.jclepro.2015.10.090
- [22] S. T. Newman, A. Nassehi, R. Imani-Asrai, and V. Dhokia, 'Energy efficient process planning for CNC machining', *CIRP J. Manuf. Sci. Technol.*, vol. 5, no. 2, pp. 127–136, Jan. 2012. DOI: 10.1016/j.cirpj.2012.03.007
- [23] Amr Salem, Hussien Hegab, and Hossam A. Kishawy, 'An integrated approach for sustainable machining processes: Assessment, performance analysis, and optimization', *Sustain. Prod. Consum.*, vol. 25, pp. 450–470, Jan. 2021. DOI: 10.1016/j.spc.2020.11.021
- [24] T. Lu, A. Gupta, A. D. Jayal, F. Badurdeen, S. C. Feng, O. W. Dillon Jr., and I. S. Jawahir, 'A Framework of Product and Process Metrics for Sustainable Manufacturing', in *Advances in Sustainable Manufacturing*, Berlin, Heidelberg, 2011, pp. 333–338. DOI: 10.1007/978-3-642-20183-7_48
- [25] K. Branker, J. Jeswiet, and I.Y. Kim, 'Greenhouse gases emitted in manufacturing a product—A new economic model', *CIRP Ann.*, vol. 60, no. 1, pp. 53–56, 2011. DOI: 10.1016/j.cirp.2011.03.002
- [26] J. Jeswiet and S. Kara, 'Carbon emissions and CES™ in manufacturing', *CIRP Ann.*, vol. 57, no. 1, pp. 17–20, Jan. 2008. DOI: 10.1016/j.cirp.2008.03.117
- [27] Jeffrey B. Dahmus and Timothy G. Gutowski, 'An Environmental Analysis of Machining', presented at the ASME 2004 International Mechanical Engineering Congress and Exposition, 2008, pp. 643–652 [Online]. DOI: 10.1115/IMECE2004-62600
- [28] Hirohisa Narita, Nelfa Desmira, and Hideo Fujimoto, 'Environmental Burden Analysis for Machining Operation Using LCA Method', in *Manufacturing Systems and Technologies for the New Frontier*, London, 2008, pp. 65–68. DOI: 10.1007/978-1-84800-267-8_13
- [29] Yusuf Altintas, *Manufacturing Automation: Metal Cutting Mechanics, Machine Tool Vibrations, and CNC Design*. Cambridge University Press, 2000, ISBN: 978-0-521-65973-4.
- [30] G. Campatelli and A. Scippa, 'Prediction of Milling Cutting Force Coefficients for Aluminum 6082-T4', *Procedia CIRP*, vol. 1, pp. 563–568, Jan. 2012. DOI: 10.1016/j.procir.2012.04.100
- [31] Baohai Wu, Xue Yan, Ming Luo, and Ge Gao, 'Cutting force prediction for circular end milling process', *Chin. J. Aeronaut.*, vol. 26, no. 4, pp. 1057–1063, Aug. 2013. DOI: 10.1016/j.cja.2013.04.003
- [32] Mithilesh Kumar Dikshit, Asit Baran Puri, Atanu Maity, and Amit Jyoti Banerjee, 'Analysis of Cutting Forces and Optimization of Cutting Parameters in High Speed Ball-end Milling Using Response Surface Methodology and Genetic Algorithm', *Procedia Mater. Sci.*, vol. 5, pp. 1623–1632, Jan. 2014. DOI: 10.1016/j.mspro.2014.07.350
- [33] N. Grossi, L. Salles, A. Scippa, and G. Campatelli, 'Speed-varying cutting force coefficient identification in milling', *Precis. Eng.*, vol. 42, pp. 321–334, Oct. 2015. DOI: 10.1016/j.precisioneng.2015.04.006
- [34] ISO, 'ISO 14044:2006 Environmental management – Life cycle assessment – Requirements and guidelines'. Jul-2006 [Online]. Available: <https://www.iso.org/standard/38498.html>. [Accessed: 19-Apr-2023]
- [35] ISO, 'ISO 14044:2006/Amd 2:2020 Environmental management – Life cycle assessment – Requirements and guidelines Amendment 2'. Sep-2020.
- [36] Steven J. Skerlos, 'Cutting Fluids and Their Environmental Impact', in *Encyclopedia of Tribology*, Q. J. Wang and Y.-W. Chung, Eds. Boston, MA: Springer US, 2013, pp. 655–660 [Online]. DOI: 10.1007/978-0-387-92897-5_614
- [37] ISO, 'ISO 14044:2006', ISO, 12-Aug-2014. [Online]. Available: <https://www.iso.org/standard/38498.html>. [Accessed: 30-May-2023]
- [38] Greenhouse Gas Protocol, 'Product Standard | GHG Protocol'. [Online]. Available: <https://ghgprotocol.org/product-standard>. [Accessed: 30-May-2023]
- [39] GDP Tooling, 'Frequently Asked Questions FAQs', *GDP Tooling*, 21-Sep-2020. [Online]. Available: <https://gdptooling.com/frequently-asked-questions-faqs/>. [Accessed: 28-May-2023]
- [40] Multicam, 'Have You Replaced Your Collets and Tool Holders?', 09-Jan-2018. [Online]. Available: <https://www.multicam.com/en/resources/blog/2018/replace-collets-and-tool-holders>. [Accessed: 28-May-2023]
- [41] Heather Goetsch, 'Defining Functional Units for LCA and TEA', 28-Jun-2022 [Online]. Available: <https://www.energy.gov/eere/life-cycle-assessment-and-techno-economic-analysis-training>
- [42] Timothy Gutowski, Jeffrey Dahmus, and Alex Thiriez, 'Electrical energy requirements for manufacturing processes', in *13th CIRP international conference on life cycle engineering*, 2006, vol. 31, no. 1, pp. 623–638.
- [43] S. Kara and W. Li, 'Unit process energy consumption models for material removal processes', *CIRP Ann.*, vol. 60, no. 1, pp. 37–40, Jan. 2011. DOI: 10.1016/j.cirp.2011.03.018
- [44] W Li and S Kara, 'An empirical model for predicting energy consumption of manufacturing processes: a case of turning process', *Proc. Inst. Mech. Eng. Part B J. Eng. Manuf.*, vol. 225, no. 9, pp. 1636–1646, 2011.
- [45] Paolo C. Priarone, Gianni Campatelli, Filippo Montevicchi, Giuseppe Venturini, and Luca Settineri, 'A modelling framework for comparing the environmental and economic performance of WAAM-based integrated manufacturing and machining', *CIRP Ann.*, vol. 68, no. 1, pp. 37–40, Jan. 2019. DOI: 10.1016/j.cirp.2019.04.005

- [46] Gianni Campatelli, Filippo Monteverchi, Giuseppe Venturini, Giuseppe Ingarao, and Paolo C. Priaone, 'Integrated WAAM-Subtractive Versus Pure Subtractive Manufacturing Approaches: An Energy Efficiency Comparison', *Int. J. Precis. Eng. Manuf.-Green Technol.*, vol. 7, no. 1, pp. 1–11, Jan. 2020. DOI: 10.1007/s40684-019-00071-y
- [47] Vincenzo Lunetto, Paolo C. Priaone, Sami Kara, and Luca Settinieri, 'A comparative LCA method for environmentally friendly manufacturing: Additive manufacturing versus Machining case', *Procedia CIRP*, vol. 98, pp. 406–411, Jan. 2021. DOI: 10.1016/j.procir.2021.01.125
- [48] Yan He, Jiong Zhang, Xiaoguang Wang, Yufeng Li, Xiaocheng Tian, and Yulin Wang, 'A process scenario oriented Life Cycle Assessment framework for machining processes', *Procedia CIRP*, vol. 105, pp. 332–338, Jan. 2022. DOI: 10.1016/j.procir.2022.02.055
- [49] Mary Sotos and GHG Protocol Team, 'GHG Protocol Scope 2 Guidance'. World Resources Institute, 2015.
- [50] EFRAG, 'Draft European Sustainability Reporting Standards ESRS E1 Climate Change Basis for Conclusions'. Mar-2023 [Online]. Available: <https://www.efrag.org/Assets/Download?assetUrl=%2Fsites%2Fwebpublishing%2FSiteAssets%2FBC%2520ESRS%2520E1%2520Climate%2520change.pdf>. [Accessed: 30-May-2023]
- [51] L. Norberto López de Lacalle, Francisco J. Campa, and Aitzol Lamikiz, '3 - Milling', in *Modern Machining Technology*, J. Paulo Davim, Ed. Woodhead Publishing, 2011, pp. 213–303 [Online]. DOI: 10.1533/9780857094940.213
- [52] Deniz Aslan and Yusuf Altintas, 'On-line chatter detection in milling using drive motor current commands extracted from CNC', *Int. J. Mach. Tools Manuf.*, vol. 132, pp. 64–80, Sep. 2018. DOI: 10.1016/j.ijmachtools.2018.04.007
- [53] Chen-Jung Li, Hsiang-Chun Tseng, Meng-Shiun Tsai, and Chih-Chun Cheng, 'Novel servo-feed-drive model considering cutting force and structural effects in milling to predict servo dynamic behaviors', *Int. J. Adv. Manuf. Technol.*, vol. 106, Jan. 2020. DOI: 10.1007/s00170-019-04778-9
- [54] Yokogawa Test & Measurement Corporation, 'WT500 Power Analyzer User's Manual IM 760201-01E 11th Edition'. Sep-2019.
- [55] SCB, 'Electricity supply and use 2001–2021 (GWh)', *Statistiska Centralbyrån*, 27-Oct-2022. [Online]. Available: <https://www.scb.se/en/finding-statistics/statistics-by-subject-area/energy/energy-supply-and-use/annual-energy-statistics-electricity-gas-and-district-heating/pong/tables-and-graphs/electricity-supply-and-use-20012021-gwh/>. [Accessed: 15-May-2023]
- [56] Scott Nicholson and Garvin Heath, 'Life Cycle Emissions Factors for Electricity Generation Technologies'. National Renewable Energy Laboratory - Data (NREL-DATA), Golden, CO (United States); National Renewable Energy Laboratory (NREL), Golden, CO (United States), p. 1 files, 2021 [Online]. DOI: 10.7799/1819907
- [57] Anna Furberg, Rickard Arvidsson, and Sverker Molander, 'Environmental life cycle assessment of cemented carbide (WC-Co) production', *J. Clean. Prod.*, vol. 209, pp. 1126–1138, 2019. DOI: 10.1016/j.jclepro.2018.10.272
- [58] Anna Furberg, Rickard Arvidsson, and Sverker Molander, 'A practice-based framework for defining functional units in comparative life cycle assessments of materials', *J. Ind. Ecol.*, vol. 26, no. 3, pp. 718–730, Jun. 2022. DOI: 10.1111/jiec.13218
- [59] Xiaotian Ma, Congcong Qi, Liping Ye, Donglu Yang, and Jinglan Hong, 'Life cycle assessment of tungsten carbide powder production: A case study in China', *J. Clean. Prod.*, vol. 149, pp. 936–944, Apr. 2017. DOI: 10.1016/j.jclepro.2017.02.184

Appendix A: Supplementary Figures and Tables

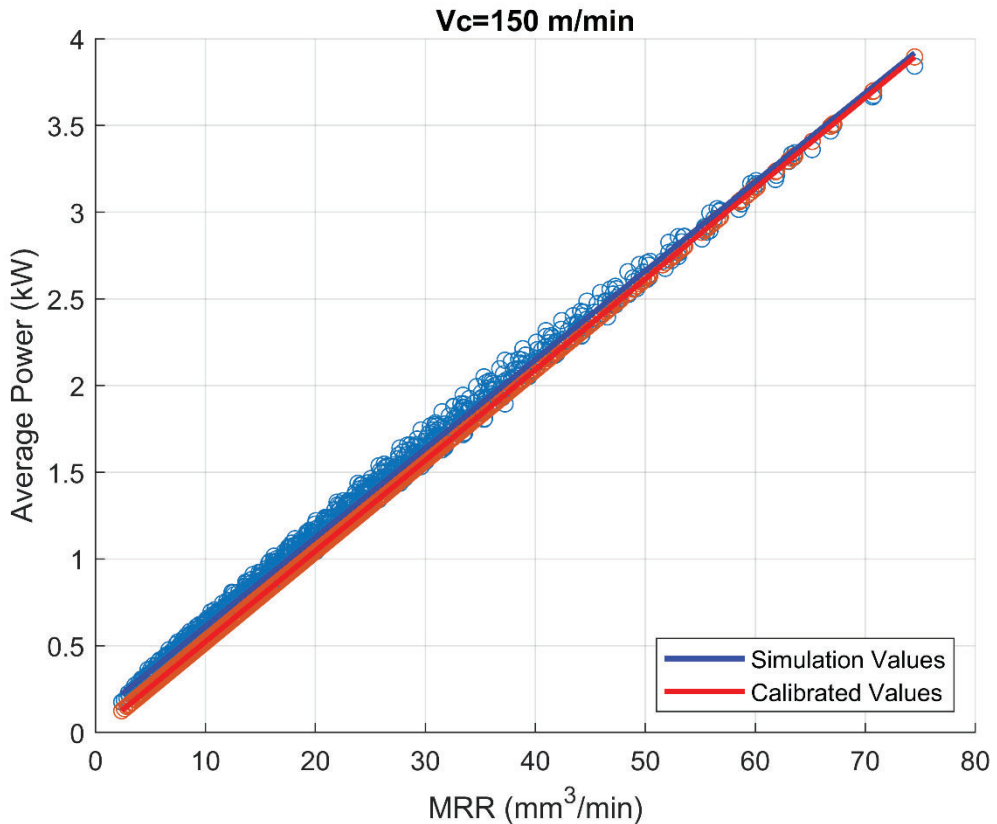


Figure 39 Simulated and Calibrated Average Power Values vs MRR

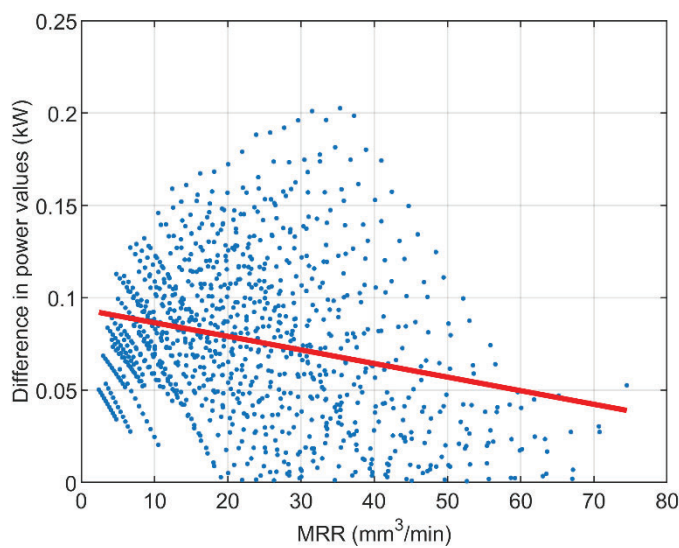


Figure 40 Absolute Error in the Power Values Predicted using the Empirical Model Vs MRR

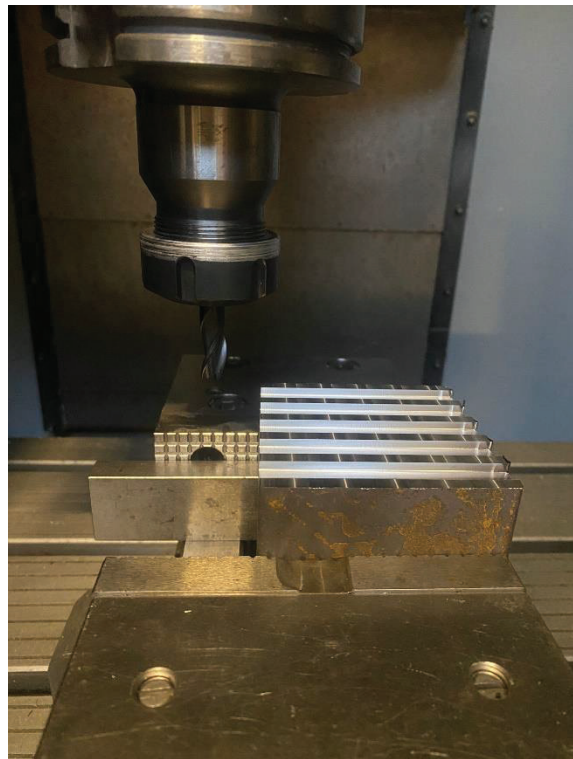


Figure 41 Slots Cut along X Axis



Figure 42 Slots Cut along Y Axis



Figure 43 Diagonal Slots

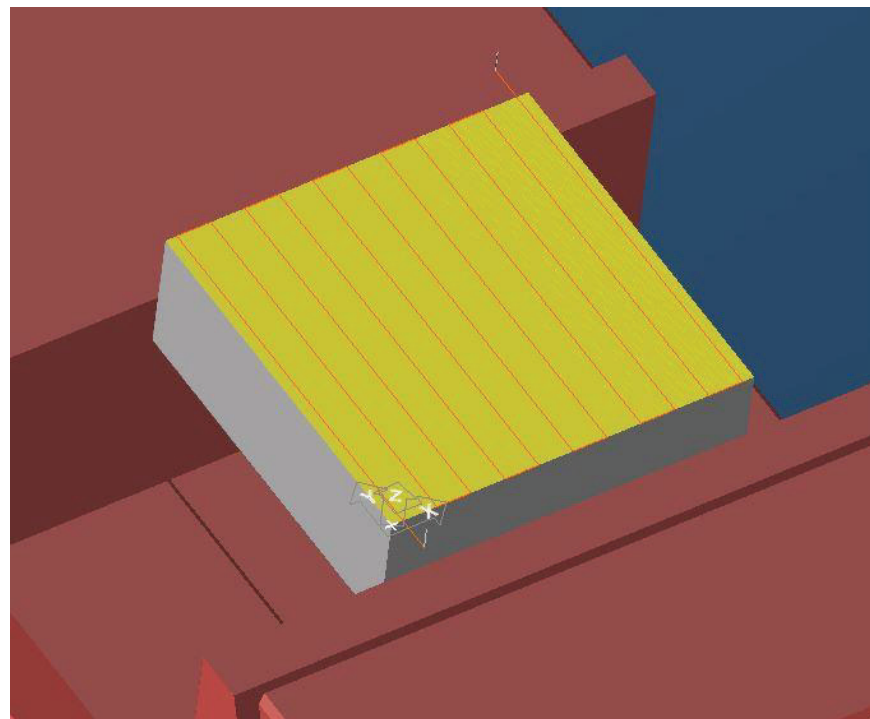


Figure 44 Face Milling Tool Path along Y Axis

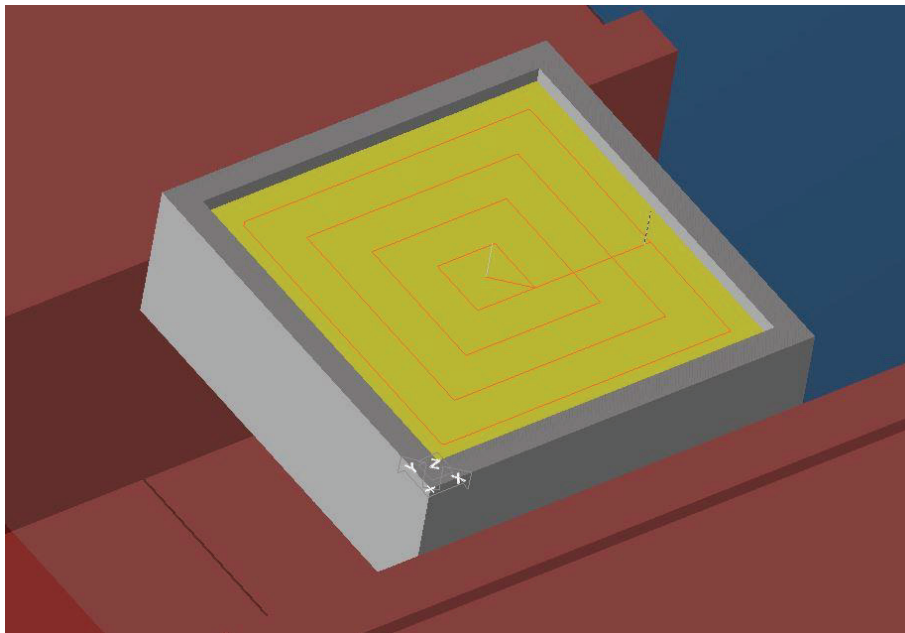


Figure 45 Pocketing Tool Path Cutting Outward from the Center

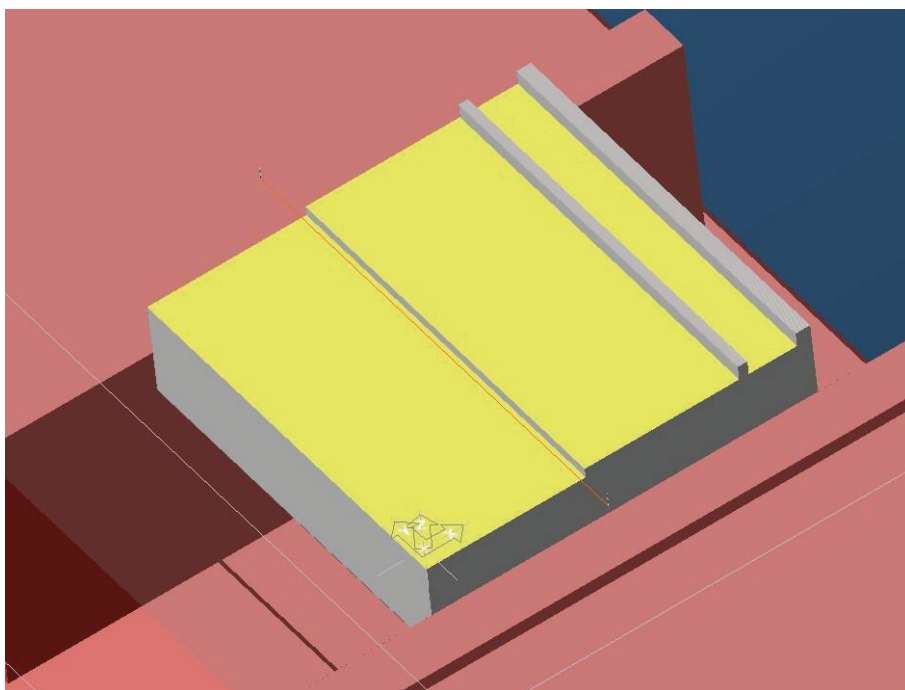


Figure 46 Shoulder Milling Tool Path and Machined Surfaces

Table 31 Trace Variables

#	Trace Variable	Description	Units
1	/Channel/!SEMA/measPos1 [u1, 1]	Actual value of position, encoder 1. [X axis]	mm
2	/Channel/!SEMA/measPos1 [u1, 2]	Actual value of position, encoder 1. [Y axis]	mm
3	/Channel/!SEMA/measPos1 [u1, 3]	Actual value of position, encoder 1. [Z axis]	mm
4	/Channel/!SEMA/actFeedRate [u1, 1]	Actual value of axis-specific feed rate [X axis]	mm/min
5	/Channel/!SEMA/actFeedRate [u1, 2]	Actual value of axis-specific feed rate [Y axis]	mm/min
6	/Channel/!SEMA/actFeedRate [u1, 3]	Actual value of axis-specific feed rate [Z axis]	mm/min
7	/Nck/!SD/nckServoDataActPower64 [u1, 1]	Active power (64 bit) [X axis]	Watt
8	/Nck/!SD/nckServoDataActPower64 [u1, 2]	Active power (64 bit) [Y axis]	Watt
9	/Nck/!SD/nckServoDataActPower64 [u1, 3]	Active power (64 bit) [Z axis]	Watt
10	/Nck/!SD/nckServoDataActPower64 [u1, 4]	Active power (64 bit) [Spindle]	Watt
11	/Nck/!SD/nckServoDataActCurr64 [u1, 1]	Torque-prod. Current act. Val. i(q) (64 bit) [X axis]	Ampere
12	/Nck/!SD/nckServoDataActCurr64 [u1, 2]	Torque-prod. Current act. Val. i(q) (64 bit) [Y axis]	Ampere
13	/Nck/!SD/nckServoDataActCurr64 [u1, 3]	Torque-prod. Current act. Val. i(q) (64 bit) [Z axis]	Ampere
14	/Nck/!SD/nckServoDataActCurr64 [u1, 4]	Torque-prod. Current act. Val. i(q) (64 bit) [Spindle]	Ampere
15	/Channel/!SEMA/actSpeedRel [u1, 1]	Actual value of rotary speed [X axis]	percent
16	/Channel/!SEMA/actSpeedRel [u1, 2]	Actual value of rotary speed [Y axis]	percent
17	/Channel/!SEMA/actSpeedRel [u1, 3]	Actual value of rotary speed [Z axis]	percent
18	/Channel/!S/actFeedRateIpo [u1, 1]	Actual value of the interpolation feed rate	mm/min
19	/Channel/!SPARP/actLineNumber [u1, 1]	Line number of current NC instruction (start:1)	-
20	/Channel/!SSP2/actSpeed [u1, 1]	Spindle speed, actual value	rpm

Table 32 Experimental and Predicted Data for Calculating the Variables in Table 17

#	Experiment			Prediction	
	Trace P_{sp}	Trace $P_{sp\ air}$	Trace P_x	Interp. $P_{sp\ air}$	Pred. P_x
1	997.7	478.5	15.3	522.1	19.3
2	1007.5	478.5	22.1	522.1	19.3
3	1147.3	385.8	7.9	414.9	8.1
4	1166.1	385.8	11.4	414.9	8.1
5	1328.8	356.2	7.2	379.4	5.5
6	1360.4	356.2	8.2	379.4	5.5
7	788.8	483.4	20.1	522.1	19.3
8	808.5	483.4	19.6	522.1	19.3
9	859.3	388.8	8.0	414.9	8.1
10	869.8	388.8	9.5	414.9	8.1
11	954.4	353.1	6.8	379.4	5.5
12	958.2	353.1	6.8	379.4	5.5

Table 33 Life Cycle Emission Factors for Electricity Generation Technologies (g CO₂-eq/kWh) [56]

	Min	1Q	Med	3Q	Max
Hydropower	0.57	8.4	21	27	75
Biopower	-1000	28	52	110	1300
Wind Power	1.3	8.1	13	22	81
Nuclear	3.1	7.7	13	31	220
Natural Gas	307	427.25	486	550.5	988
Photovoltaic	11	30	43	62	226

Trace configuration header

```

<traceCaptureSetup_V20>
  <collectionSettings atCapacity="discard" powerOnStart="false" timeLimit="72"
appendData="false" deferOffload="false" endless="false" capacity="4.81587e+06"
autoRestart="false" />
  <sessionSettings clientPrivilegeRead="password" clientPrivilegeManage="exclusive"
archiveSetting="NCU" expirationPeriod="0" sessionName="KTHCUTo403X1" />
  <sampleRateSettings driveSampleRate1="0.00012500" servoSampleRate="0.003"
ipo2SampleRate="0.006" ipo1SampleRate="0.006" />
  <signalSettings>
    <signal eventChannel="1" domain="NCU_1" event="1" description="Actual value of position,
encoder 1." displayRes="5" key="s1" dataType="double" unitsType="posn"
name="/Channel/!SEMA/measPos1 [u1, 1]" />
    <signal eventChannel="1" domain="NCU_1" event="1" description="Actual value of position,
encoder 1." displayRes="5" key="s2" dataType="double" unitsType="posn"
name="/Channel/!SEMA/measPos1 [u1, 2]" />
    <signal eventChannel="1" domain="NCU_1" event="1" description="Actual value of position,
encoder 1." displayRes="5" key="s3" dataType="double" unitsType="posn"
name="/Channel/!SEMA/measPos1 [u1, 3]" />
    <signal eventChannel="1" domain="NCU_1" event="1" description="Actual value of the
interpolation feedrate" displayRes="5" key="s20" dataType="double" unitsType="veloLin"
name="/Channel/!S/actFeedRateIpo [u1, 1]" />
    <signal eventChannel="1" domain="NCU_1" event="255" description="Active power (64 bit)"
displayRes="5" key="s8" dataType="double" unitsType="power"
name="/Nck/!SD/nckServoDataActPower64 [u1, 1]" />
    <signal eventChannel="1" domain="NCU_1" event="255" description="Active power (64 bit)"
displayRes="5" key="s9" dataType="double" unitsType="power"
name="/Nck/!SD/nckServoDataActPower64 [u1, 2]" />
    <signal eventChannel="1" domain="NCU_1" event="255" description="Active power (64 bit)"
displayRes="5" key="s10" dataType="double" unitsType="power"
name="/Nck/!SD/nckServoDataActPower64 [u1, 3]" />
    <signal eventChannel="1" domain="NCU_1" event="255" description="Active power (64 bit)"
displayRes="5" key="s16" dataType="double" unitsType="power"
name="/Nck/!SD/nckServoDataActPower64 [u1, 4]" />
    <signal eventChannel="1" domain="NCU_1" event="255" description="Torque-prod. Current act.
Val. i(q) (64 bit)" displayRes="5" key="s17" dataType="double" unitsType="current"
name="/Nck/!SD/nckServoDataActCurr64 [u1, 1]" />
    <signal eventChannel="1" domain="NCU_1" event="255" description="Torque-prod. Current act.
Val. i(q) (64 bit)" displayRes="5" key="s18" dataType="double" unitsType="current"
name="/Nck/!SD/nckServoDataActCurr64 [u1, 2]" />
    <signal eventChannel="1" domain="NCU_1" event="255" description="Torque-prod. Current act.
Val. i(q) (64 bit)" displayRes="5" key="s19" dataType="double" unitsType="current"
name="/Nck/!SD/nckServoDataActCurr64 [u1, 3]" />
    <signal eventChannel="1" domain="NCU_1" event="255" description="Torque-prod. Current act.
Val. i(q) (64 bit)" displayRes="5" key="s21" dataType="double" unitsType="current"
name="/Nck/!SD/nckServoDataActCurr64 [u1, 4]" />
    <signal eventChannel="1" domain="NCU_1" event="1" description="Spindle speed, actual value"
displayRes="5" key="s23" dataType="double" unitsType="veloRot"
name="/Channel/!SSP2/actSpeed [u1, 1]" />
    <signal eventChannel="1" domain="NCU_1" event="1" description="Line number of current NC
instruction (start:1)" displayRes="0" key="s22" dataType="dword" unitsType="none"
name="/Channel/!SPARP/actLineNumber [u1, 1]" />
    <signal eventChannel="1" domain="NCU_1" event="1" description="Actual value of axis-specific
feedrate" displayRes="5" key="s4" dataType="double" unitsType="velo"
name="/Channel/!SEMA/actFeedRate [u1, 1]" />
    <signal eventChannel="1" domain="NCU_1" event="1" description="Actual value of axis-specific
feedrate" displayRes="5" key="s5" dataType="double" unitsType="velo"
name="/Channel/!SEMA/actFeedRate [u1, 2]" />

```

```

<signal eventChannel="1" domain="NCU_1" event="1" description="Actual value of axis-specific
feedrate" displayRes="5" key="s6" dataType="double" unitsType="velo"
name="/Channel/!SEMA/actFeedRate [u1, 3]" />
<signal eventChannel="1" domain="NCU_1" event="1" description="Actual value of rotary speed"
displayRes="5" key="s7" dataType="double" unitsType="percent"
name="/Channel/!SEMA/actSpeedRel [u1, 1]" />
<signal eventChannel="1" domain="NCU_1" event="1" description="Actual value of rotary speed"
displayRes="5" key="s14" dataType="double" unitsType="percent"
name="/Channel/!SEMA/actSpeedRel [u1, 2]" />
<signal eventChannel="1" domain="NCU_1" event="1" description="Actual value of rotary speed"
displayRes="5" key="s15" dataType="double" unitsType="percent"
name="/Channel/!SEMA/actSpeedRel [u1, 3]" />
</signalSettings>
<triggerSettings useStopTrigger="false" useStartTrigger="false" >
  <startTrigger patternTimeLimit="0.0100" patternQualifier="entered" repeatCount="1"
combineLogic="and" delay="0.0000" >
    <triggerCondition eventChannel="1" mode="equalTo" level2="0.0" domain="" event="1"
description="" displayRes="0" key="t1" dataType="none" bitMask="oooooooo" name=""
level="0" />
  </startTrigger>
  <stopTrigger patternTimeLimit="0.0100" patternQualifier="entered" repeatCount="1"
combineLogic="and" delay="0.5" >
    <triggerCondition eventChannel="1" mode="equalTo" level2="0.0" domain="" event="1"
description="" displayRes="0" key="t1" dataType="none" bitMask="oooooooo" name=""
level="0" />
  </stopTrigger>
</triggerSettings>
</traceCaptureSetup_V20>

```

